December 1995 • NREL/TP-442-6472

Effects of Surface Roughness and Vortex Generators on the NACA 4415 Airfoil

R. L. Reuss
M. J. Hoffmann
G. M. Gregorek
The Ohio State University
Columbus, Ohio

National Renewable Energy Laboratory
1617 Cole Boulevard
Golden, Colorado 80401-3393
A national laboratory of the U.S. Department of Energy
Managed by Midwest Research Institute
for the U.S. Department of Energy
under contract No. DE-AC36-83CH10093

Foreword

Airfoils for wind turbines have been selected by comparing data from different wind tunnels, tested under different conditions, making it difficult to make accurate comparisons. Most wind tunnel data sets do not contain airfoil performance in stall commonly experienced by turbines operating in the field. Wind turbines commonly experience extreme roughness for which there is very little data. Finally recent tests have shown that dynamic stall is a common occurrence for most wind turbines operating in yawed, stall or turbulent conditions. Very little dynamic stall data exists for the airfoils of interest to wind turbine designer. In summary, very little airfoil performance data exists which is appropriate for wind turbine design.

Recognizing the need for a wind turbine airfoil performance data base the National Renewable Energy Laboratory (NREL), funded by the US Department of Energy, awarded a contract to Ohio State University (OSU) to conduct a wind tunnel test program. Under this program OSU has tested a series of popular wind turbine airfoils. A standard test matrix has been developed to assure that each airfoil was tested under the same conditions. The test matrix was developed in partnership with industry and is intended to include all of the operating conditions experienced by wind turbines. These conditions include airfoil performance at high angles of attack, rough leading edge (bug simulation), steady and unsteady angles of attack.

Special care has been taken to report as much of the test conditions and raw as practical so that designers can make their own comparisons and focus on details of the data relevant to their design goals. Some of the airfoil coordinates are proprietary to NREL or an industry partner. To protect the information which defines the exact shape of the airfoil the coordinates have not been included in the report. Instructions on how to obtain these coordinates may be obtained by contacting C.P. (Sandy) Butterfield at NREL.

C. P. (Sandy) Butterfield
Wind Technology Division
National Renewable Energy Laboratory
1617 Cole Blvd.
Golden, Colorado, 80401 USA
Internet Address: Sandy_Butterfield@NREL.GOV
Phone 303-384-6902
FAX 303-384-6901

Abstract

Wind turbines in the field can be subjected to many and varying wind conditions, including high winds with the rotor locked or with yaw excursions. In some cases, the rotor blades may be subjected to unusually large angles of attack that possibly result in unexpected loads and deflections. To better understand loadings at unusual angles of attack, a wind tunnel test was performed.

An 18-inch constant-chord model of the NACA 4415 airfoil section was tested under two dimensional steady state conditions in the Ohio State University Aeronautical and Astronautical Research Laboratory 7x10 Subsonic Wind Tunnel. The objective of these tests was to document section lift and moment characteristics under various model and air flow conditions. Surface pressure data were acquired at -60° through +230° geometric angles of attack, at a nominal 1 million Reynolds number. Also, cases with and without leading edge grit roughness were investigated. Leading edge roughness was used to simulate blade conditions encountered on wind turbines in the field. Additionally, surface pressure data were acquired for Reynolds numbers of 1.5 and 2.0 million, with and without leading edge grit roughness, but the angle of attack was limited to a -20° to 40° range.

In general, results showed lift curve slope sensitivities to Reynolds number and roughness. The maximum lift coefficient was reduced as much as 20 % by leading edge roughness. Moment coefficient showed little sensitivity to roughness beyond 50° angle of attack, but the expected decambering effect of a thicker boundary layer with roughness did show at lower angles.

Tests were also conducted with vortex generators located at the 30% chord location on the upper surface only, at 1 and 1.5 million Reynolds numbers, with and without leading edge grit roughness. In general, with leading edge grit roughness applied, the vortex generators restored the baseline level of maximum lift coefficient but with a more sudden stall break and at a lower angle of attack than the baseline.

Table of Contents Page

List of Figures Page

List of Tables Page

List of Symbols

AOA	Angle of Attack, degrees
□□	Angle of Attack, degrees
c	Chord Length, inches
C_{dmin}	Minimum Drag Coefficient
C_{dp}	Section Pressure (Form) Drag Coefficient
C_{dw}	Section Drag Coefficient, calculated from Wake momentum deficit
C_l	Section Lift Coefficient
C_{lmax}	Section Maximum Lift Coefficient
C_m	Section Pitching Moment Coefficient
C_{mo}	Section Pitching Moment Coefficient at zero degrees angle of attack
$C_{m\frac{1}{4}}$	Section Pitching Moment Coefficient about the quarter chord
C_p	Pressure Coefficient
C_{pmin}	Minimum Pressure Coefficient
k	Roughness element height, inches
psi	Units of pressure, pounds per square inch
q	Dynamic pressure, psi
Re	Reynolds number
x	Axis parallel to airfoil reference line, Coordinate in inches
y	Axis perpendicular to airfoil reference line, Coordinate in inches

Acknowledgements

This work was made possible by the efforts and financial support of the National Renewable Energy Laboratory which provided major funding and technical monitoring; the U.S. Department of Energy, which is credited for its funding of this document through the National Renewable Energy Laboratory under contract number DE-AC36-83CH10093 and U.S. Windpower Incorporated which provided funding for models and provided technical assistance. The staff of the Ohio State University Aeronautical and Astronautical Research Laboratory appreciate the contributions made by personnel from both organizations.

Introduction

Wind turbines in the field can be subjected to many and varying wind conditions, including high winds with rotor locked or with yaw excursions. In some cases the rotor blades may be subjected to unusually large angles of attack that possibly result in unexpected loads and deflections. To better understand loadings at unusual angles of attack, a wind tunnel test was performed. An 18-inch constant chord model of the NACA 4415 airfoil section was tested under two dimensional steady state conditions in the Ohio State University Aeronautical and Astronautical Research Laboratory (OSU/AARL) 7x10 Subsonic Wind Tunnel (7x10). The objective of these tests was to document section lift and moment characteristics under various model and air flow conditions. These included a normal angle of attack range of -20° to +40°, an extended angle of attack range of -60° to +230°, applications of leading edge grit roughness (LEGR), and use of vortex generators (VGs), all at chord Reynolds numbers as high as possible for the particular model configuration. To realistically satisfy these conditions the 7x10 offered a tunnel-height-to-model-chord ratio of 6.7, suggesting low interference effects even at the relatively high lift and drag conditions expected during the test. Significantly, it also provided chord Reynolds numbers up to 2.0 million.

Knowing the NACA 4415 model would later be run in the OSU/AARL 3x5 Subsonic Wind Tunnel (3x5), the present test setup and methods were kept as similar as possible to those for the 3x5. Later, a direct comparison could be made of data obtained in the two wind tunnels. Consequently, most of the data acquisition equipment was moved from the 3x5 to the 7x10. Minor changes were made to the system in order to adapt the equipment to the larger facility. Also, so that the NACA 4415 model could be used in both tunnels, it was specially designed to include a central 3 foot span sensing section with removable, contoured, spanwise extensions.

In all LEGR cases a "standard" grit pattern was applied. The grit pattern was developed by U.S. Windpower, OSU/AARL, and the University of Texas, Permian Basin. The VGs were provided to OSU/AARL by U.S. Windpower. Detailed discussion of the grit pattern and VGs can be found in the Section, Model Details.

Reynolds numbers of 1, 1.5, and 2 million were tested, for normal angle of attack range cases (-20° to +40°). At 1 million Reynolds number, the model was additionally swept through the extended angle of attack range. The model would buffet at higher dynamic pressures, thus precluding higher Reynolds number data for the extended angle of attack range. However, both clean and LEGR data were taken for all useable tunnel conditions. Finally, VG effects were evaluated over the normal angle of attack range, for Reynolds numbers of 1 and 1.5 million, and for clean and LEGR cases. The VGs were tested at the 30% chord upper surface station only; any attempt at higher Reynolds numbers with VGs consistently resulted in VGs separating from the model. Scheduling constraints precluded any significant effort to alleviate the VG attachment problem.

Test Facility

Tests described here were performed in the OSU/AARL 7x10 subsonic wind tunnel. A schematic of the tunnel is shown in figure 1. There are two test sections in this tunnel; a 7-foot x 10-foot section in which these tests were conducted, and a 16-foot x 14-foot section in which very low-speed and high angle of attack testing is performed with large models. The wind tunnel is a closed-circuit, single-return, continuous flow system. A velocity range of 35 to 180 knots is developed in the 7x10 test section by a six-blade, fixed-pitch, 20-foot diameter fan directly driven by a 2000 horsepower, variable-speed motor. The tunnel's steel outer shell is water spray cooled to control internal air temperature. Its test section floor contains a rotating table which allows adjustment of the model angle of attack through a 290° range about a vertical axis. A large, long-traverse, wake survey probe was not available and, consequently, none was installed in the test section.

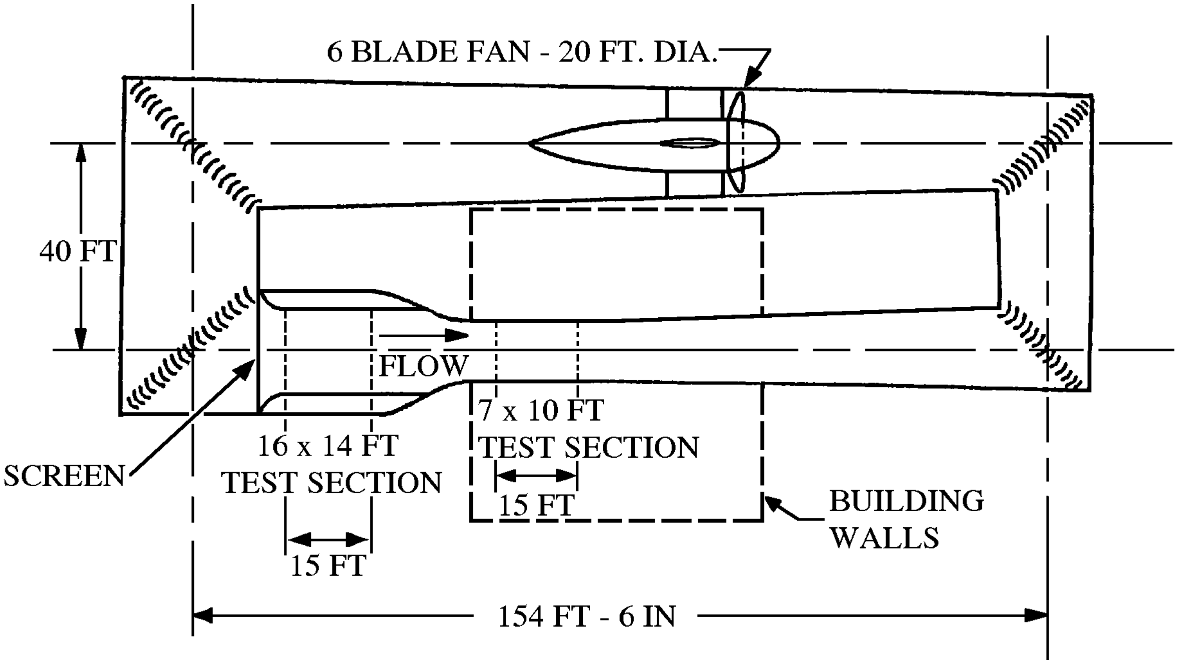

Figure 1. OSU/AARL 7x10 Subsonic Wind Tunnel

Model Details

An 18-inch constant chord NACA 4415 airfoil model was designed by OSU/AARL personnel and manufactured by others. Figure 2 shows the airfoil section; the section's measured coordinates are given in Appendix A. The model was made of a carbon composite skin over a foam core. The main load bearing member is a 1½-inch diameter steel tube which passes through the foam core at the airfoil quarter chord station. Steel and composite ribs and end plates transfer loads from the composite skin to the steel tube. The final surface was hand worked using templates to attain given coordinates within a tolerance of ±0.01 inches.

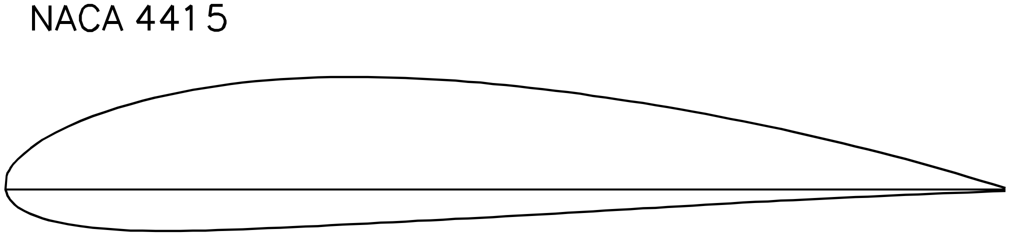

Figure 2. NACA 4415 Airfoil Section

Since the model had to also be used in the 3x5 subsonic wind tunnel for additional tests, it was designed with a 3-foot span main sensing section and 2-foot extension panels for each end, shown in figure 3. The extensions, used for 7x10 tunnel testing, were fabricated with the same contour as the main section and they slid over the steel tube and fastened to the endplates of the main section. Other minor model features were included, such as an extension to the model support tube and an adaptation of the support tube end to the different angle of attack potentiometer mountings in each facility.

To minimize pressure response times, the lengths of surface pressure tap leadout lines were made as short as possible. Although response time was not particularly important for the present test, it was important for

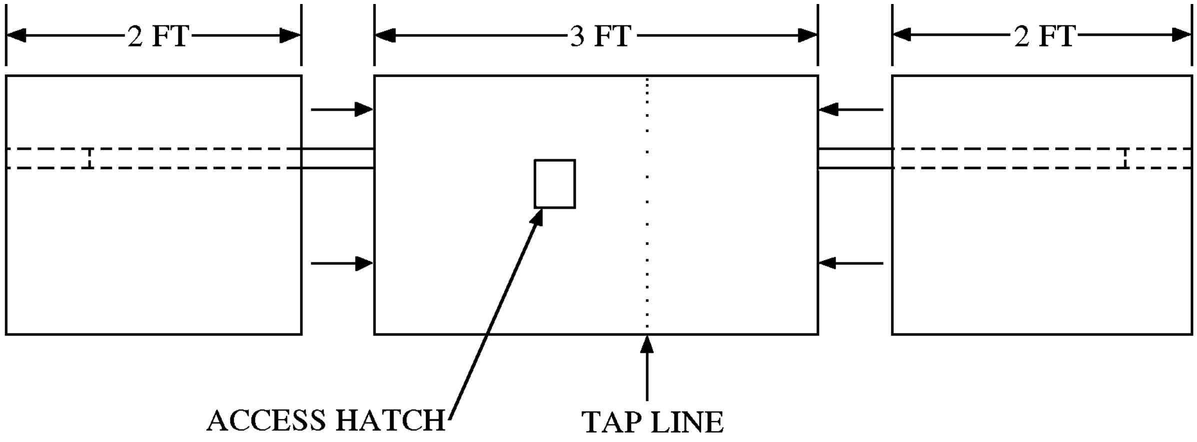

Figure 3. Model Design

the unsteady testing to be done later in the 3x5 wind tunnel. Therefore, a compartment was built into the model to hold the pressure scanning modules. This compartment was accessed through a panel door fitted flush with the model contour on the lower (pressure) surface.

For test cases involving roughness, a standard, repeatable pattern with grit as roughness elements was desired. In the past tests, grit was lightly blown into a thin layer of spray adhesive or onto a tape adhesive to obtain a roughened surface on models. For these tests, a different method was developed and used. A roughness pattern was jointly developed by OSU/AARL and U.S. Windpower personnel using a molded insect pattern taken from a wind turbine in the field by personnel at the University of Texas, Permian Basin. The resultant particle density was 32 particles per square inch in the middle of the pattern, and thinning to 8 particles per square inch at the edge of the pattern. Figure 4 shows the pattern template produced by U.S. Windpower from the above specifications. The pattern was repeatedly cut into a steel sheet 4-inches wide and 3-feet long, with holes just large enough for one piece of grit. Based on average particle size from the field specimen, standard #40 lapidary grit was chosen for the roughness elements, giving k/c=0.0019 for an 18-inch chord model.

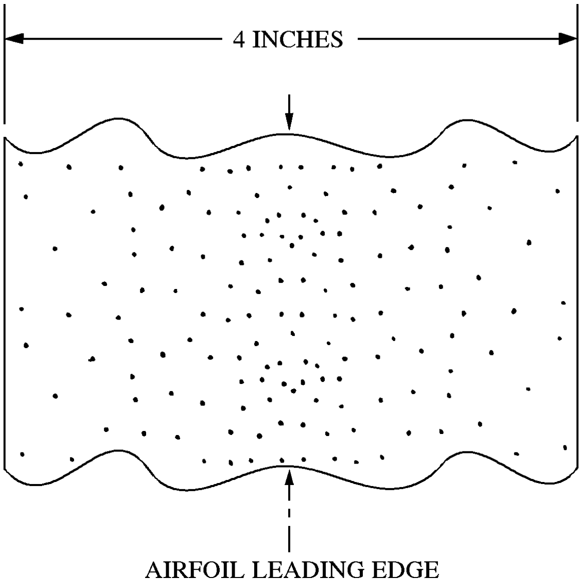

Figure 4. Roughness Pattern

To use the template, 4-inch wide double-tack tape was stuck to one side of the template and grit was poured and brushed from the opposite side. The tape was then removed from the template and transferred to the model. This scheme allowed the same roughness pattern to be replicated for any test.

VGs were applied to the model for some data points. U.S. Windpower provided the VGs with the geometry shown in figure 5. The VGs were pairs of right isosceles triangular shapes set on their longest sides at 30° included angle to each other and 15° to the chord line. The pairs were repeated every 1.61 inches in the spanwise direction. This VG configuration was fabricated in 1.53-inch-wide injection molded plastic strips with a 0.036-inch base-plate thickness. For ease of installation and to minimize damage to the model surface, these strips were fastened at the 30% chord upper surface station using rubber cement between the VG base-plate and model and thin tape (0.003 inch thick) over the base plate leading and trailing edges.

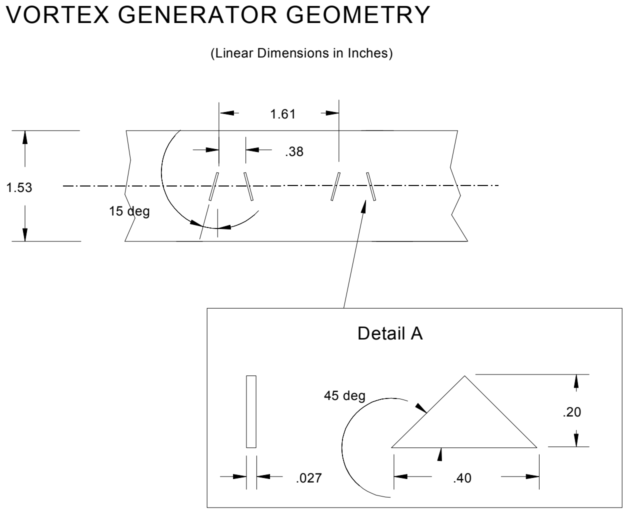

Figure 5. Vortex Generator Geometry

Test Equipment and Procedures

Data Acquisition

Data were acquired and processed from up to 60 surface pressure taps, three individual tunnel pressure transducers, and an angle of attack potentiometer. The data acquisition system included an IBM PC compatible 80386 based computer connected to a Pressure Systems Incorporated (PSI) data scanning system. The PSI system included a 780B Data Acquisition and Control Unit (DACU), 780B Pressure Calibration Unit (PCU), 81-IFC scanning module interface, two ESP-32 5-psid range pressure scanning modules (ESPs), and a 30-channel Remotely Addressed Millivolt Module (RAMM-30). Figure 6 shows the data acquisition system schematic.

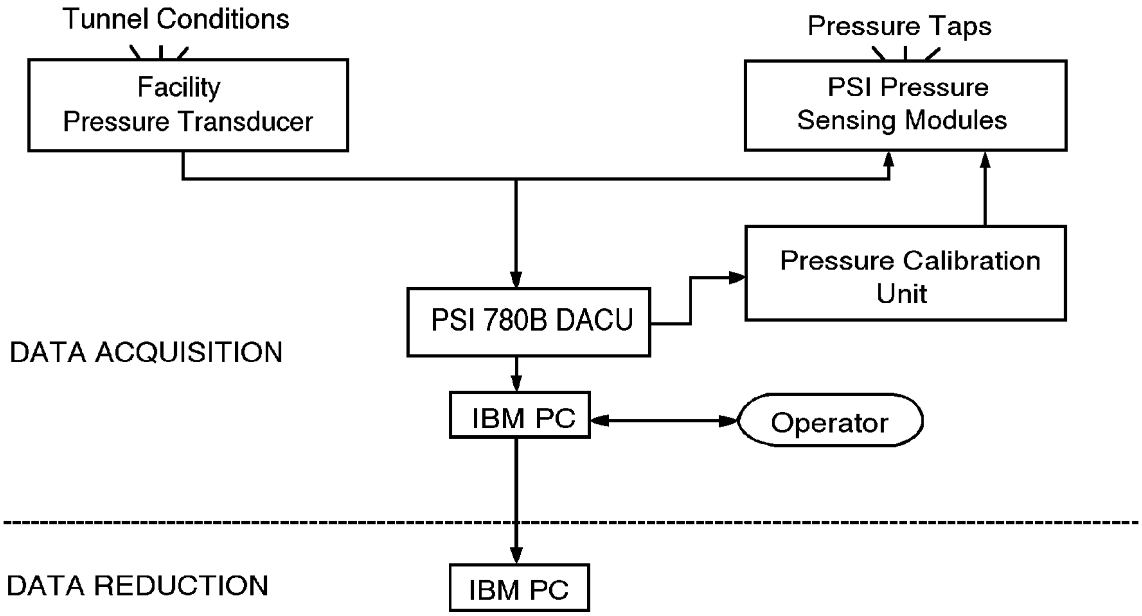

Figure 6. Data Acquisition Schematic

Three individual pressure transducers read tunnel total pressure, tunnel east static pressure, and tunnel west static pressure. Before the test began, these transducers were bench calibrated using a water manometer to determine their sensitivities and offsets. Related values were entered into the data acquisition and reduction program so the transducers could be shunt resistor calibrated before each series of wind tunnel runs.

The angle of attack potentiometer was a linear rotary potentiometer and was regularly calibrated during the tunnel pressure transducers shunt calibration. The angle of attack calibration was accomplished by taking voltage readings at known values of set angle of attack. This calibration method gave angle of attack readings within ±0.25° of actual over the entire angle range.

Two ESPs were calibrated simultaneously using the DACU and PCU. At the operator's request, the DACU commanded the PCU to apply known regulated pressures to the ESPs and read the output voltages from each integrated pressure sensor. From these values, the DACU calculated the calibration coefficients and stored them internally until the coefficients were requested by the controlling computer. This calibration was done several times during a run set because the ESPs were installed inside the model and their outputs tended to drift with temperature changes during a test sequence. Frequent online calibrations minimized the effect.

Finally, at the operator's request, pressure measurements from the airfoil surface taps and all other channels of information were acquired and stored by the DACU and subsequently passed to the controlling computer for final processing.

Data Reduction

The data reduction routine was incorporated as a section of the data acquisition program. This combination of data acquisition and reduction routines allowed data to be reduced online during a test. By quickly reducing selected runs, integrity checks could be made to ensure the equipment was working properly and to enable timely decisions about the test matrix.

The ambient pressure and tunnel air temperature were manually input into the computer and were updated regularly. These values, as well as the measurements from the tunnel pressure transducers, were used to calculate tunnel airspeed. As a continuous check of readings, both the tunnel individual pressure transducers and the ESPs, read the tunnel total and static pressures.

A typical datum point was derived by acquiring twenty data scans of all channels over a 1-second window at each angle of attack and tunnel condition. The reduction portion of the program processed each data scan to coefficient forms C_p, C_l, $C_{m1/4}$, and C_{dp} using the measured surface pressure voltages, calibration coefficients, tap locations and wind tunnel conditions. All scan sets for a given condition were then ensemble averaged to provide one set. All data were saved in electronic form. The data were not corrected for any tunnel wall effects, etc.

Test Matrix

The test was designed to allow an extended angle of attack range of -60° to 230° and Reynolds numbers of 1, 1.5, and 2 million with and without LEGR. Tabular data in Appendix B contains the actual Reynolds number for each angle of attack. The angle of attack increment was four degrees when $\alpha<-20°$ or $\alpha>40°$, two degrees when $-20°<\alpha<10°$ or $20°<\alpha<40°$, and one degree when $10°<\alpha<20°$. All test speeds and angles of attack were set for model clean and LEGR conditions.

For some cases, VGs were mounted at the 30% chord position on the model's upper surface only. The VG strips were provided by U.S. Windpower and were the exact type used on wind turbines in the field. Test conditions while the VGs were applied included clean and LEGR data at 1 and 1.5 million Reynolds numbers over an angle of attack range of -20° to 40°.

Unexpected complications during testing forced adjustments to this desired test matrix. Those complications and their effects are elaborated in the next section, Results and Discussion.

Results and Discussion

The NACA 4415 airfoil model was tested at three Reynolds numbers in the 7x10. Unfortunately, due to less than expected model rigidity, the model flexed and fluttered when near perpendicular to the flow at the higher test airspeeds. The tunnel airspeed was reduced for those conditions to reduce dynamic effects and to preserve the model's structural integrity. Consequently, the Reynolds number was not constant for the entire extended angle of attack sweeps and only the nominal 1 million Reynolds number condition was obtained. Reynolds number was as low as 0.6 million during the nominal 1 million Reynolds number extended angle of attack cases. Also, no wake survey probe was available for the test; only pressure drag from surface pressure integrations is presented.

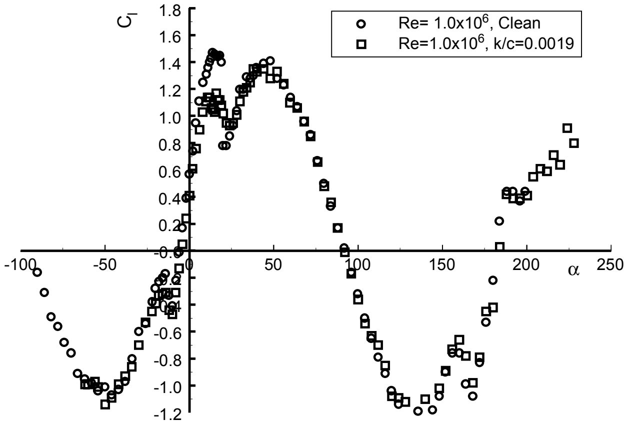

Figure 7. C_l vs □□, Extended Range

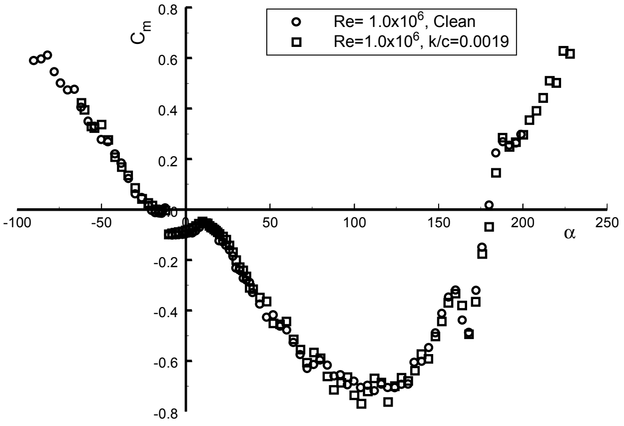

Figure 8. $C_{m1/4}$ vs □□, Extended Range

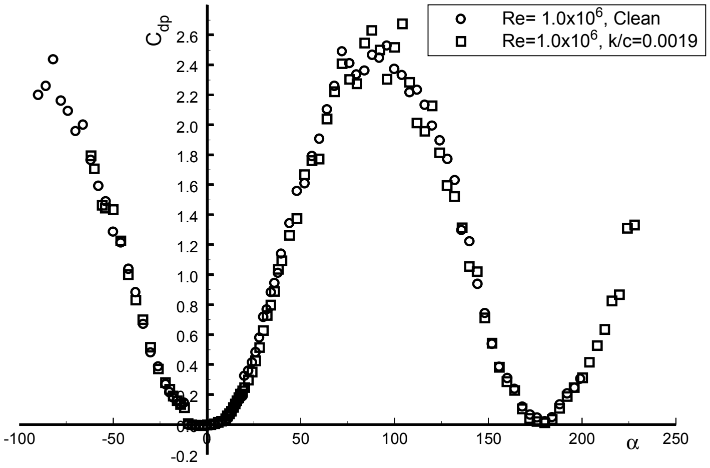

Figure 9. C_{dp} vs □□, Extended Range

Figure 7 shows the lift coefficient versus angle of attack for the extended angle of attack sweeps, for the model clean and with LEGR at 1 million Reynolds Number. Increases in lift coefficient occurred when the model was in its post stall region for both positive and negative angles of attack, but the maximum lift coefficient occurred just before positive stall and is 1.47. For the clean case, this model exhibits a gradual trailing edge stall. Correspondingly, for the LEGR data, the maximum lift coefficient prior to stall is 1.14 and occurs at a slightly lower angle of attack in comparison with the clean case. However, the overall maximum lift of the LEGR case does not occur before stall, but beyond it near 45° angle of attack. This can be observed in figure 7. Similar magnitudes of C_l= 1.4 are also apparent in the large angle of attack clean cases.

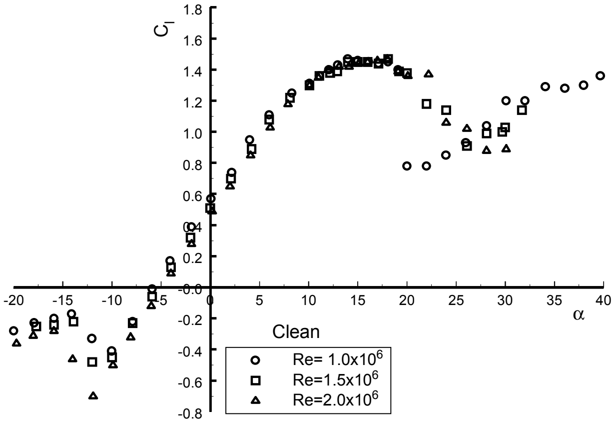

Figure 10. C_l vs α, Clean

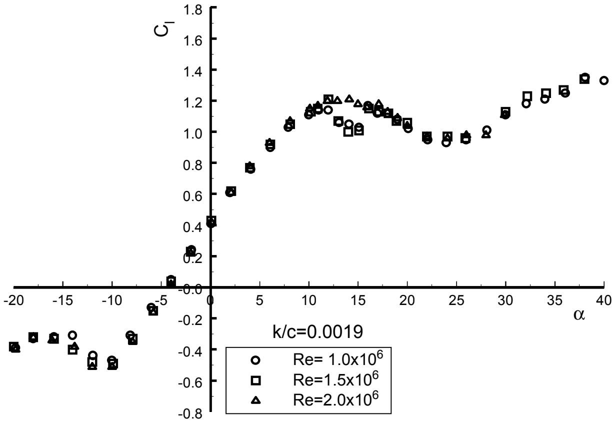

Figure 11. C_l vs α, LEGR, k/c=0.0019

The quarter chord pitching moment results are shown in figure 8 for the lowest Reynolds number of 1 million. The pitching moment is most negative when the airfoil is at high angles of attack near 110°. This observation is consistent for both the clean and LEGR cases. The pressure drag is shown in figure 9. The highest pressure drag occurs when the model is near 90° angle of attack. There is some scatter in the data at such conditions, caused by the severely detached, unstable flow on the leeward side of the model.

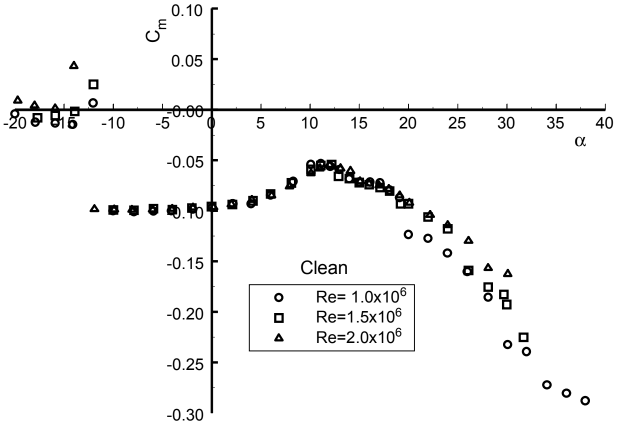

Figure 12. $C_{m\frac{1}{4}}$ vs α, Clean

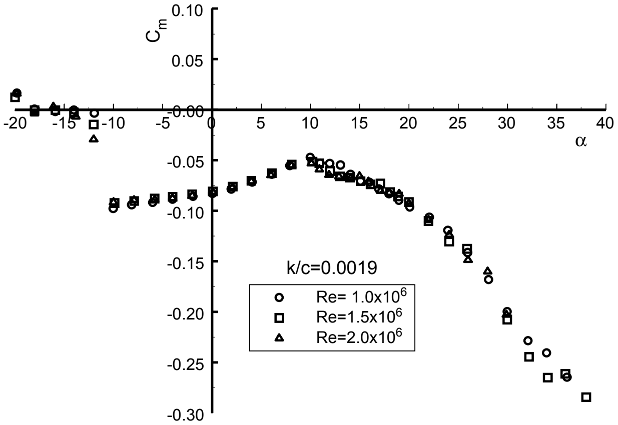

Figure 13. $C_{m\frac{1}{4}}$ vs α, LEGR, k/c=0.0019

A number of test runs were made for nominal angles of attack from -20° to +40°. For some of the cases there is no data shown for the highest angles of attack; these data were discounted as unreliable because the model was buffeting. Figure 10 and 11 show lift coefficients for all the test Reynolds numbers, for the clean model and LEGR cases. The maximum positive lift coefficient for the clean cases is about 1.47 and the LEGR data has a C_{lmax} about 1.21. For the clean cases, the negative maximum lift appears more sensitive to Reynolds number than the positive maximum. Also note that for the 1 million Reynolds number case, the model with

LEGR seems to stall less abruptly than the clean airfoil. The average lift curve slope for these data is about 0.093.

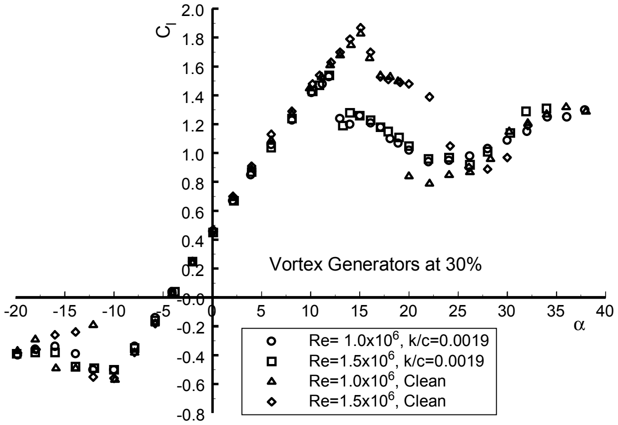

Figure 14. C_l vs □□, Vortex Generators

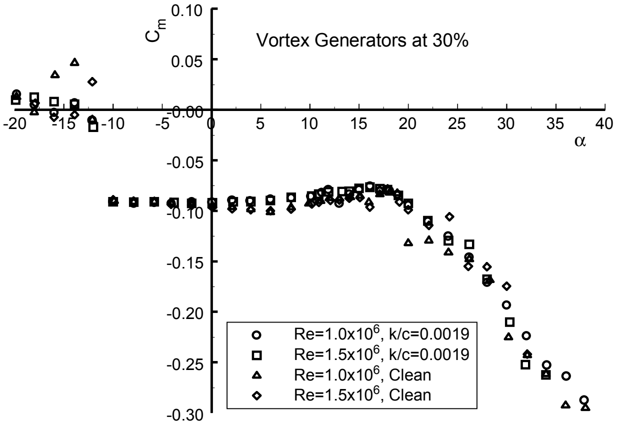

Figure 15. $C_{m¼}$ vs □□, Vortex Generators

Figure 12 shows the pitching moment about the quarter chord for the clean cases and figure 13 shows the LEGR cases. The LEGR data show a slightly more positive pitching moment near 0° angle of attack; however beyond stall, the pitching moment is slightly more negative for the model with LEGR than the clean model. The C_{mo} about the quarter chord for the clean case is -0.096 and -0.081 for the LEGR case.

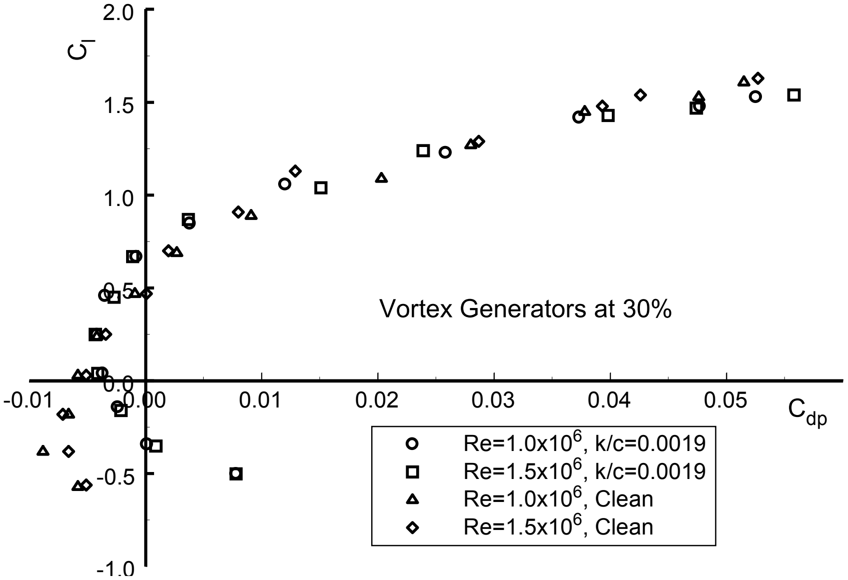

Figure 16. Drag Polar, Vortex Generators, C_l vs C_{dp}

VGs were fitted to the model at the 30% chord location, upper surface (suction side) only. The lift coefficient and pitching moment coefficients for the VG cases are shown in figure 14 and 15, respectively. The maximum lift coefficient for the clean case with VGs is near 1.85 and near 1.5 for the LEGR case. This is a 19% reduction in maximum lift when the airfoil has leading edge roughness. The stall of this airfoil is more abrupt when the VGs are applied, and occurs at a slightly lower angle of attack than without VGs. The pitching moment shows slightly different characteristics with the VGs than without. The pitching moment is almost a constant -0.10, from -10° to +15° angle of attack with VGs applied, but noticeable variation exists without VGs. Figure 16 shows a pressure drag polar for the VG cases; it is included only for completeness sake. This form of drag coefficient is inherently inaccurate because it does not include friction drag and should only be used for comparisons within the present data sets.

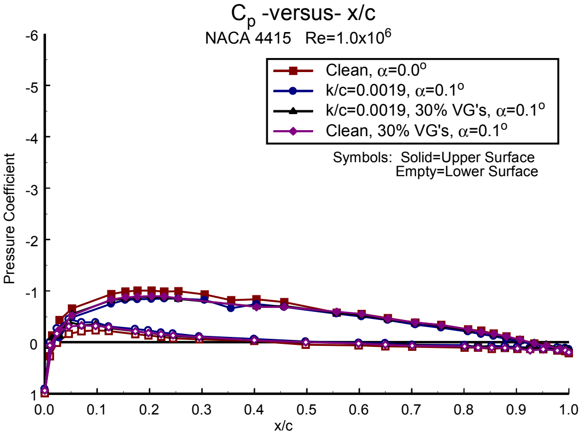

Figure 17. C_p vs x/c, α=0°

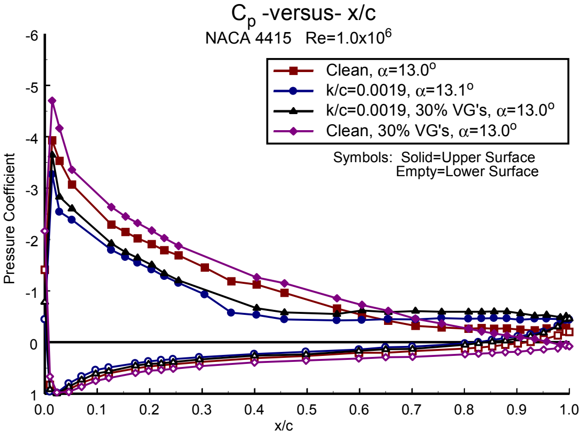

Figure 18. C_p vs x/c, α=13°

Representative surface pressure distributions are for a Reynolds number of 1 million and show cases of clean, LEGR, and VGs with and without LEGR. Figure 17 shows the pressure distributions for 0° angle of attack. A trend toward reduced pressure magnitudes with LEGR can be observed. At angles of attack near stall, the trending is more apparent. For example, figure 18 shows pressure distributions for a 13° angle of attack. The data show the model has upper surface flow separation near the 40% chord station for the LEGR case. It further shows the VGs increase the pressure magnitudes for both the clean and LEGR cases. Also, the VGs have caused the separation point to move slightly aft.

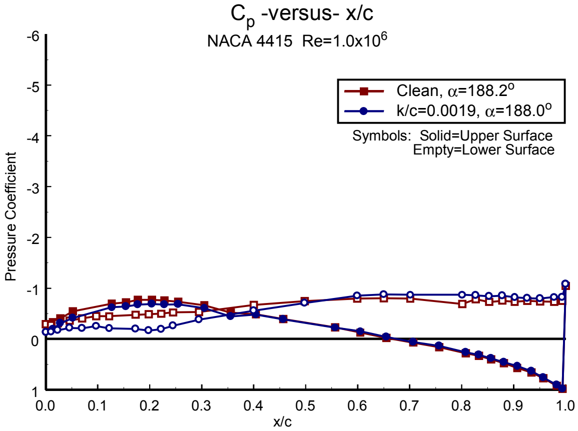

Figure 19. C_p vs x/c, α=188°

Figure 19 shows the pressure data for the model at an angle of attack of 188°, including clean and LEGR cases. Clean and LEGR pressure distributions are shown. Notice the distributions are almost identical near the trailing edge of the airfoil, and slightly different at the leading edge. This difference shows an effect of the roughness even though the leading edge is located, for this unusual case, down stream of the trailing edge.

The pressure distributions and coefficient data for other test conditions are in Appendix B.

Summary

A NACA 4415 model was installed in the OSU/AARL 7x10 subsonic wind tunnel and tested at three Reynolds numbers and with model clean, roughened, and with VGs. Table 1 is a summary of the aerodynamic coefficient data for the NACA 4415.

Table 1. NACA 4415 Aerodynamic Parameters Summary

CASE	Re num	C_{lmax}	$dC_l/d\alpha$	C_{mo}
Clean	$1.0x10^6$	1.47	0.097	-0.097
Clean	$1.5x10^6$	1.45	0.092	-0.096
Clean	$2.0x10^6$	1.47	0.094	-0.096
k/c=0.0019	$1.0x10^6$	1.14	0.088	-0.083
k/c=0.0019	$1.5x10^6$	1.21	0.091	-0.081
k/c=0.0019	$2.0x10^6$	1.21	0.095	-0.081
Clean VG's	$1.0x10^6$	1.83	0.105	-0.095
Clean VG's	$1.5x10^6$	1.87	0.109	-0.096
k/c=0.0019 VG's	$1.0x10^6$	1.53	0.101	-0.091
k/c=0.0019 VG's	$1.5x10^6$	1.54	0.104	-0.092

For the clean NACA 4415 model, Reynolds number changes from 1 to 2 million did not have a significant effect on the maximum positive lift or the pitching moment at zero degrees angle of attack. However, the addition of leading edge grit roughness to the model reduced the maximum lift coefficient by 18% and caused a 16% change in the pitching moment at 0° angle of attack. Also, the lift curve slope showed increases with Reynolds number. Adding VGS on the model upper surface at the 30% chord station caused the maximum lift coefficient to increase by 29% in the clean cases and about 27% for the roughened cases. The VGs apparently energized the boundary layer sufficiently to increase the lift curve slope and to delay stall to a higher angle of attack resulting in a higher maximum lift coefficient. However, the positive stall with VGs was more abrupt than the stall without VGs.

Appendix A: Model and Surface Pressure Tap Coordinates

Table A1. NACA 4415 Measured Model Coordinates
18 inch desired chord

Chord Station (in)	Upper Ordinate (in)	Chord Station (in)	Lower Ordinate (in)
0.0000	0.0936	0.0000	0.0936
0.0018	0.1404	0.0018	0.0414
0.0036	0.1530	0.0036	0.0306
0.0072	0.1764	0.0054	0.0144
0.0108	0.1980	0.0108	-0.0054
0.0198	0.2358	0.0180	-0.0324
0.0522	0.3222	0.0468	-0.1062
0.0792	0.3708	0.0720	-0.1530
0.1368	0.4518	0.1332	-0.2304
0.2160	0.5436	0.2070	-0.2952
0.3168	0.6426	0.3060	-0.3618
0.3924	0.7074	0.3798	-0.4032
0.4806	0.7740	0.4680	-0.4446
0.6156	0.8658	0.6012	-0.4968
0.7488	0.9468	0.7326	-0.5382
0.9036	1.0315	0.8874	-0.5778
1.0548	1.1052	1.0368	-0.6102
1.1718	1.1592	1.1052	-0.6318
1.3662	1.2420	1.3464	-0.6624
1.5768	1.3266	1.5570	-0.6912
1.7424	1.3878	1.7226	-0.7092
1.9062	1.4436	1.8882	-0.7236
2.0394	1.4868	2.0196	-0.7326
2.4192	1.5966	2.3994	-0.7506
2.9718	1.7262	2.9520	-0.7578
3.3516	1.8000	3.3318	-0.7560
3.8106	1.8720	3.7908	-0.7470
4.2156	1.9242	4.1976	-0.7344
4.8942	1.9872	4.8780	-0.7074
5.8392	2.0304	5.8230	-0.6624
6.7266	2.0340	6.7122	-0.6174
7.5186	2.0106	7.4934	-0.5742
8.5176	1.9440	8.5068	-0.5202

Table A1. NACA 4415 Measured Model Coordinates
18 inch desired chord

Chord Station (in)	Upper Ordinate (in)	Chord Station (in)	Lower Ordinate (in)
9.3708	1.8630	9.3618	-0.4716
10.3014	1.7514	10.2942	-0.4176
12.0690	1.4778	12.9384	-0.2682
13.8474	1.1358	13.8456	-0.2214
14.5332	0.9810	14.5368	-0.1890
14.9994	0.8712	15.0012	-0.1674
15.8652	0.6498	15.5052	-0.1440
16.3368	0.5220	15.8688	-0.1278
16.8300	0.3870	16.3098	-0.1098
17.1738	0.2916	16.8372	-0.0846
17.3862	0.2304	17.3034	-0.0648
17.5482	0.1854	17.4636	-0.0576
17.6958	0.1404	17.6220	-0.0486
17.8974	0.0810	17.7048	-0.0450
17.9478	0.0648	17.7840	-0.0414
18.0540	0.0342	17.8362	-0.0378
		17.9064	-0.0342
		18.0540	-0.0234

End of Table A1

Table A2. NACA 4415 Surface Pressure Tap Locations		
Tap Number	Chord Station	Ordinate
1	1.0000	-0.0016
2	0.9933	-0.0019
3	0.9778	-0.0025
4	0.9511	-0.0036
5	0.9262	-0.0046
6	0.9018	-0.0056
7	0.8781	-0.0067
8	0.8531	-0.0078
9	0.8272	-0.0090
10	0.8008	-0.0103
11	0.7502	-0.0128
12	0.7009	-0.0154
13	0.6504	-0.0184
14	0.5994	-0.0214
15	0.5512	-0.0242
16	0.4985	-0.0273
17	0.3997	-0.0325
18	0.2953	-0.0377
19	0.2454	-0.0400
20	0.2221	-0.0408
21	0.1977	-0.0415
22	0.1727	-0.0419
23	0.1466	-0.0417
24	0.1221	-0.0411
25	0.0967	-0.0395
26	0.0702	-0.0363

Table A2. NACA 4415 Surface Pressure Tap Locations

Tap Number	Chord Station	Ordinate
27	0.0461	-0.0318
28	0.0225	-0.0236
29	0.0102	-0.0162
30	0.0000	0.0005
31	0.0140	0.0321
32	0.0278	0.0436
33	0.0519	0.0583
34	0.0000	0.0000
35	0.1037	0.0796
36	0.1271	0.0868
37	0.1541	0.0936
38	0.1769	0.0984
39	0.2036	0.1031
40	0.2283	0.1066
41	0.2551	0.1097
42	0.3050	0.1127
43	0.3560	0.1135
44	0.4040	0.1123
45	0.4569	0.1092
46	0.5057	0.1047
47	0.5573	0.0988
48	0.6049	0.0923
49	0.6553	0.0843
50	0.7074	0.0749
51	0.7574	0.0648
52	0.8082	0.0536
53	0.8325	0.0479

Table A2. NACA 4415 Surface Pressure Tap Locations

Tap Number	Chord Station	Ordinate
54	0.8568	0.0420
55	0.8811	0.0359
56	0.9071	0.0288
57	0.9341	0.0212
58	0.9572	0.0146
59	0.9830	0.0069
60	0.9935	0.0036

End of Table A2

Appendix B: Integrated Coefficients and Pressure Distributions

List of Tables Page

List of Figures Page

Table B1. NACA 4415, Clean, Re = 1 million

RUN	AOA	C_l	C_{dp}	$C_{m¼}$	Re x10^{-6}
100	-90.0	-0.16	2.2000	0.5904	0.68
101	-85.8	-0.31	2.2603	0.5968	0.68
102	-81.9	-0.49	2.4366	0.6121	0.68
103	-77.9	-0.56	2.1612	0.5465	0.69
104	-74.0	-0.68	2.0917	0.5009	0.70
105	-69.9	-0.76	1.9575	0.4743	0.72
106	-66.0	-0.91	2.0011	0.4763	0.75
107	-61.9	-0.95	1.7662	0.4050	0.76
108	-57.9	-0.98	1.5935	0.3492	0.77
109	-53.9	-1.04	1.4896	0.3294	0.81
110	-50.0	-1.01	1.2866	0.2781	0.85
111	-46.0	-1.07	1.2137	0.2693	0.86
112	-41.8	-1.03	1.0391	0.2201	0.89
113	-38.0	-0.97	0.8834	0.1836	0.93
114	-33.9	-0.80	0.6706	0.1227	0.99
115	-30.0	-0.60	0.4798	0.0618	1.01
116	-25.9	-0.54	0.3860	0.0464	1.01
117	-22.0	-0.38	0.2704	0.0147	1.01
118	-20.0	-0.28	0.2160	-0.0040	1.01
119	-17.9	-0.23	0.1793	-0.0124	1.00
120	-15.9	-0.20	0.1596	-0.0133	1.01
121	-14.1	-0.17	0.1374	-0.0146	1.01
122	-12.0	-0.33	0.1445	0.0066	1.01
123	-10.0	-0.41	-0.0010	-0.1000	1.00
124	-7.9	-0.22	-0.0047	-0.1009	1.00
125	-5.9	-0.01	-0.0072	-0.1004	1.00
126	-4.1	0.17	-0.0094	-0.0999	1.00

Table B1. NACA 4415, Clean, Re = 1 million

RUN	AOA	C_l	C_{dp}	$C_{m\frac{1}{4}}$	Re $x10^{-6}$
127	-1.9	0.39	-0.0089	-0.0985	1.00
128	0.1	0.57	-0.0085	-0.0967	1.00
129	2.2	0.74	-0.0018	-0.0931	1.01
130	4.0	0.95	0.0005	-0.0930	1.01
131	6.0	1.11	0.0059	-0.0844	1.00
132	8.3	1.25	0.0185	-0.0709	1.00
133	10.1	1.31	0.0227	-0.0542	1.00
134	11.1	1.36	0.0371	-0.0530	1.00
135	12.1	1.40	0.0562	-0.0561	1.00
136	13.0	1.43	0.0719	-0.0591	1.00
137	14.0	1.47	0.0974	-0.0683	0.99
138	15.0	1.46	0.1207	-0.0716	0.99
139	16.1	1.45	0.1430	-0.0716	0.99
140	17.1	1.44	0.1615	-0.0721	1.00
141	18.1	1.45	0.1786	-0.0796	1.00
142	19.1	1.40	0.1895	-0.0869	0.99
143	20.0	0.78	0.3236	-0.1235	0.99
144	22.0	0.78	0.3600	-0.1272	0.99
145	24.0	0.85	0.4142	-0.1418	0.99
146	26.0	0.93	0.4838	-0.1602	0.98
147	28.1	1.04	0.5785	-0.1856	0.98
148	30.1	1.20	0.7180	-0.2323	0.99
149	32.0	1.20	0.7659	-0.2395	0.99
150	34.1	1.29	0.8821	-0.2722	0.99
151	36.1	1.28	0.9434	-0.2803	0.99
152	38.0	1.30	1.0111	-0.2882	0.98
153	39.7	1.36	1.1393	-0.3286	0.97

Table B1. NACA 4415, Clean, Re = 1 million

RUN	AOA	C_l	C_{dp}	$C_{m¼}$	Re x10^{-6}
154	44.1	1.39	1.3420	-0.3749	0.90
155	48.0	1.41	1.5573	-0.4263	0.88
156	52.1	1.28	1.6107	-0.4184	0.86
157	56.0	1.23	1.7930	-0.4617	0.84
158	60.0	1.14	1.9070	-0.4772	0.82
159	64.0	1.07	2.1034	-0.5273	0.79
160	68.0	0.96	2.2595	-0.5748	0.78
161	72.1	0.86	2.4907	-0.6301	0.76
162	76.0	0.67	2.4105	-0.6149	0.75
163	79.8	0.50	2.3370	-0.5969	0.75
164	84.0	0.33	2.3618	-0.6163	0.73
165	88.1	0.17	2.4671	-0.6596	0.73
166	91.9	0.02	2.4479	-0.6541	0.73
167	96.1	-0.16	2.5284	-0.6944	0.73
168	99.9	-0.32	2.3743	-0.6803	0.74
169	104.0	-0.50	2.3324	-0.7062	0.74
170	108.1	-0.65	2.2165	-0.6965	0.73
171	112.0	-0.79	2.2337	-0.7181	0.74
172	116.2	-0.91	2.1340	-0.6920	0.70
173	120.0	-1.04	1.9940	-0.7056	0.67
174	124.1	-1.14	1.8963	-0.7061	0.69
175	128.2	-1.25	1.7731	-0.6927	0.67
176	132.1	-1.34	1.6303	-0.6917	0.67
177	135.8	-1.19	1.2975	-0.6049	0.69
178	140.0	-1.28	1.2218	-0.6017	0.71
179	144.2	-1.18	0.9391	-0.5466	0.74
180	148.2	-1.08	0.7431	-0.4885	0.77

Table B1. NACA 4415, Clean, Re = 1 million

RUN	AOA	C_l	C_{dp}	$C_{m¼}$	Re $x10^{-6}$
181	151.9	-0.90	0.5381	-0.4119	0.80
182	156.0	-0.76	0.3841	-0.3472	0.99
183	160.1	-0.76	0.3106	-0.3194	1.00
184	164.1	-0.99	0.2364	-0.4379	1.00
185	168.2	-1.08	0.1191	-0.4879	1.01
186	172.2	-0.83	0.0658	-0.3205	1.01
187	176.0	-0.53	0.0462	-0.1489	1.00
188	180.1	-0.22	0.0222	0.0175	1.00
189	184.0	0.22	0.0485	0.2242	1.00
190	188.2	0.44	0.1330	0.2681	0.99
191	192.0	0.44	0.2072	0.2540	0.98
192	196.1	0.37	0.2464	0.2636	0.99
193	199.1	0.44	0.3054	0.2975	0.99

End of Table B1

Table B2. NACA 4415, Clean, Re = 1.5 million

RUN	AOA	C_l	C_{dp}	$C_{m\frac{1}{4}}$	Re x10^{-6}
200	-20.3	-0.31	0.2266	-0.0002	1.49
201	-17.7	-0.25	0.1878	-0.0078	1.50
202	-15.9	-0.24	0.1696	-0.0055	1.51
203	-13.9	-0.22	0.1514	-0.0014	1.50
204	-12.0	-0.48	0.1610	0.0252	1.50
205	-10.0	-0.45	-0.0038	-0.0991	1.51
206	-7.9	-0.23	-0.0063	-0.0992	1.47
207	-5.9	-0.06	-0.0080	-0.0977	1.50
208	-4.0	0.13	-0.0083	-0.0986	1.49
209	-2.0	0.32	-0.0063	-0.0970	1.49
210	0.0	0.51	-0.0033	-0.0957	1.49
211	2.1	0.70	0.0007	-0.0936	1.49
212	4.2	0.89	0.0079	-0.0899	1.50
213	6.0	1.08	0.0097	-0.0833	1.49
214	8.1	1.22	0.0196	-0.0722	1.49
215	10.1	1.30	0.0328	-0.0590	1.49
216	11.1	1.36	0.0401	-0.0549	1.49
217	12.2	1.38	0.0561	-0.0542	1.50
218	12.9	1.39	0.0750	-0.0656	1.49
219	14.0	1.45	0.0988	-0.0680	1.49
220	15.0	1.45	0.1242	-0.0719	1.49
221	16.0	1.45	0.1445	-0.0740	1.49
222	17.1	1.44	0.1671	-0.0768	1.48
223	18.1	1.47	0.1878	-0.0804	1.49
224	19.2	1.39	0.2014	-0.0930	1.49
225	20.0	1.38	0.2200	-0.0928	1.49
226	22.0	1.18	0.2505	-0.1060	1.49

Table B2. NACA 4415, Clean, Re = 1.5 million					
RUN	AOA	C_l	C_{dp}	$C_{m¼}$	Re $x10^{-6}$
227	24.0	1.14	0.3029	-0.1178	1.48
228	26.1	0.91	0.4791	-0.1588	1.47
229	28.1	0.99	0.5556	-0.1753	1.47
230	30.0	1.03	0.6184	-0.1926	1.50
231	31.7	1.14	0.7250	-0.2250	1.46
232	29.7	1.00	0.5957	-0.1827	1.44
End of Table B2					

Table B3. NACA 4415, Clean, Re = 2 million

RUN	AOA	C_l	C_{dp}	$C_{m¼}$	Re x10^{-6}
240	-19.7	-0.36	0.2403	0.0094	1.91
241	-18.0	-0.31	0.2090	0.0047	1.95
242	-15.9	-0.28	0.1823	0.0016	1.96
243	-14.0	-0.46	0.2044	0.0437	1.98
244	-11.9	-0.70	-0.0043	-0.0979	2.00
245	-9.9	-0.50	-0.0069	-0.0984	2.00
246	-8.1	-0.32	-0.0086	-0.0986	2.00
247	-6.0	-0.12	-0.0086	-0.0985	1.99
248	-4.0	0.09	-0.0073	-0.0977	1.98
249	-1.9	0.28	-0.0052	-0.0965	1.98
250	0.2	0.49	-0.0011	-0.0961	1.98
251	2.0	0.65	0.0050	-0.0931	1.97
252	4.1	0.85	0.0114	-0.0888	1.97
253	6.1	1.03	0.0207	-0.0844	1.99
254	7.9	1.18	0.0272	-0.0754	1.98
255	10.1	1.30	0.0395	-0.0626	1.98
256	11.0	1.35	0.0457	-0.0577	1.98
257	12.0	1.40	0.0542	-0.0544	1.97
258	13.1	1.42	0.0772	-0.0577	1.98
259	14.1	1.42	0.0985	-0.0602	1.99
260	15.1	1.44	0.1267	-0.0707	1.98
261	16.0	1.45	0.1514	-0.0727	1.99
262	17.0	1.46	0.1711	-0.0747	1.98
263	18.0	1.47	0.1915	-0.0782	1.98
264	19.1	1.39	0.2074	-0.0846	1.98
265	20.1	1.36	0.2259	-0.0918	1.98
266	22.2	1.37	0.2760	-0.1039	1.98

Table B3. NACA 4415, Clean, Re = 2 million					
RUN	AOA	C_l	C_{dp}	$C_{m¼}$	Re $x10^{-6}$
267	24.0	1.06	0.2943	-0.1140	1.98
268	26.1	1.02	0.3585	-0.1293	1.98
269	28.1	0.88	0.5041	-0.1563	1.99
270	30.1	0.89	0.5464	-0.1622	1.97
End of Table B3					

Table B4. NACA 4415, LEGR k/c=0.0019, Re = 1 million					
RUN	AOA	C_l	C_{dp}	$C_{m¼}$	Re x10^{-6}
280	-61.8	-0.99	1.7932	0.4227	0.67
281	-60.0	-0.99	1.7074	0.3957	0.68
282	-55.9	-0.97	1.4644	0.3295	0.71
283	-54.1	-1.01	1.4450	0.3232	0.70
284	-49.9	-1.14	1.4347	0.3376	0.72
285	-46.0	-1.09	1.2261	0.2758	0.74
286	-41.9	-0.99	1.0009	0.2079	0.76
287	-37.9	-0.93	0.8313	0.1689	0.79
288	-34.1	-0.86	0.7006	0.1361	0.81
289	-30.0	-0.70	0.5168	0.0852	0.83
290	-25.9	-0.53	0.3703	0.0427	0.86
291	-22.1	-0.45	0.2805	0.0259	0.87
292	-19.8	-0.39	0.2350	0.0166	1.01
293	-18.0	-0.33	0.1914	0.0008	1.00
294	-15.9	-0.32	0.1601	-0.0019	1.00
295	-14.0	-0.31	0.1342	-0.0002	1.01
296	-11.9	-0.44	0.1134	-0.0035	1.00
297	-10.0	-0.47	0.0063	-0.0977	1.00
298	-8.1	-0.31	-0.0005	-0.0942	1.01
299	-6.0	-0.13	-0.0035	-0.0917	1.01
300	-4.0	0.05	-0.0056	-0.0886	1.01
301	-1.9	0.24	-0.0057	-0.0858	1.00
302	0.1	0.41	-0.0025	-0.0828	1.00
303	2.0	0.61	-0.0007	-0.0786	1.01
304	4.1	0.76	0.0044	-0.0716	1.01
305	6.1	0.90	0.0149	-0.0638	1.01
306	7.9	1.03	0.0235	-0.0553	1.01

Table B4. NACA 4415, LEGR k/c=0.0019, Re = 1 million

RUN	AOA	C_l	C_{dp}	$C_{m\frac{1}{4}}$	Re x10^{-6}
307	10.0	1.11	0.0390	-0.0472	1.00
308	11.0	1.14	0.0580	-0.0529	1.00
309	12.0	1.14	0.0732	-0.0532	1.00
310	13.1	1.06	0.0891	-0.0548	1.00
311	14.1	1.05	0.1143	-0.0638	1.00
312	15.1	1.03	0.1379	-0.0706	1.00
313	16.0	1.17	0.1595	-0.0718	0.99
314	17.0	1.12	0.1801	-0.0786	0.99
315	18.0	1.12	0.2022	-0.0833	0.99
316	19.0	1.08	0.2249	-0.0897	1.00
317	20.1	1.02	0.2475	-0.0964	1.00
318	22.1	0.95	0.2977	-0.1062	0.99
319	24.0	0.93	0.3501	-0.1192	0.98
320	26.0	0.95	0.4259	-0.1416	1.00
321	28.1	1.01	0.5148	-0.1682	0.99
322	30.0	1.11	0.6266	-0.1998	1.00
323	32.1	1.18	0.7276	-0.2285	0.99
324	34.0	1.21	0.7972	-0.2406	0.98
325	36.1	1.25	0.8890	-0.2645	0.99
326	38.1	1.35	1.0358	-0.3102	0.98
327	40.0	1.33	1.0939	-0.3154	0.96
328	44.0	1.35	1.2620	-0.3482	0.94
329	48.0	1.28	1.3750	-0.3639	0.87
330	52.1	1.33	1.6677	-0.4511	0.84
331	56.0	1.24	1.7629	-0.4540	0.76
332	59.8	1.10	1.7734	-0.4433	0.73
333	64.0	1.06	2.0405	-0.5140	0.71

Table B4. NACA 4415, LEGR k/c=0.0019, Re = 1 million

RUN	AOA	C_l	C_{dp}	$C_{m1/4}$	Re x10^{-6}
334	68.1	0.96	2.2212	-0.5543	0.69
335	72.0	0.85	2.4084	-0.6069	0.68
336	76.1	0.66	2.3040	-0.5660	0.65
337	80.0	0.48	2.2756	-0.5893	0.65
338	84.1	0.36	2.5464	-0.6607	0.64
339	88.0	0.17	2.6311	-0.7143	0.64
340	92.3	-0.01	2.5010	-0.6862	0.62
341	96.1	-0.17	2.3053	-0.6641	0.63
342	100.1	-0.36	2.5181	-0.7360	0.63
343	104.2	-0.54	2.6748	-0.7695	0.63
344	108.1	-0.63	2.2847	-0.7204	0.61
345	112.0	-0.70	2.0133	-0.6691	0.62
346	116.2	-0.85	1.9573	-0.6849	0.62
347	120.1	-1.08	2.1285	-0.7624	0.62
348	124.1	-1.09	1.8139	-0.6995	0.64
349	128.1	-1.12	1.5957	-0.6655	0.66
350	131.9	-1.25	1.5222	-0.6791	0.67
351	136.1	-1.21	1.3145	-0.6380	0.68
352	139.9	-1.10	1.0548	-0.5733	0.70
353	144.0	-1.25	1.0219	-0.5912	0.75
354	148.2	-1.02	0.7121	-0.5028	0.83
355	152.0	-0.89	0.5430	-0.4434	0.86
356	155.9	-0.73	0.3831	-0.3692	1.00
357	160.0	-0.66	0.2870	-0.3328	1.00
358	164.0	-0.78	0.2284	-0.3798	1.00
359	168.1	-0.98	0.1049	-0.4940	1.00
360	172.1	-0.79	0.0408	-0.3651	0.99

Table B4. NACA 4415, LEGR k/c=0.0019, Re = 1 million

RUN	AOA	C_l	C_{dp}	$C_{m¼}$	Re $x10^{-6}$
361	176.0	-0.45	0.0202	-0.1763	1.00
362	180.1	-0.42	0.0126	-0.0687	1.00
363	184.1	0.03	0.0341	0.1459	1.00
364	188.0	0.42	0.1082	0.2852	0.99
365	192.1	0.39	0.1868	0.2488	1.00
366	195.9	0.39	0.2469	0.2670	0.99
367	200.3	0.41	0.3122	0.2968	1.00
368	203.9	0.55	0.4158	0.3545	1.00
369	208.1	0.61	0.5278	0.3916	0.98
370	212.1	0.59	0.6358	0.4431	0.95
371	216.0	0.71	0.8246	0.5104	0.92
372	219.9	0.64	0.8669	0.5026	0.79
373	224.1	0.91	1.3109	0.6291	0.68
374	228.0	0.80	1.3315	0.6177	0.64

End of Table B4

Table B5. NACA 4415, LEGR k/c=0.0019, Re = 1 million, repeated runs

RUN	AOA	C_l	C_{dp}	$C_{m¼}$	Re x10^{-6}
380	0.1	0.43	-0.0041	-0.0813	1.00
381	2.1	0.61	-0.0013	-0.0757	1.00
382	4.0	0.77	0.0014	-0.0698	1.00
383	8.1	1.03	0.0239	-0.0544	1.00
384	9.9	1.10	0.0384	-0.0471	1.00

End of Table B5

Table B6. NACA 4415, LEGR k/c=0.0019, Re = 1.5 million

RUN	AOA	C_l	C_{dp}	$C_{m¼}$	Re x10^{-6}
390	-20.0	-0.38	0.2328	0.0125	1.48
391	-18.0	-0.32	0.1924	-0.0001	1.49
392	-15.9	-0.33	0.1594	-0.0002	1.50
393	-14.0	-0.40	0.1389	-0.0025	1.50
394	-12.0	-0.48	0.1016	-0.0144	1.49
395	-9.9	-0.49	0.0035	-0.0922	1.51
396	-7.9	-0.33	-0.0011	-0.0902	1.50
397	-5.8	-0.15	-0.0036	-0.0877	1.51
398	-4.0	0.04	-0.0050	-0.0859	1.51
399	-2.0	0.23	-0.0055	-0.0834	1.51
400	0.1	0.43	-0.0044	-0.0807	1.50
401	2.1	0.62	-0.0028	-0.0759	1.50
402	4.0	0.77	0.0027	-0.0703	1.50
403	6.1	0.92	0.0114	-0.0627	1.49
404	8.1	1.05	0.0221	-0.0540	1.49
405	10.2	1.13	0.0440	-0.0511	1.49
406	10.9	1.15	0.0540	-0.0527	1.48
407	12.0	1.21	0.0791	-0.0605	1.48
408	13.0	1.07	0.0984	-0.0658	1.49
409	14.0	1.00	0.1177	-0.0670	1.48
410	15.1	1.01	0.1347	-0.0704	1.48
411	16.1	1.15	0.1619	-0.0737	1.50
412	17.1	1.13	0.1786	-0.0728	1.49
413	18.1	1.12	0.2020	-0.0812	1.49
414	18.9	1.07	0.2185	-0.0857	1.48
415	20.0	1.06	0.2413	-0.0913	1.49
416	22.0	0.97	0.3020	-0.1100	1.49

Table B6. NACA 4415, LEGR k/c=0.0019, Re = 1.5 million

RUN	AOA	C_l	C_{dp}	$C_{m¼}$	Re x10^{-6}
417	24.1	0.97	0.3734	-0.1302	1.49
418	25.9	0.96	0.4195	-0.1374	1.49
419	30.0	1.13	0.6412	-0.2075	1.49
420	32.2	1.23	0.7631	-0.2444	1.49
421	34.1	1.25	0.8423	-0.2649	1.49
422	35.9	1.27	0.8915	-0.2612	1.47
423	38.0	1.34	0.9942	-0.2843	1.45

End of Table B6

Table B7. NACA 4415, LEGR k/c=0.0019, Re = 2 million

RUN	AOA	C_l	C_{dp}	$C_{m¼}$	Re x10^{-6}
430	-19.8	-0.40	0.2376	0.0161	1.99
431	-18.0	-0.32	0.1929	-0.0035	2.00
432	-16.1	-0.34	0.1685	0.0032	1.99
433	-13.8	-0.38	0.1385	-0.0063	2.00
434	-12.0	-0.51	0.0884	-0.0290	2.00
435	-10.0	-0.51	0.0056	-0.0913	2.00
436	-7.9	-0.35	-0.0010	-0.0893	2.00
437	-5.8	-0.16	-0.0032	-0.0885	1.99
438	-4.0	0.02	-0.0041	-0.0874	1.99
439	-2.0	0.22	-0.0042	-0.0849	2.00
440	0.1	0.42	-0.0036	-0.0814	2.00
441	2.1	0.61	-0.0025	-0.0762	1.99
442	4.0	0.78	0.0023	-0.0705	1.99
443	6.0	0.93	0.0112	-0.0646	1.99
444	8.1	1.07	0.0190	-0.0547	1.98
445	10.1	1.15	0.0436	-0.0529	1.98
446	10.9	1.17	0.0604	-0.0587	1.98
447	11.9	1.20	0.0828	-0.0640	1.98
448	12.9	1.20	0.1053	-0.0659	1.98
449	14.1	1.21	0.1244	-0.0671	1.98
450	15.0	1.18	0.1424	-0.0655	1.98
451	15.9	1.16	0.1583	-0.0710	1.98
452	17.1	1.18	0.1856	-0.0801	1.98
453	18.0	1.13	0.2009	-0.0818	1.98
454	19.0	1.09	0.2172	-0.0830	1.98
455	20.0	1.04	0.2432	-0.0923	1.98
456	22.0	0.97	0.3005	-0.1088	1.97

Table B7. NACA 4415, LEGR k/c=0.0019, Re = 2 million

RUN	AOA	C_l	C_{dp}	$C_{m¼}$	Re x10^{-6}
457	24.1	0.96	0.3630	-0.1233	1.99
458	26.0	0.98	0.4367	-0.1483	1.99
459	28.0	0.98	0.5049	-0.1598	1.98
460	29.9	1.11	0.6299	-0.2027	1.99

End of Table B7

Table B8. NACA 4415, LEGR k/c=0.0019, VGs, Re = 1 million

RUN	AOA	C_l	C_{dp}	$C_{m1/4}$	Re x10^{-6}
470	-19.8	-0.40	0.2338	0.0153	1.00
471	-18.0	-0.36	0.2006	0.0052	1.00
472	-16.0	-0.34	0.1634	-0.0025	1.00
473	-13.9	-0.39	0.1429	0.0069	1.00
474	-12.1	-0.50	0.1069	-0.0101	1.01
475	-10.0	-0.50	0.0078	-0.0910	1.00
476	-7.9	-0.34	0.0001	-0.0926	1.00
477	-5.8	-0.14	-0.0024	-0.0918	1.00
478	-4.1	0.04	-0.0037	-0.0926	1.00
479	-2.0	0.25	-0.0042	-0.0910	1.00
480	0.1	0.46	-0.0035	-0.0914	1.00
481	2.1	0.67	-0.0008	-0.0894	1.00
482	3.9	0.85	0.0038	-0.0900	1.00
483	6.0	1.06	0.0120	-0.0885	1.00
484	8.1	1.23	0.0258	-0.0872	1.00
485	10.1	1.42	0.0373	-0.0856	1.00
486	11.2	1.48	0.0477	-0.0818	0.99
487	11.9	1.53	0.0525	-0.0789	1.00
488	13.0	1.24	0.1127	-0.0925	0.99
489	14.0	1.20	0.1348	-0.0833	1.00
490	15.0	1.26	0.1513	-0.0790	0.99
491	16.1	1.21	0.1675	-0.0755	0.99
492	17.1	1.18	0.1886	-0.0805	0.98
493	18.1	1.10	0.2025	-0.0798	1.00
494	18.9	1.07	0.2171	-0.0838	1.00
495	20.0	1.02	0.2474	-0.0946	0.98
496	22.0	0.94	0.3056	-0.1102	0.99

Table B8. NACA 4415, LEGR k/c=0.0019, VGs, Re = 1 million

RUN	AOA	C_l	C_{dp}	$C_{m¼}$	Re $x10^{-6}$
497	24.1	0.95	0.3632	-0.1250	0.98
498	26.2	0.98	0.4393	-0.1458	1.00
499	28.0	1.03	0.5236	-0.1708	1.00
500	30.0	1.09	0.6138	-0.1933	0.99
501	32.0	1.15	0.7147	-0.2236	1.00
502	34.1	1.25	0.8272	-0.2527	1.00
503	36.1	1.25	0.8954	-0.2637	1.00
504	37.9	1.30	0.9902	-0.2875	0.99
505	40.1	1.38	1.1250	-0.3265	0.97

End of Table B8

Table B9. NACA 4415, LEGR k/c=0.0019, VGs, Re = 1.5 million

RUN	AOA	C_l	C_{dp}	$C_{m¼}$	Re x10^{-6}
510	-19.9	-0.39	0.2360	0.0100	1.50
511	-18.0	-0.38	0.2108	0.0127	1.50
512	-16.0	-0.38	0.1766	0.0081	1.49
513	-13.9	-0.48	0.1443	0.0058	1.50
514	-12.0	-0.49	0.1024	-0.0170	1.49
515	-10.0	-0.50	0.0078	-0.0910	1.49
516	-7.9	-0.35	0.0009	-0.0913	1.50
517	-5.8	-0.16	-0.0021	-0.0910	1.50
518	-3.8	0.04	-0.0041	-0.0917	1.50
519	-2.0	0.25	-0.0043	-0.0926	1.49
520	0.1	0.45	-0.0027	-0.0920	1.50
521	2.2	0.67	-0.0011	-0.0910	1.50
522	4.0	0.87	0.0037	-0.0908	1.50
523	6.0	1.04	0.0151	-0.0897	1.49
524	8.1	1.24	0.0239	-0.0864	1.49
525	10.2	1.43	0.0398	-0.0853	1.48
526	10.9	1.47	0.0474	-0.0834	1.49
527	11.9	1.54	0.0558	-0.0811	1.49
528	13.3	1.19	0.1091	-0.0807	1.48
529	14.0	1.28	0.1290	-0.0803	1.49
530	15.0	1.26	0.1494	-0.0777	1.48
531	16.1	1.23	0.1690	-0.0766	1.49
532	17.1	1.18	0.1877	-0.0780	1.48
533	17.9	1.15	0.2015	-0.0790	1.48
534	19.0	1.11	0.2220	-0.0846	1.49
535	20.0	1.05	0.2448	-0.0925	1.49
536	22.0	0.96	0.3014	-0.1098	1.49

Table B9. NACA 4415, LEGR k/c=0.0019, VGs, Re = 1.5 million

RUN	AOA	C_l	C_{dp}	$C_{m¼}$	Re $x10^{-6}$
537	24.1	0.97	0.3733	-0.1294	1.50
538	26.2	0.92	0.4145	-0.1330	1.49
539	28.0	1.01	0.5205	-0.1675	1.50
540	30.3	1.14	0.6523	-0.2102	1.48
541	31.9	1.29	0.7868	-0.2522	1.47
542	34.0	1.31	0.8559	-0.2624	1.44

End of Table B9

Table B10. NACA 4415, Clean, VGs, Re = 1 million

RUN	AOA	C_l	C_{dp}	$C_{m¼}$	Re x10^{-6}
550	-19.8	-0.37	0.2488	0.0132	1.00
551	-18.0	-0.29	0.2027	-0.0020	1.01
552	-15.9	-0.49	0.2320	0.0345	1.01
553	-13.9	-0.49	0.2083	0.0467	1.01
554	-12.1	-0.19	0.1309	-0.0094	1.01
555	-9.9	-0.57	-0.0058	-0.0900	0.99
556	-7.9	-0.38	-0.0088	-0.0908	0.99
557	-5.8	-0.18	-0.0066	-0.0906	0.99
558	-4.1	0.03	-0.0058	-0.0916	1.00
559	-2.0	0.24	-0.0042	-0.0917	1.01
560	0.1	0.47	-0.0009	-0.0948	1.00
561	2.1	0.69	0.0027	-0.0960	1.00
562	4.0	0.89	0.0091	-0.0983	1.00
563	6.0	1.09	0.0203	-0.1011	1.00
564	8.1	1.27	0.0280	-0.0963	1.00
565	9.9	1.45	0.0378	-0.0926	1.00
566	11.1	1.53	0.0476	-0.0900	1.00
567	12.0	1.61	0.0515	-0.0871	1.00
568	13.0	1.68	0.0621	-0.0879	1.00
569	14.1	1.75	0.0726	-0.0863	1.00
570	15.1	1.83	0.0840	-0.0850	1.00
571	16.0	1.66	0.1424	-0.0912	0.99
572	17.1	1.54	0.1764	-0.0833	0.98
573	18.1	1.53	0.1930	-0.0818	1.00
574	18.9	1.50	0.2024	-0.0825	1.00
575	20.0	0.84	0.3357	-0.1318	0.99
576	22.1	0.79	0.3646	-0.1292	1.00

Table B10. NACA 4415, Clean, VGs, Re = 1 million

RUN	AOA	C_l	C_{dp}	$C_{m¼}$	Re x10^{-6}
577	24.1	0.85	0.4184	-0.1410	0.99
578	26.2	0.87	0.4620	-0.1477	0.98
579	28.3	0.96	0.5444	-0.1683	1.00
580	30.2	1.15	0.6992	-0.2248	0.99
581	32.1	1.21	0.7818	-0.2426	0.99
582	34.0	1.27	0.8679	-0.2615	0.98
583	36.0	1.32	0.9726	-0.2923	0.98
584	38.0	1.29	1.0186	-0.2950	0.99
585	40.1	1.31	1.1088	-0.3141	1.01

End of Table B10

Table B11. NACA 4415, Clean, VGs, Re = 1.5 million

RUN	AOA	C_l	C_{dp}	$C_{m\frac{1}{4}}$	Re $x10^{-6}$
590	-20.1	-0.40	0.2616	0.0187	1.49
591	-17.9	-0.36	0.2231	0.0068	1.50
592	-16.0	-0.26	0.1800	-0.0072	1.49
593	-13.9	-0.24	0.1567	-0.0047	1.50
594	-12.1	-0.55	0.1713	0.0279	1.50
595	-10.0	-0.56	-0.0051	-0.0892	1.49
596	-7.9	-0.38	-0.0066	-0.0904	1.49
597	-5.8	-0.18	-0.0071	-0.0907	1.49
598	-4.1	0.03	-0.0051	-0.0933	1.50
599	-2.0	0.25	-0.0034	-0.0945	1.50
600	0.1	0.47	0.0001	-0.0963	1.49
601	2.1	0.70	0.0020	-0.0980	1.49
602	4.0	0.91	0.0080	-0.0987	1.49
603	6.0	1.13	0.0129	-0.0999	1.49
604	8.1	1.29	0.0287	-0.0983	1.49
605	10.2	1.48	0.0393	-0.0932	1.49
606	10.9	1.54	0.0426	-0.0915	1.49
607	12.1	1.63	0.0527	-0.0897	1.49
608	13.0	1.70	0.0614	-0.0891	1.48
609	14.0	1.79	0.0726	-0.0876	1.50
610	15.1	1.87	0.0853	-0.0869	1.49
611	16.1	1.70	0.1435	-0.0962	1.48
612	17.1	1.53	0.1702	-0.0792	1.50
613	17.9	1.51	0.1812	-0.0783	1.49
614	19.1	1.49	0.2078	-0.0911	1.48
615	20.0	1.48	0.2353	-0.0989	1.49
616	22.1	1.39	0.2795	-0.1142	1.48

Table B11. NACA 4415, Clean, VGs, Re = 1.5 million

RUN	AOA	C_l	C_{dp}	$C_{m¼}$	Re x10^{-6}
617	24.2	1.05	0.2830	-0.1058	1.50
618	26.1	0.90	0.4752	-0.1549	1.49
619	28.0	0.89	0.5040	-0.1553	1.48
620	30.0	0.97	0.5849	-0.1745	1.48
621	32.1	1.19	0.7734	-0.2418	1.49

End of Table B11

Steady-State Pressure Distributions

Re = 1.0 million

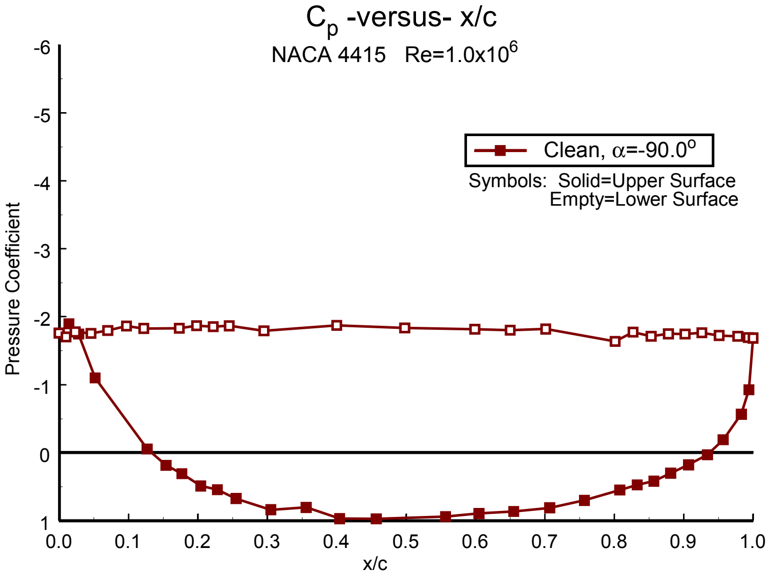

Figure B1. α= -90°

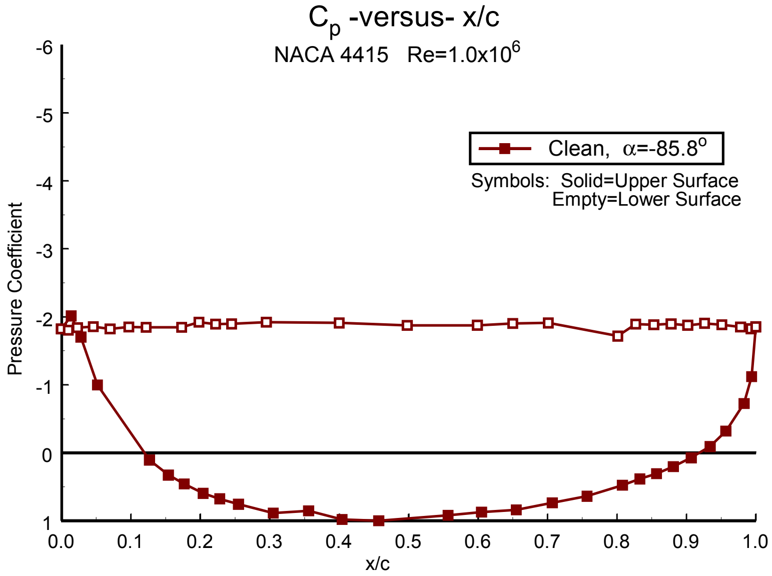

Figure B2. α= -86°

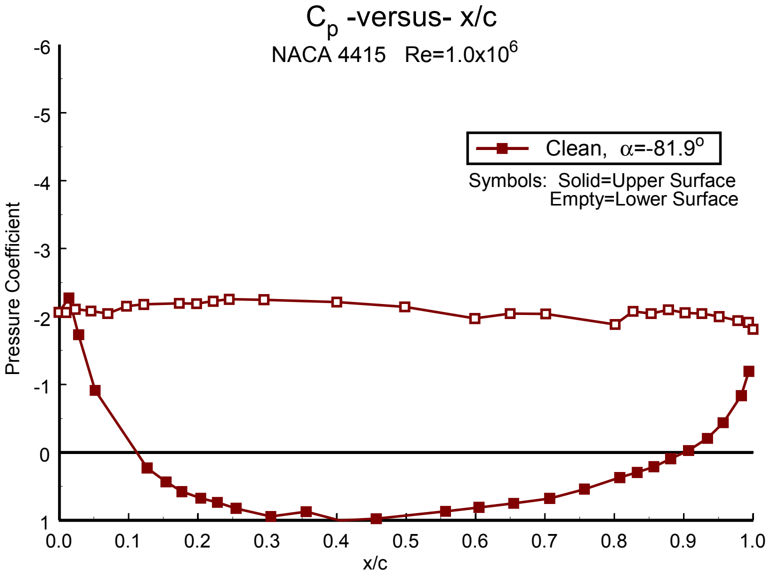

Figure B3. α= -82°

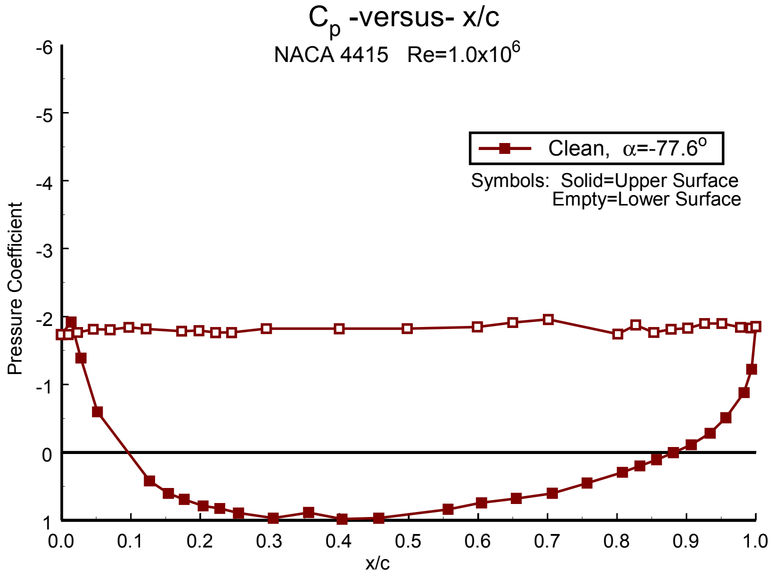

Figure B4. α= -78°

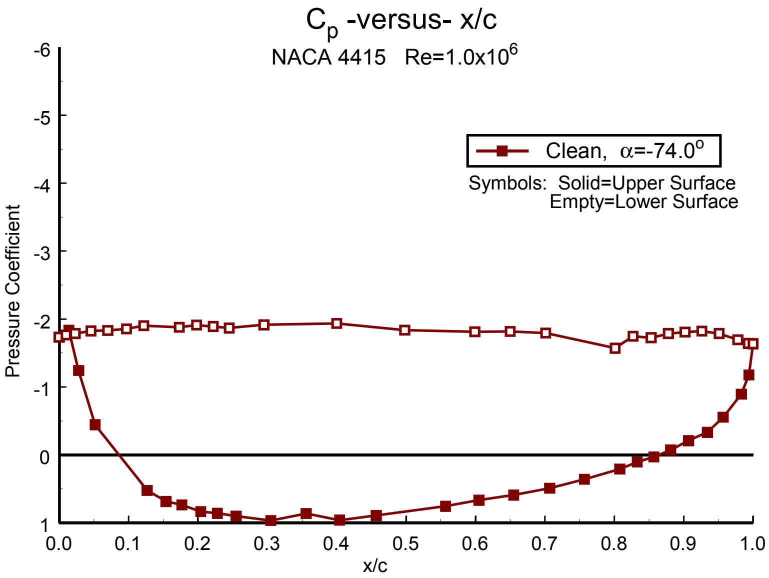

Figure B5. □□ -74°

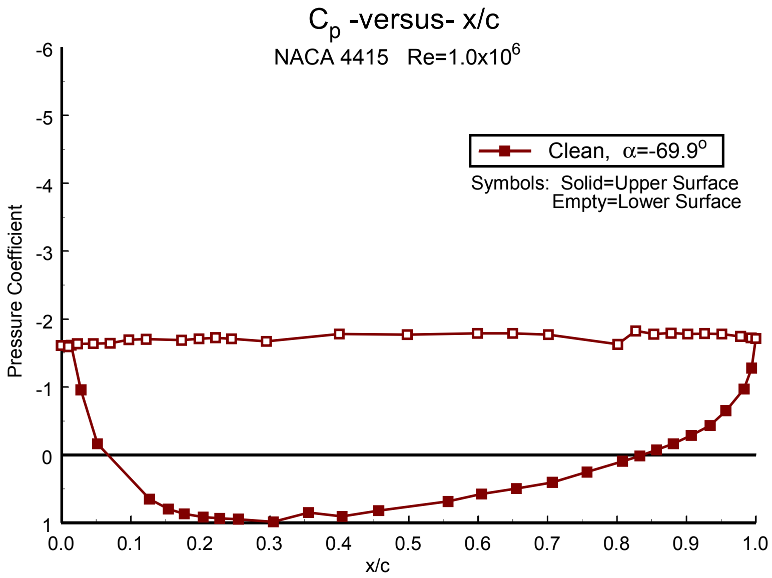

Figure B6. □□ -70°

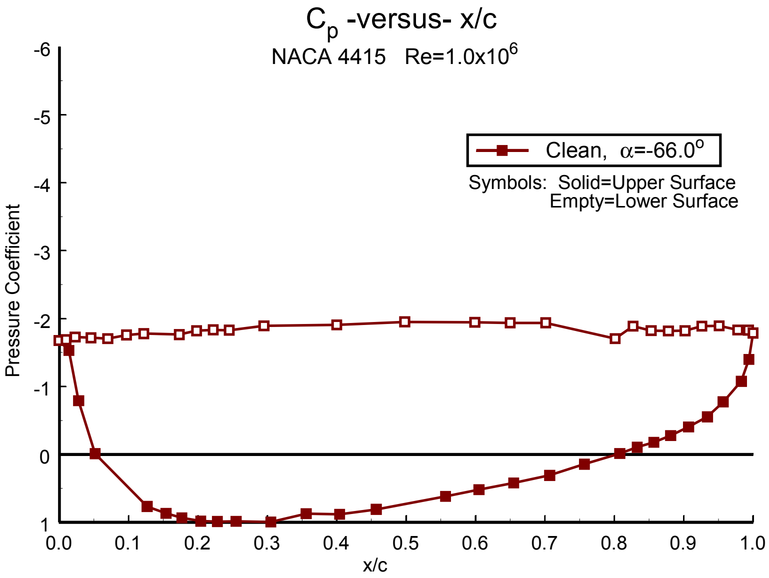

Figure B7. □□ -66°

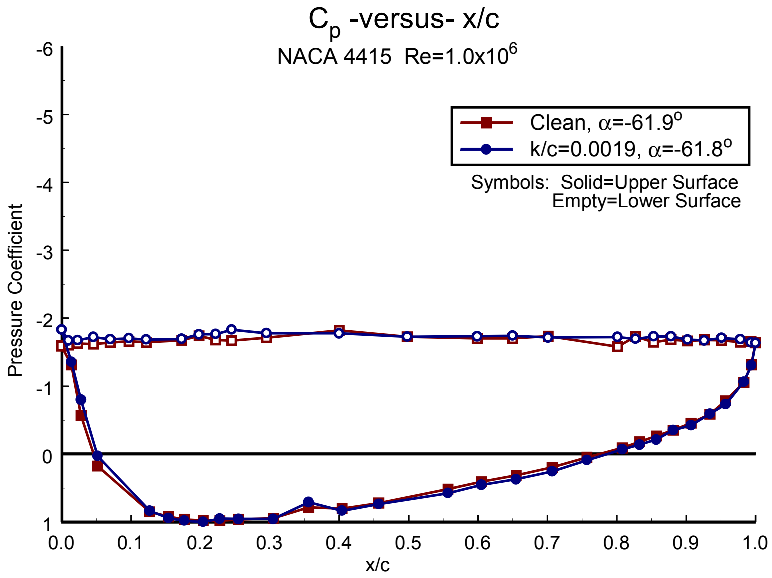

Figure B8. □□ -62°

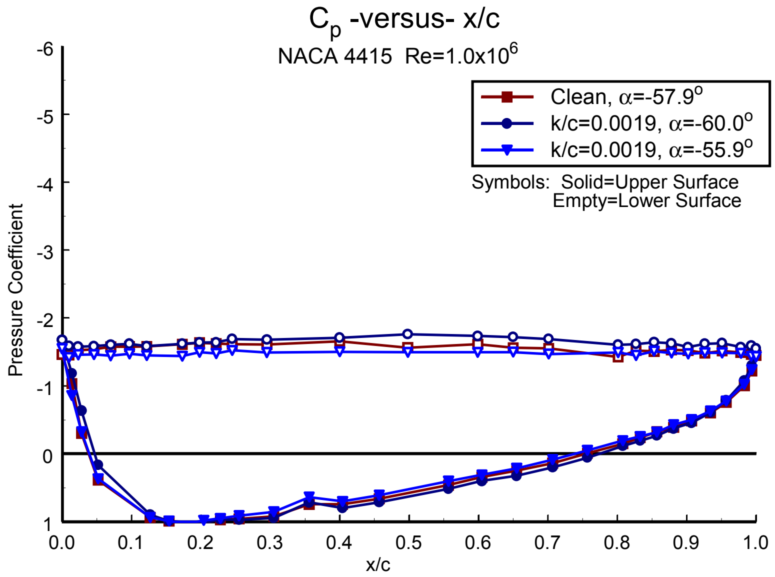

Figure B9. □□= -58°

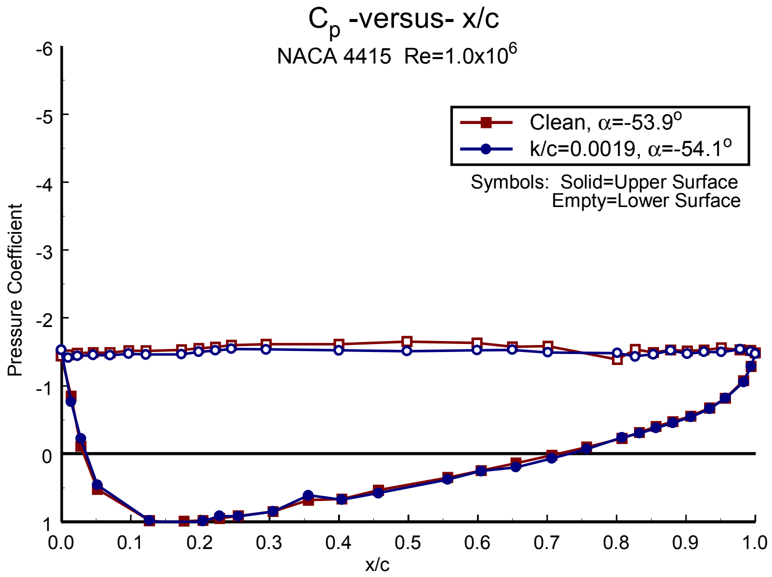

Figure B10. □□= -54°

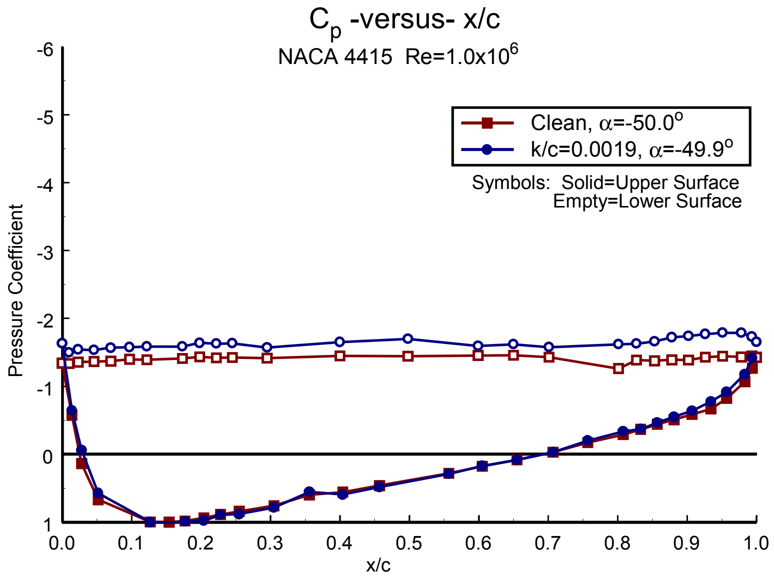

Figure B11. □□= -50°

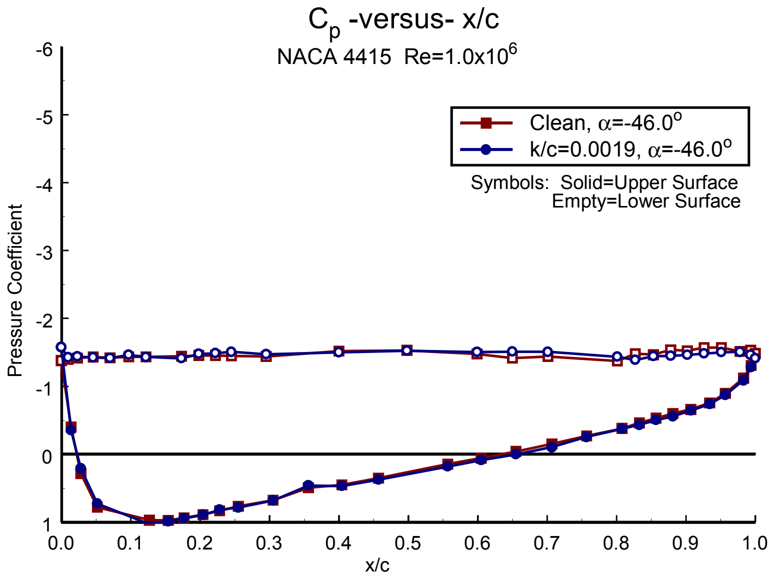

Figure B12. □□= -46°

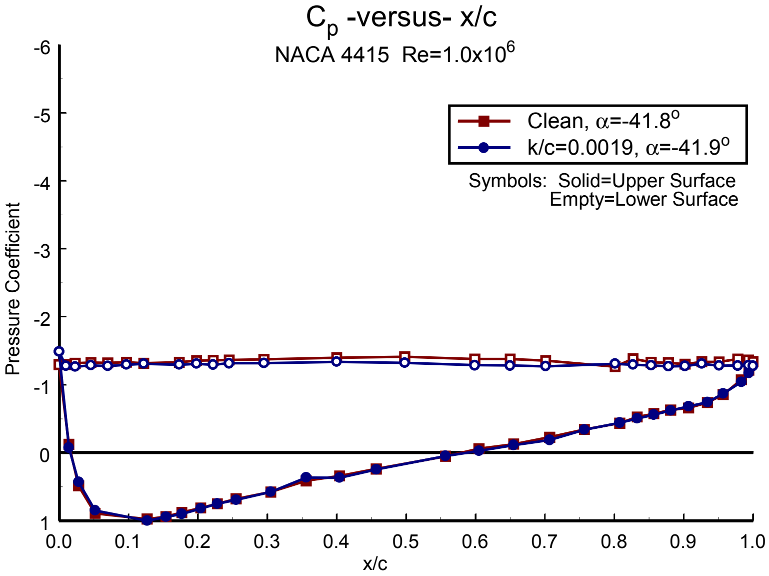

Figure B13. α = -42°

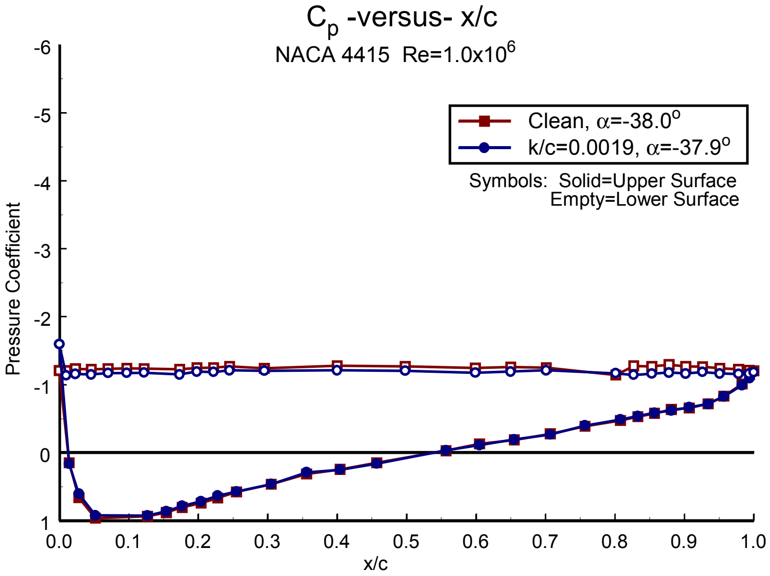

Figure B14. α = -38°

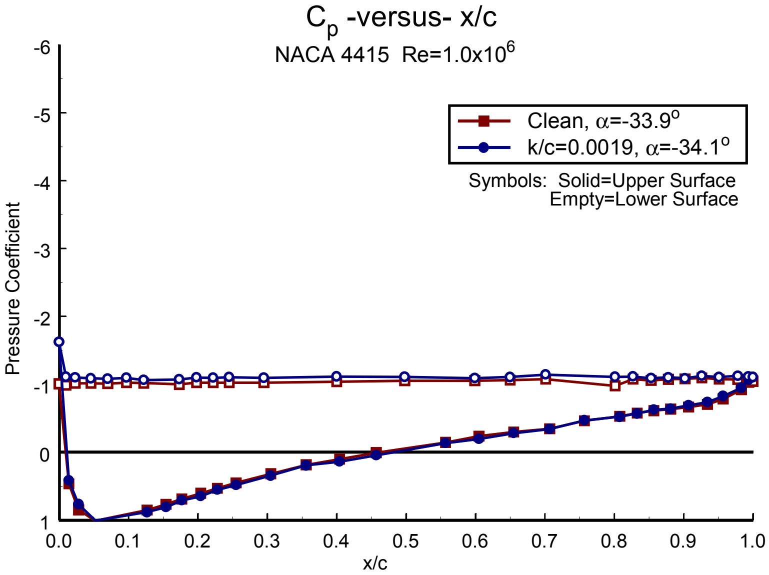

Figure B15. α = -34°

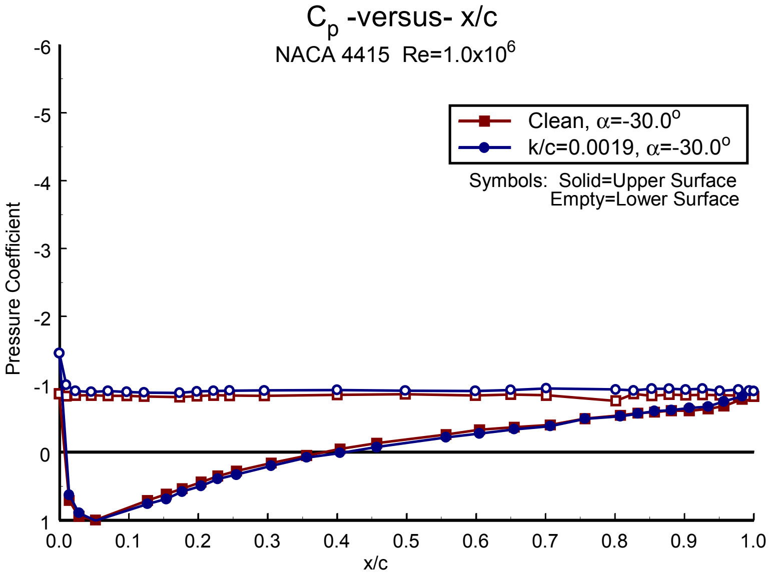

Figure B16. α = -30°

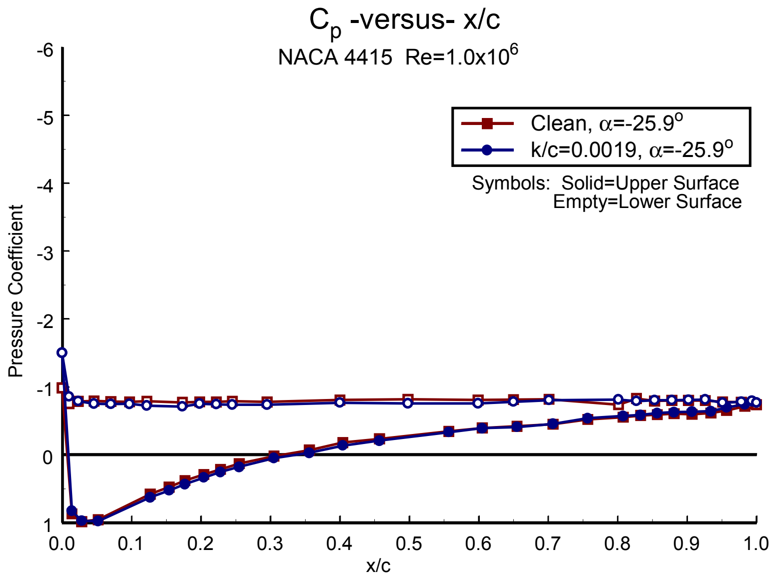

Figure B17. □= -26°

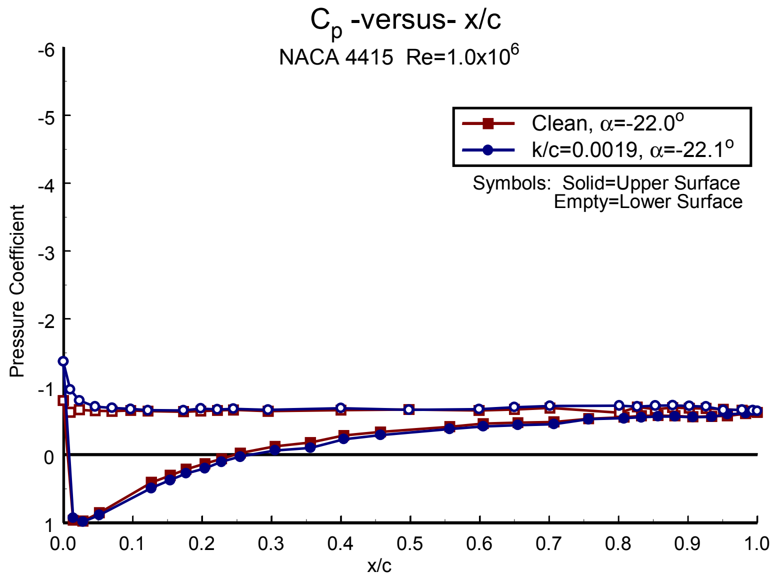

Figure B18. □= -22°

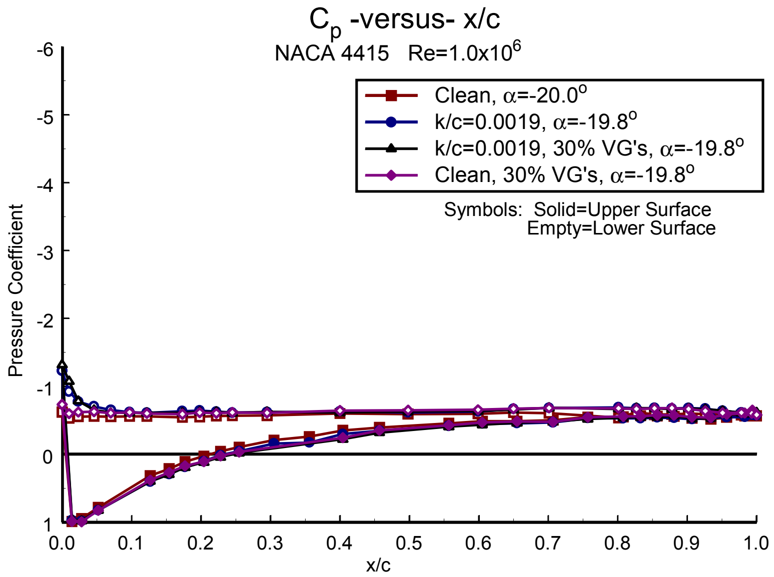

Figure B19. □= -20°

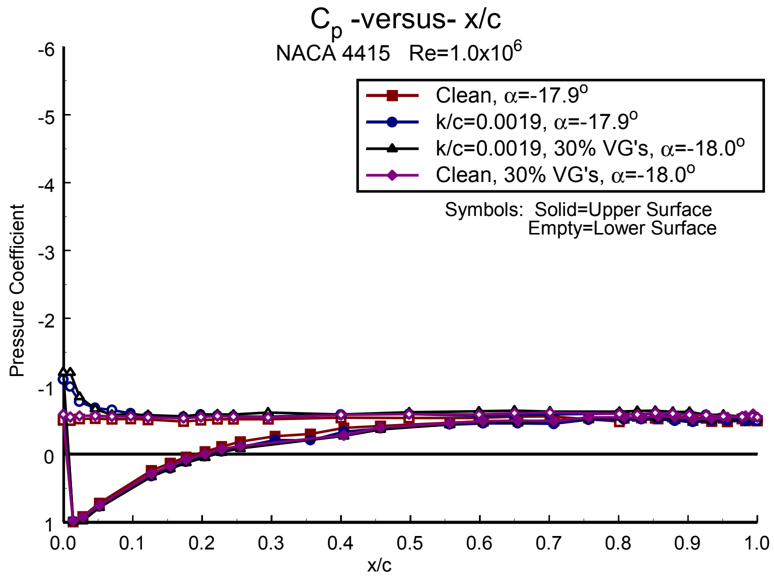

Figure B20. □= -18°

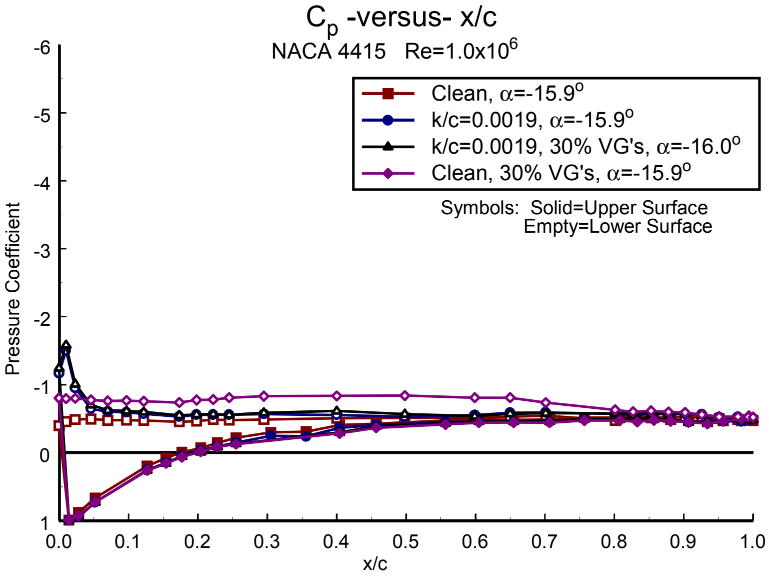

Figure B21. □= -16°

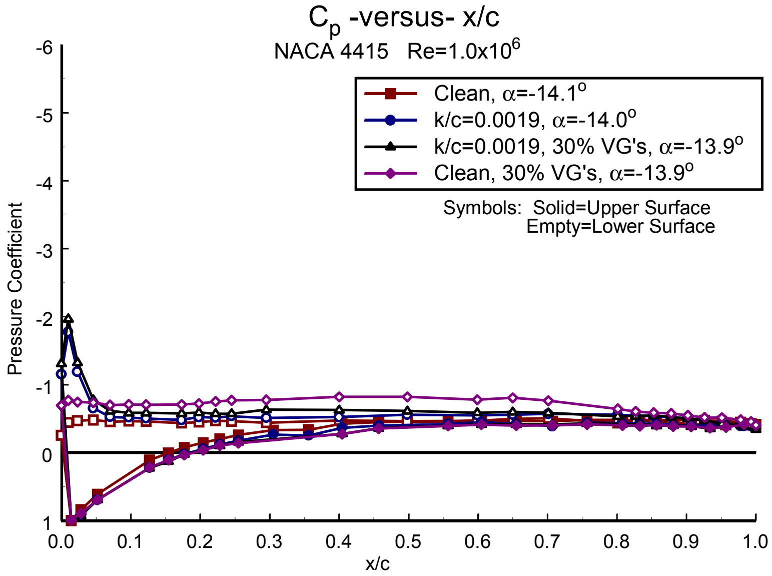

Figure B22. □= -14°

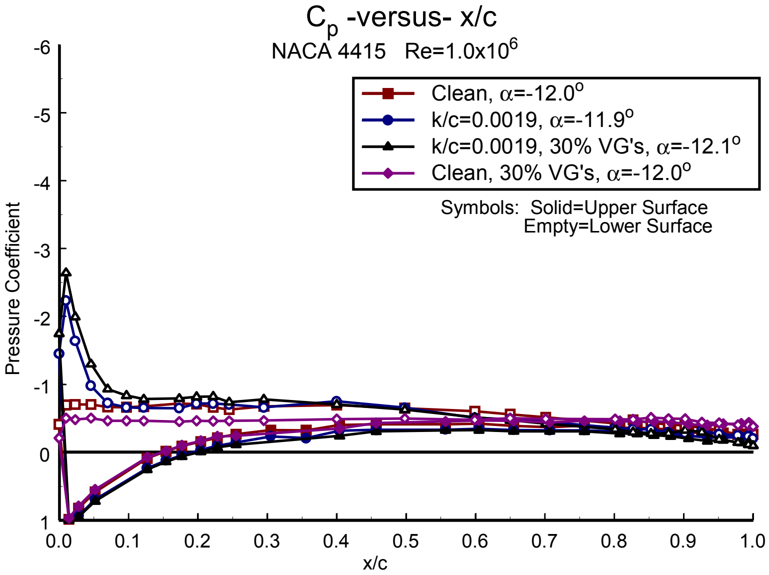

Figure B23. □= -12°

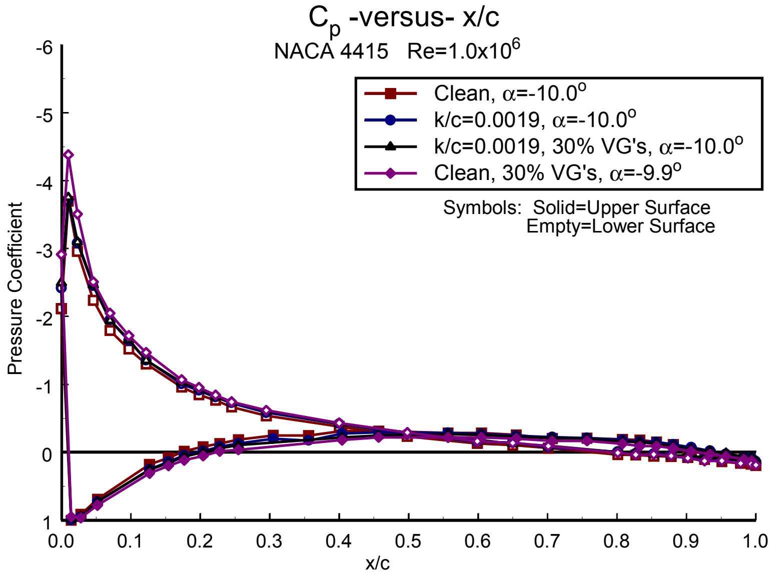

Figure B24. □= -10°

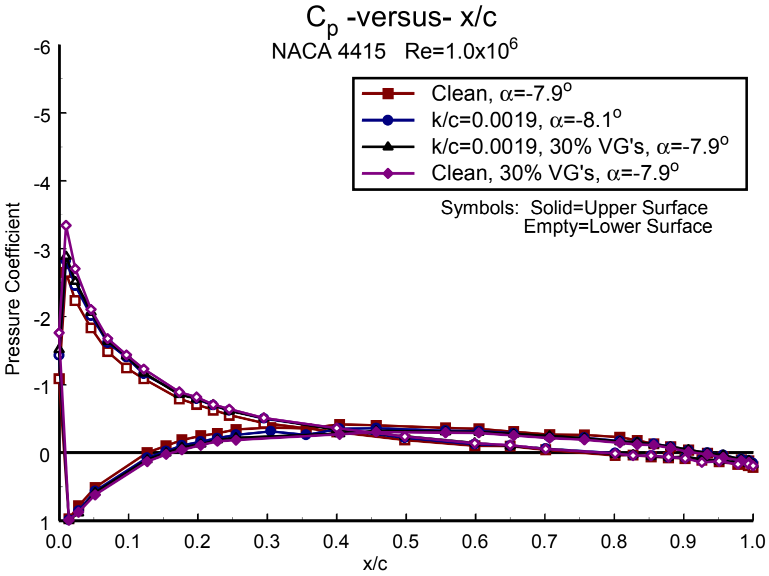

Figure B25. α= -8°

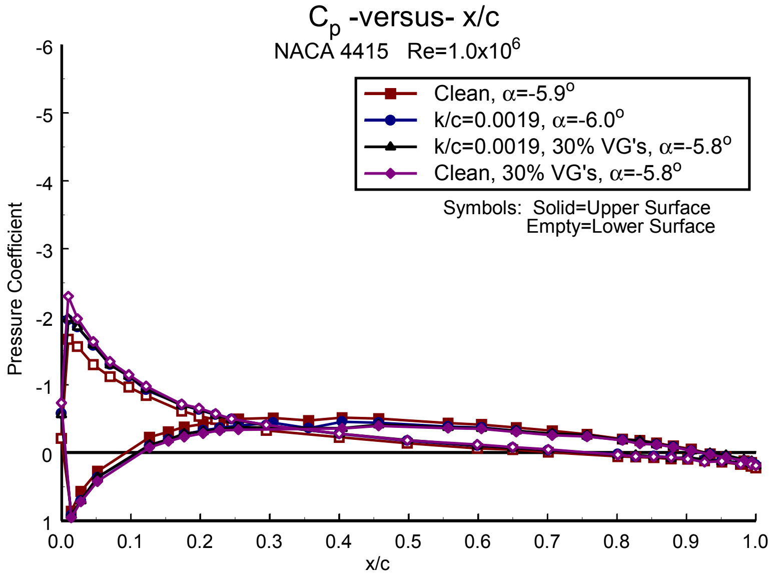

Figure B26. α= -6°

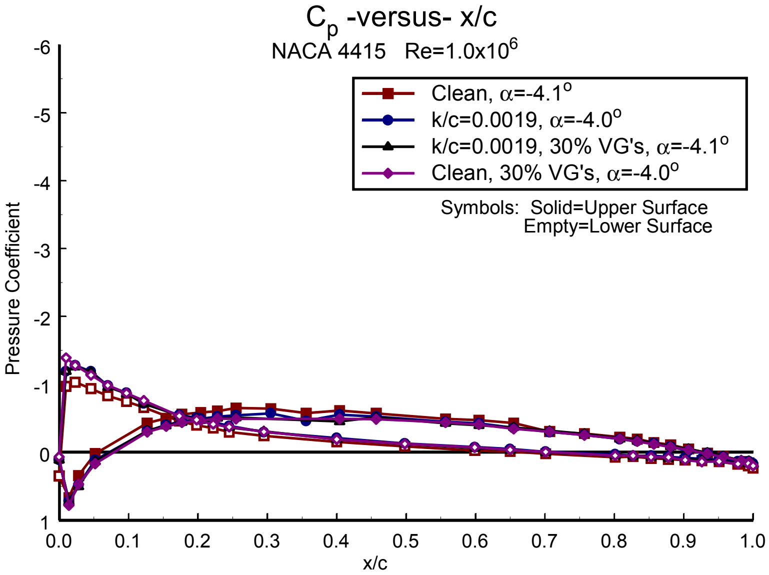

Figure B27. α= -4°

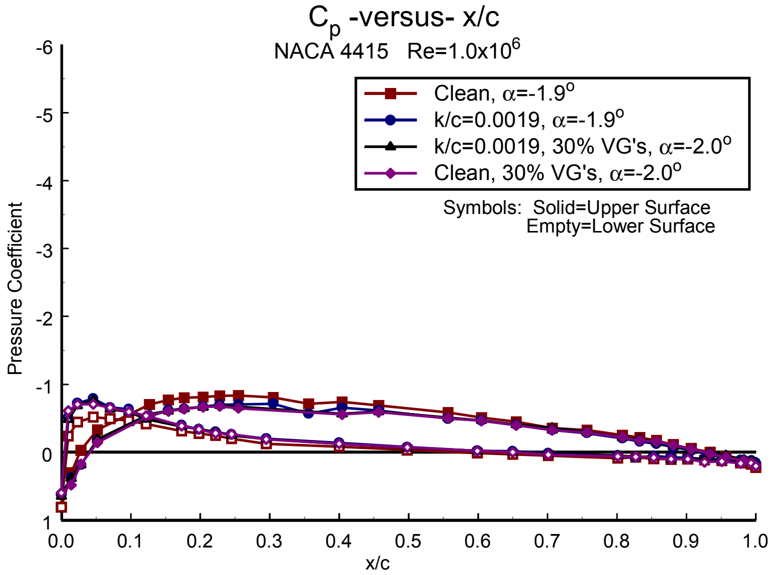

Figure B28. α= -2°

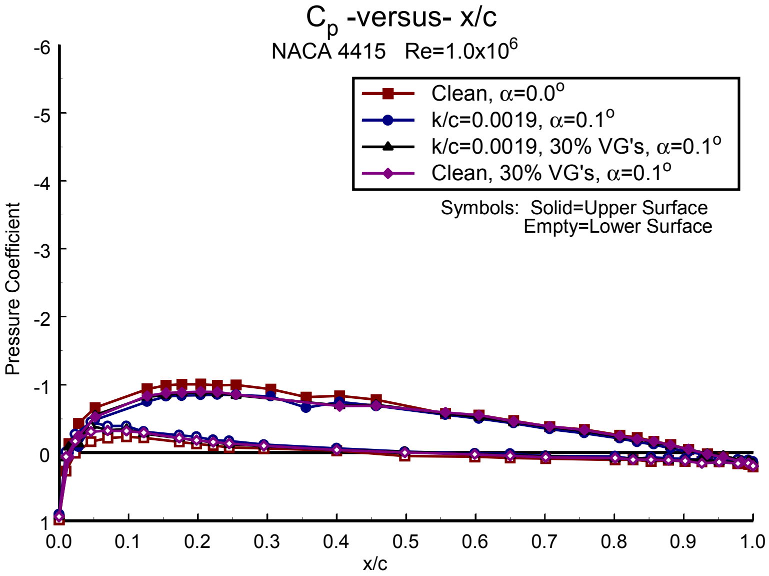

Figure B29. α = 0°

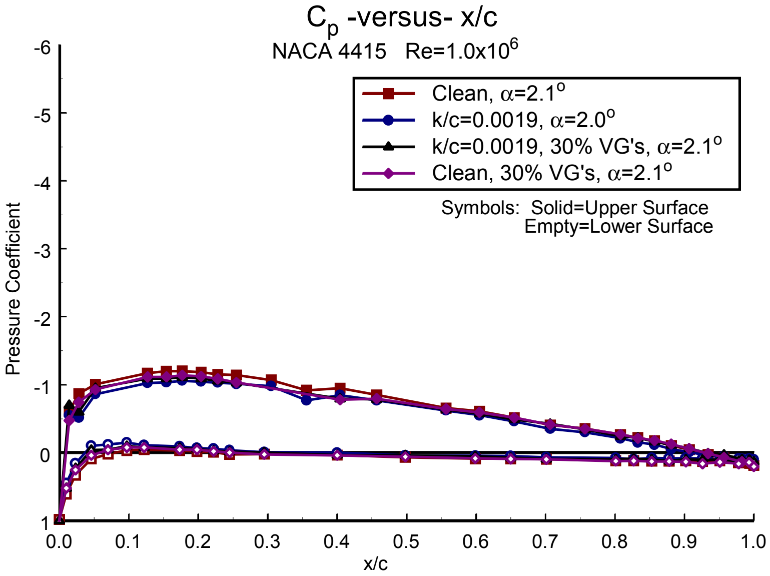

Figure B30. α = 2°

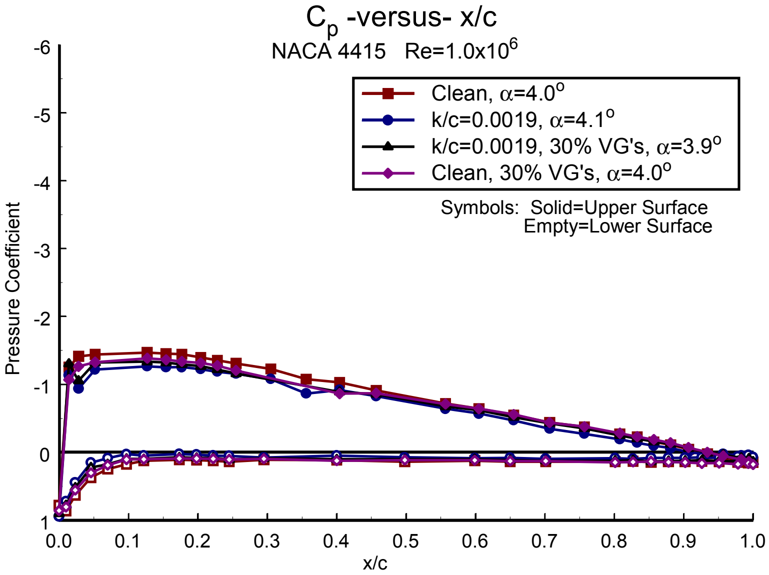

Figure B31. α = 4°

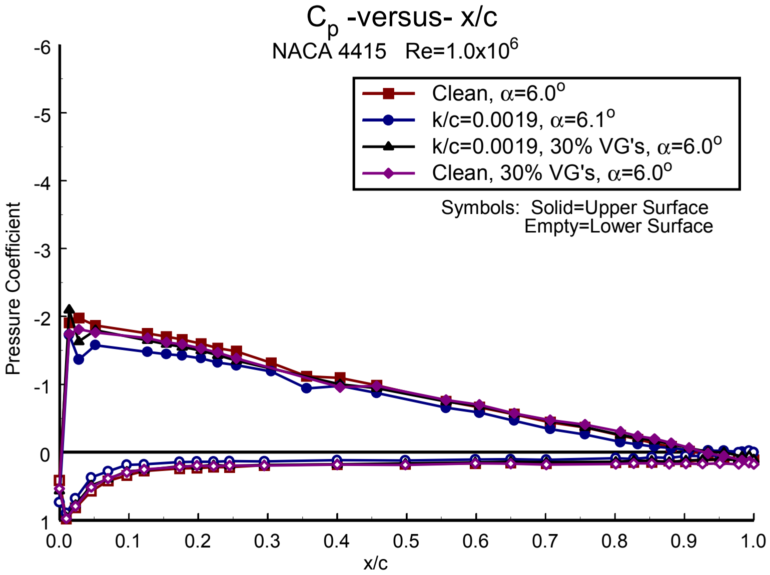

Figure B32. α = 6°

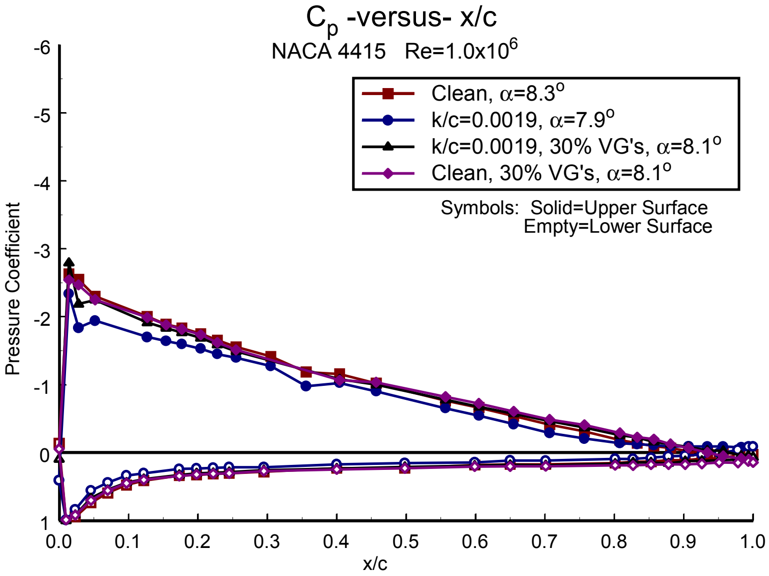

Figure B33. α = 8°

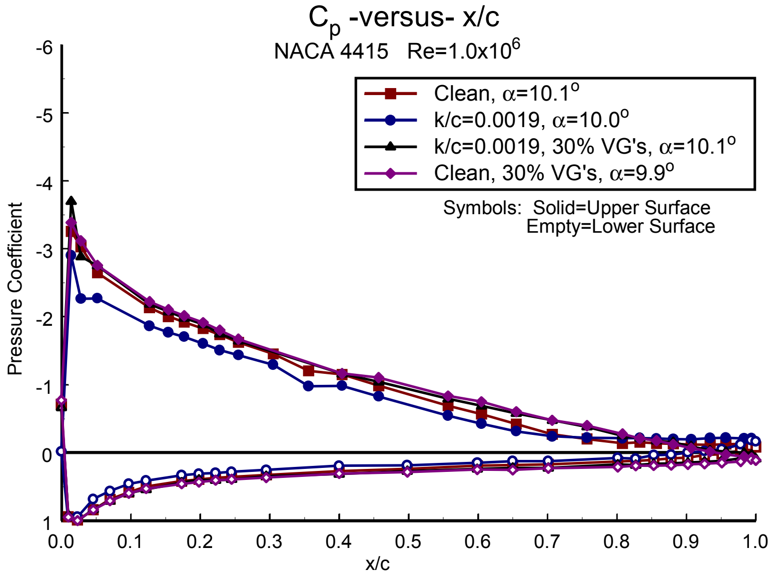

Figure B34. α = 10°

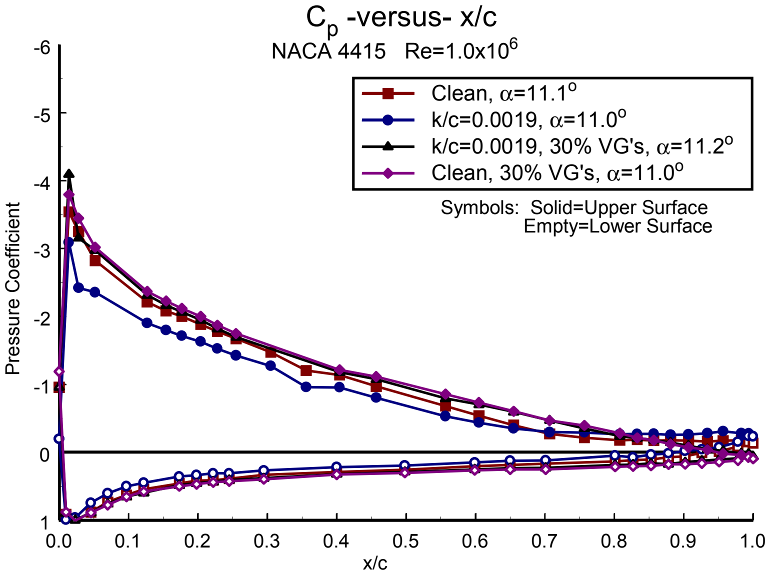

Figure B35. α = 11°

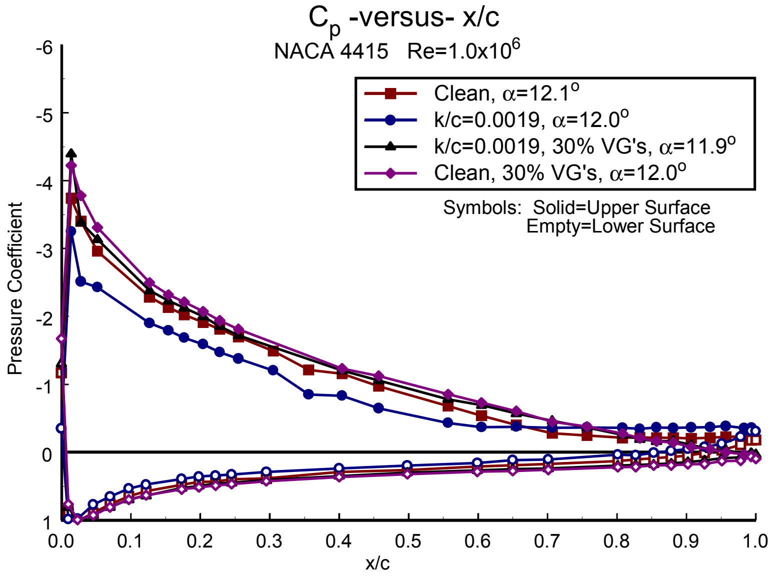

Figure B36. α = 12°

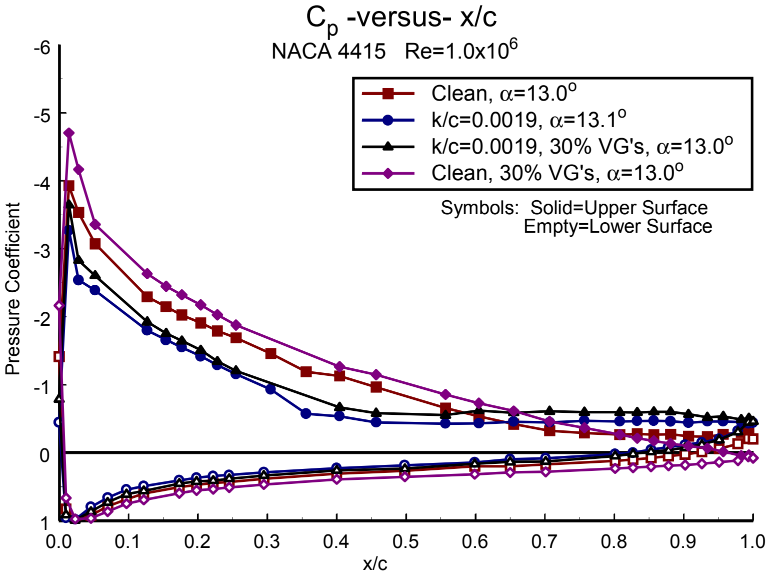

Figure B37. α = 13°

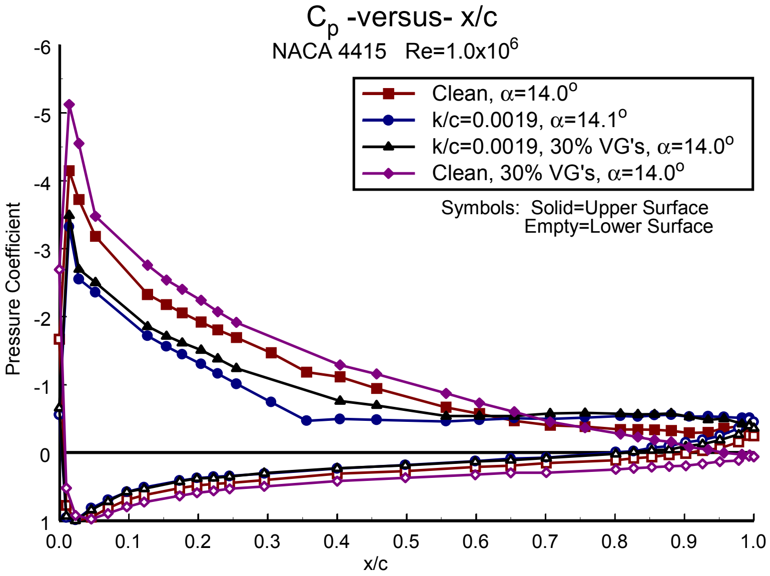

Figure B38. α = 14°

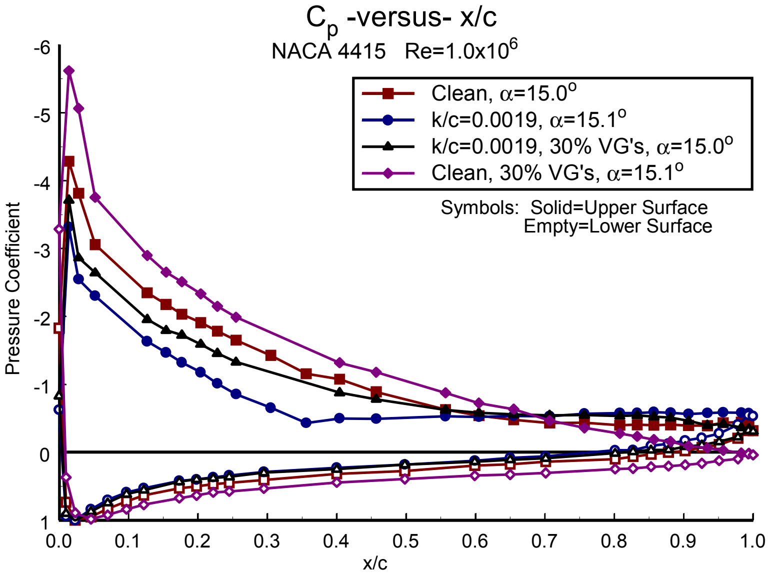

Figure B39. α = 15°

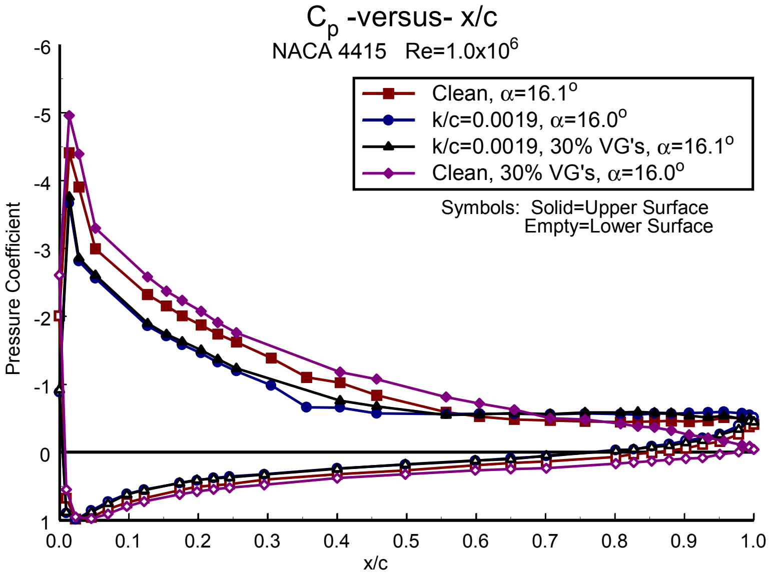

Figure B40. α = 16°

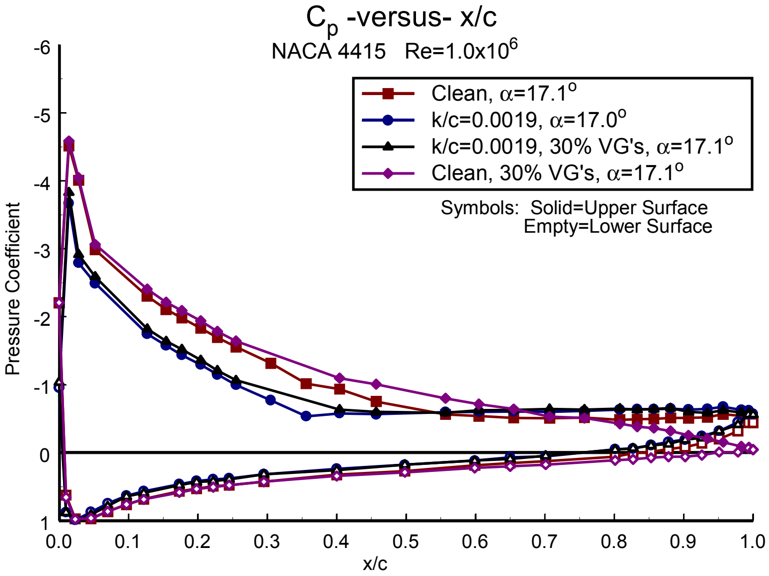

Figure B41. □⊟ 17°

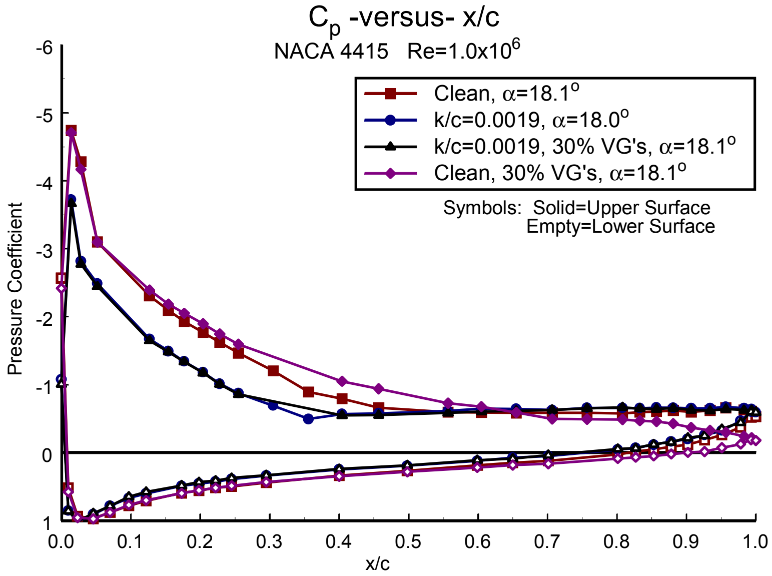

Figure B42. □⊟ 18°

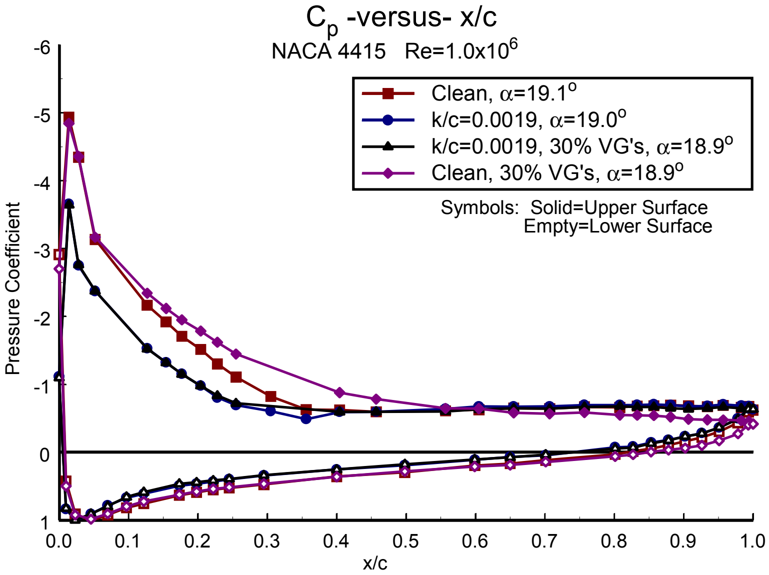

Figure B43. □⊟ 19°

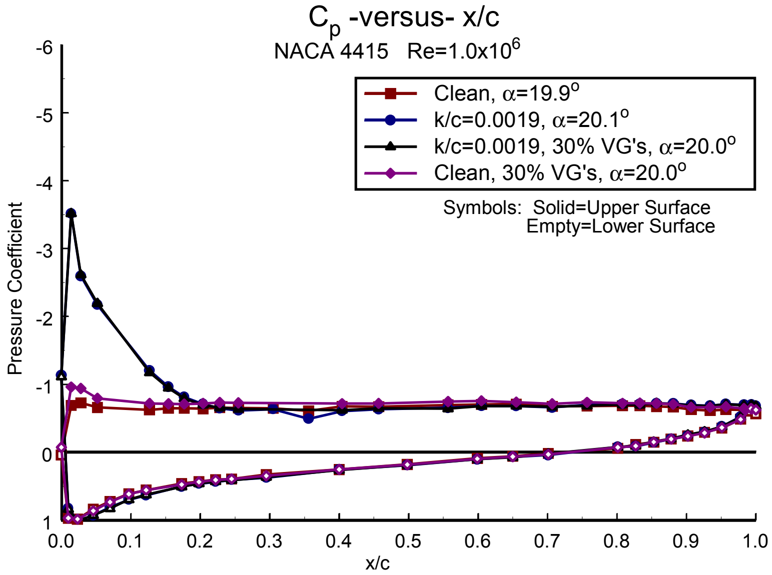

Figure B44. □⊟ 20°

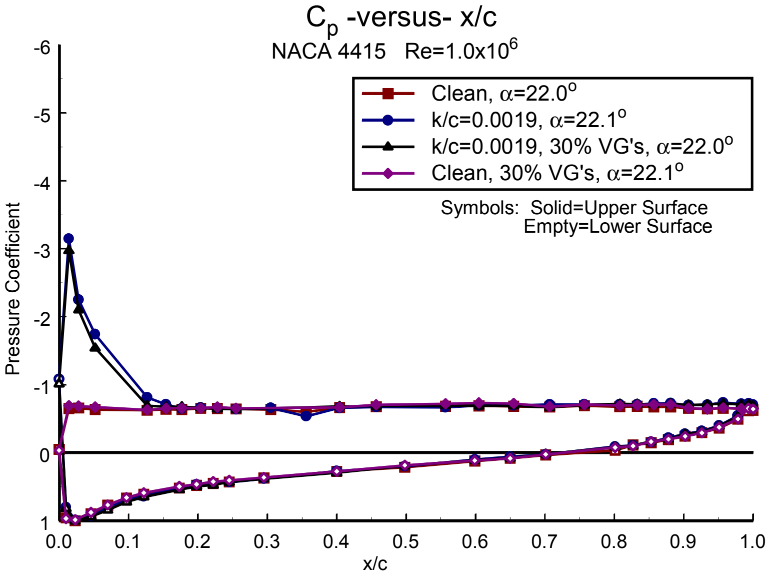

Figure B45. □□= 22°

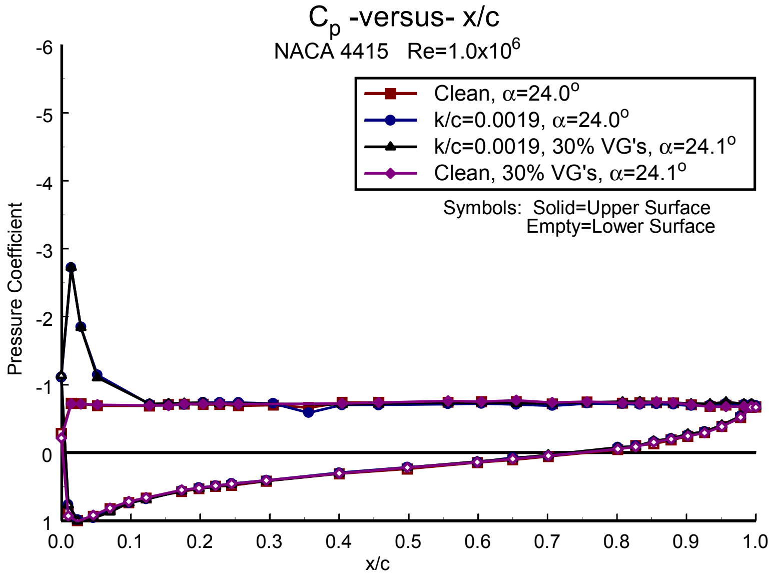

Figure B46. □□= 24°

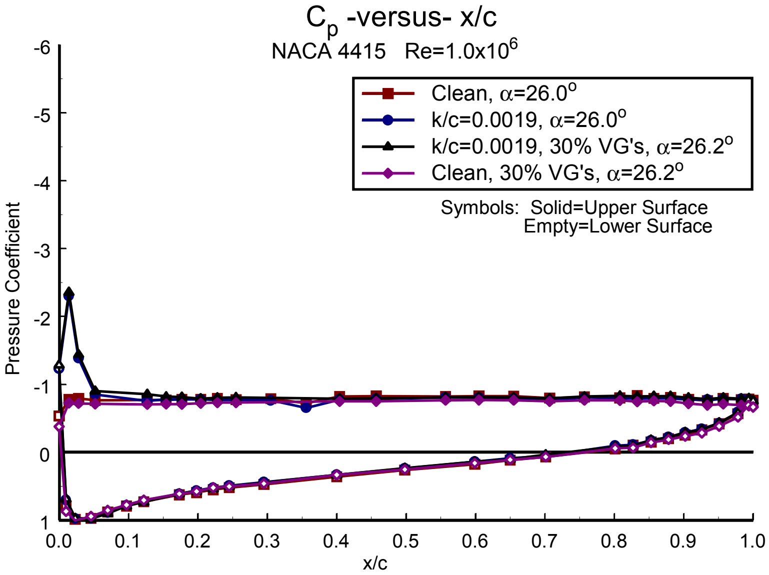

Figure B47. □□= 26°

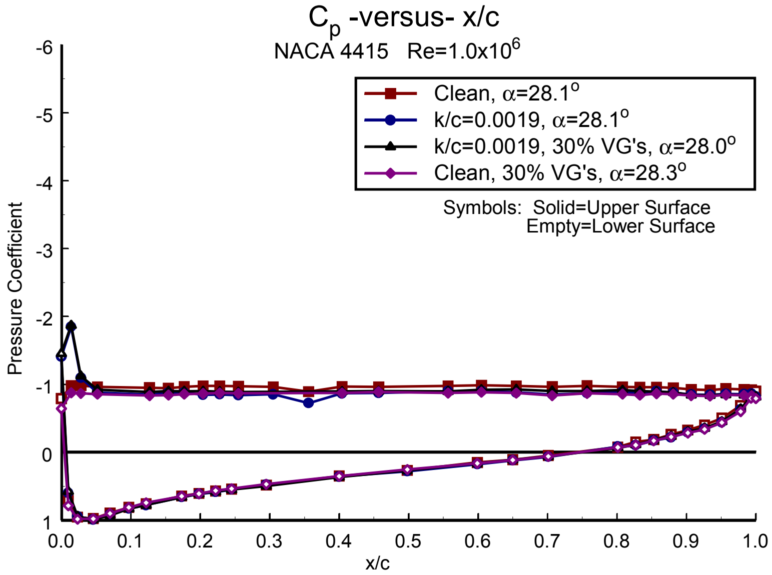

Figure B48. □□= 28°

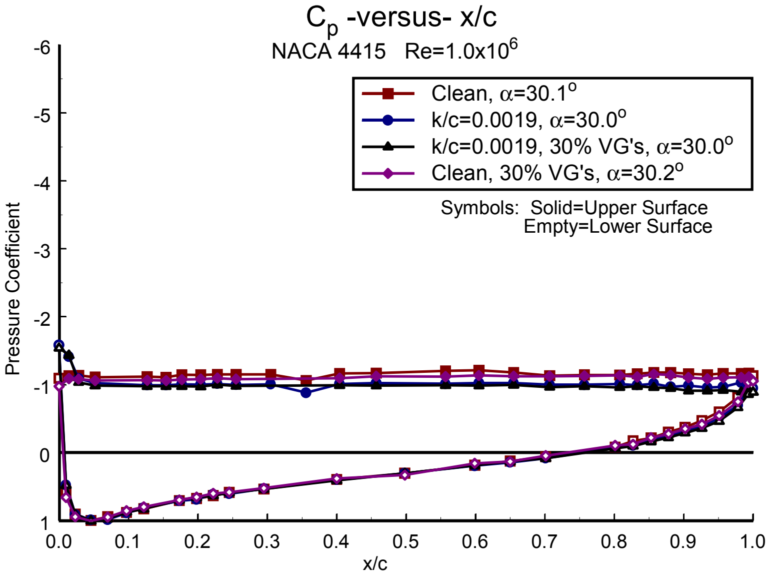

Figure B49. α = 30°

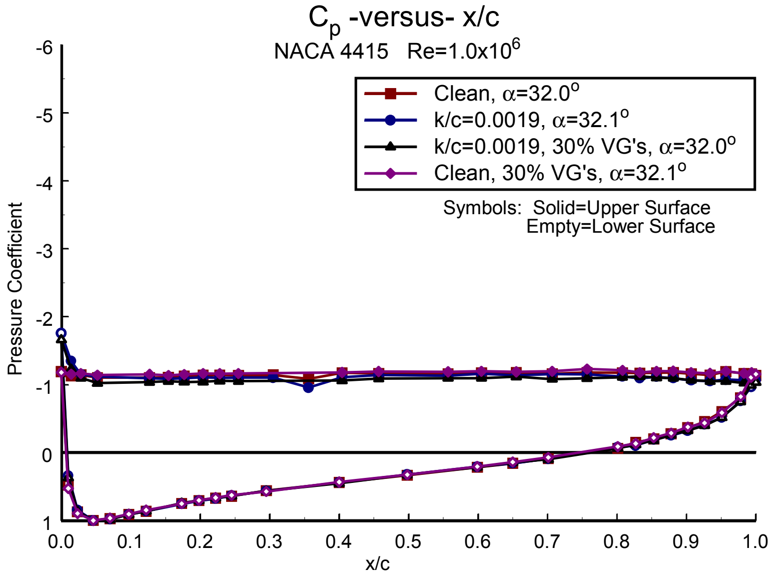

Figure B50. α = 32°

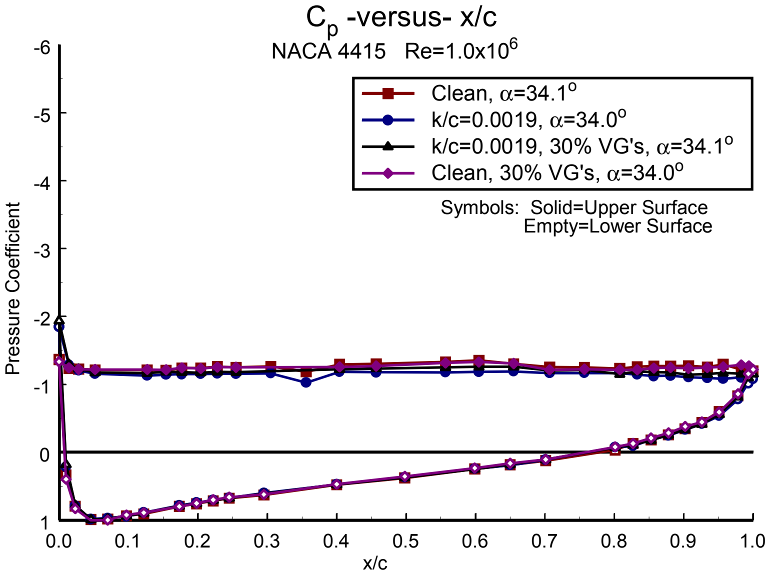

Figure B51. α = 34°

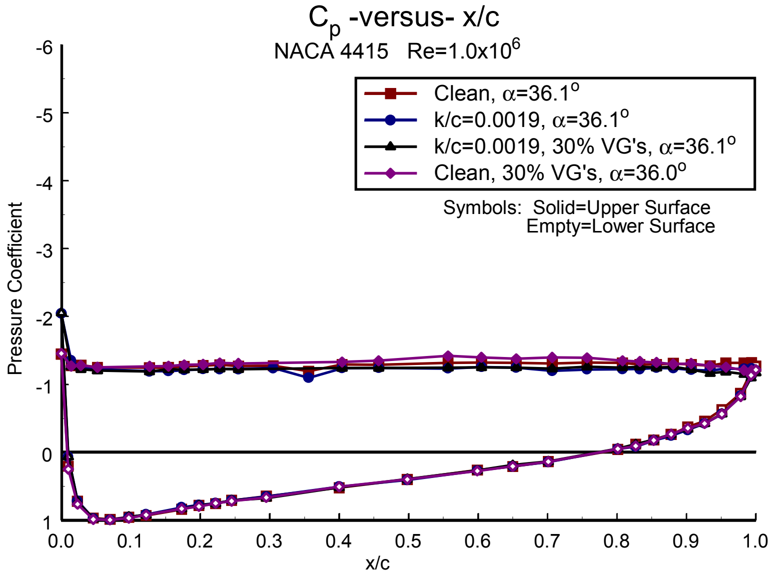

Figure B52. α = 36°

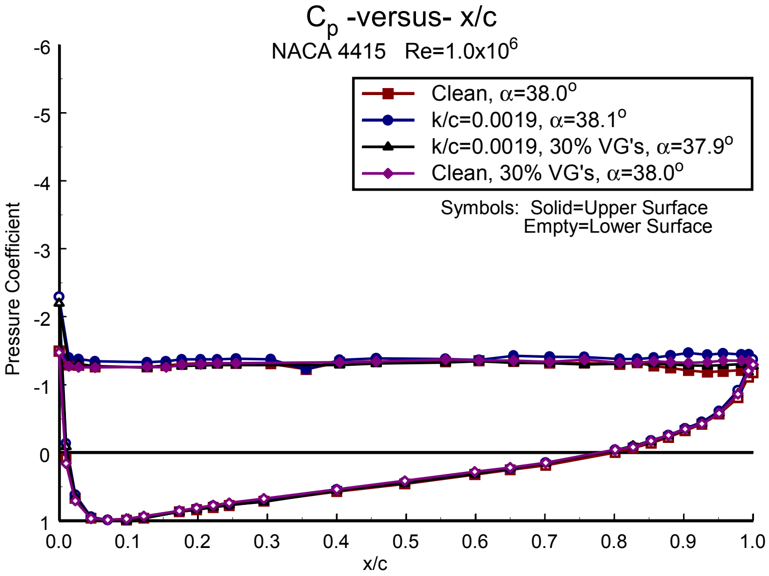

Figure B53. α = 38°

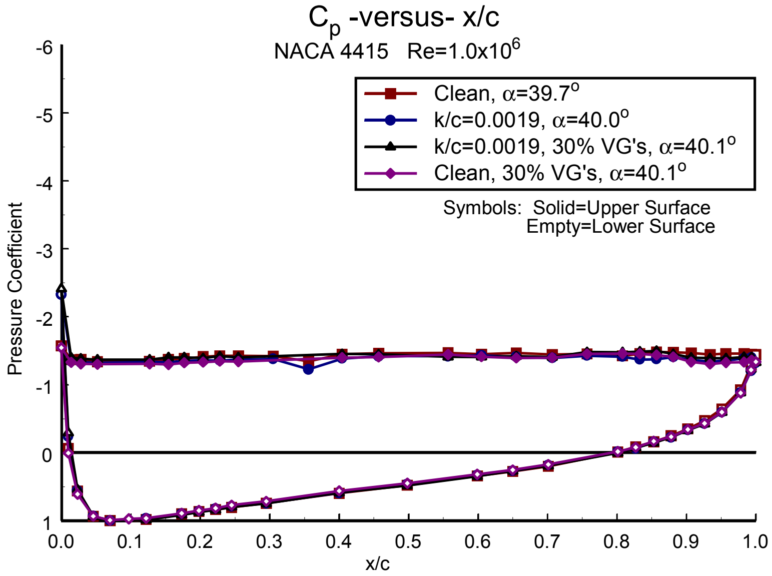

Figure B54. α = 40°

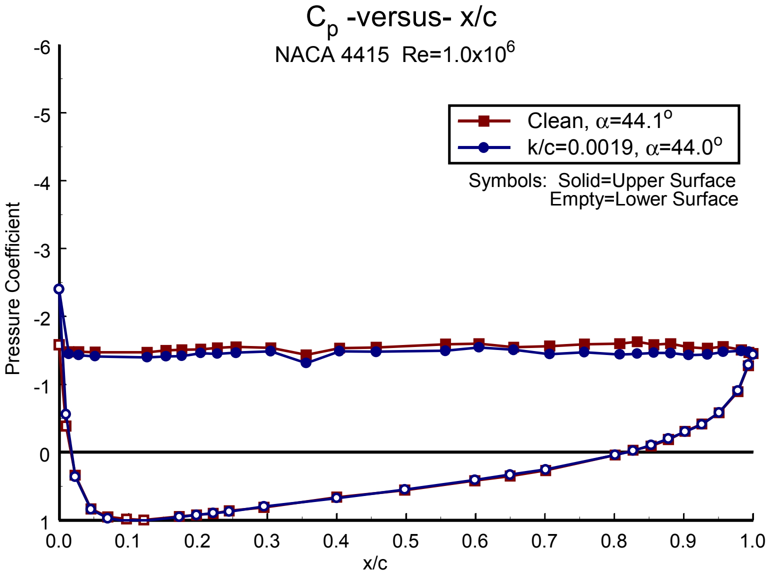

Figure B55. α = 44°

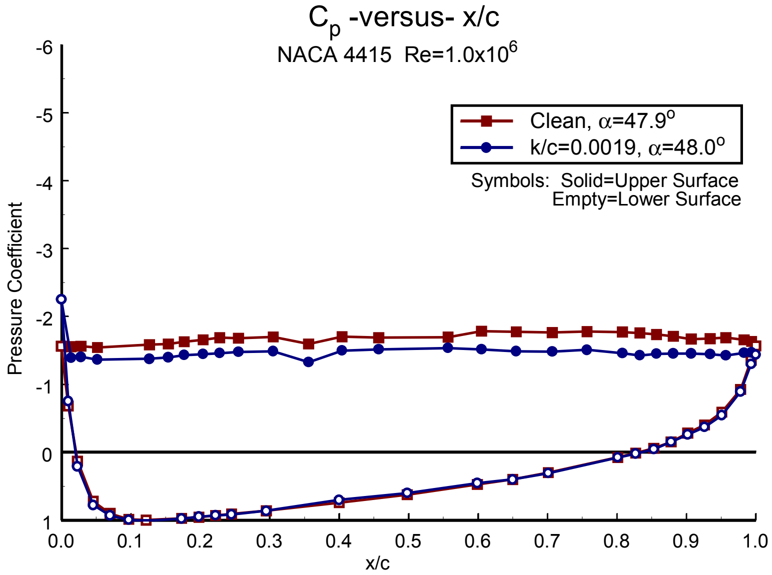

Figure B56. α = 48°

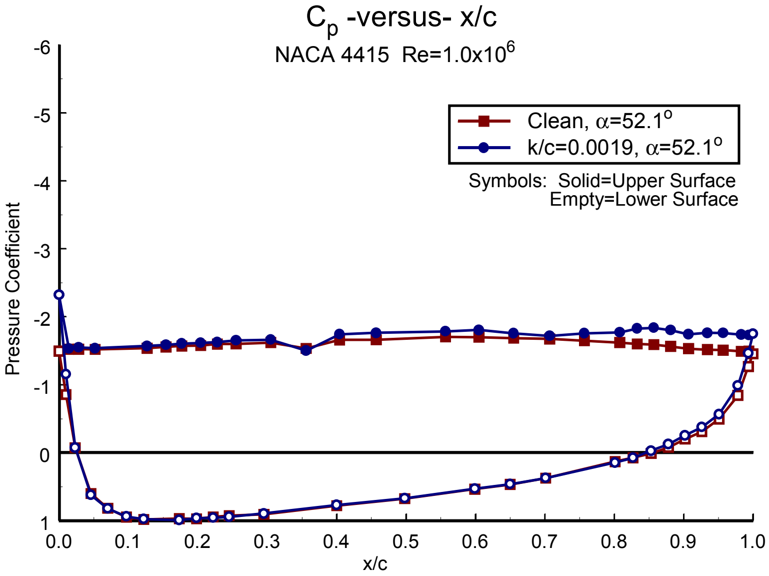

Figure B57. □□ 52°

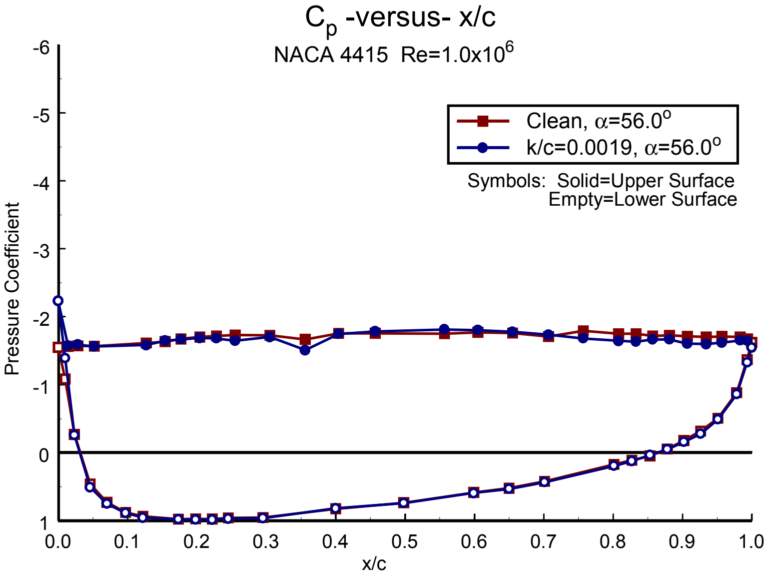

Figure B58. □□ 56°

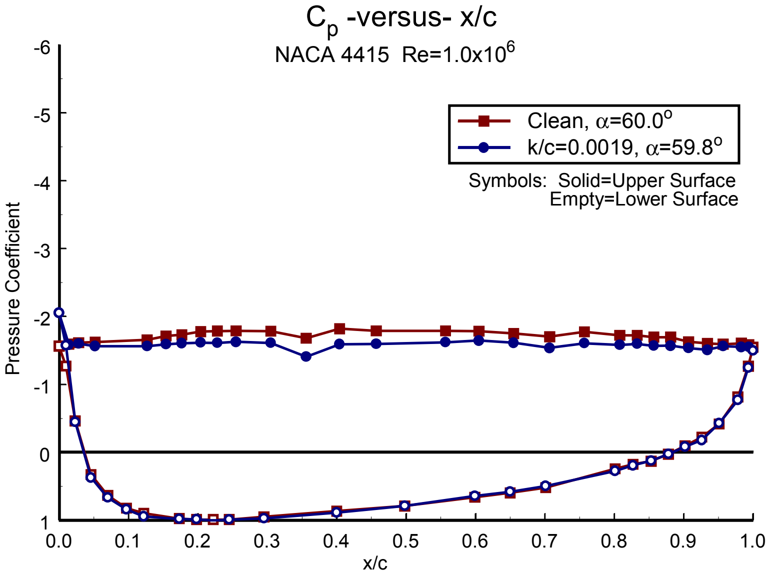

Figure B59. □□ 60°

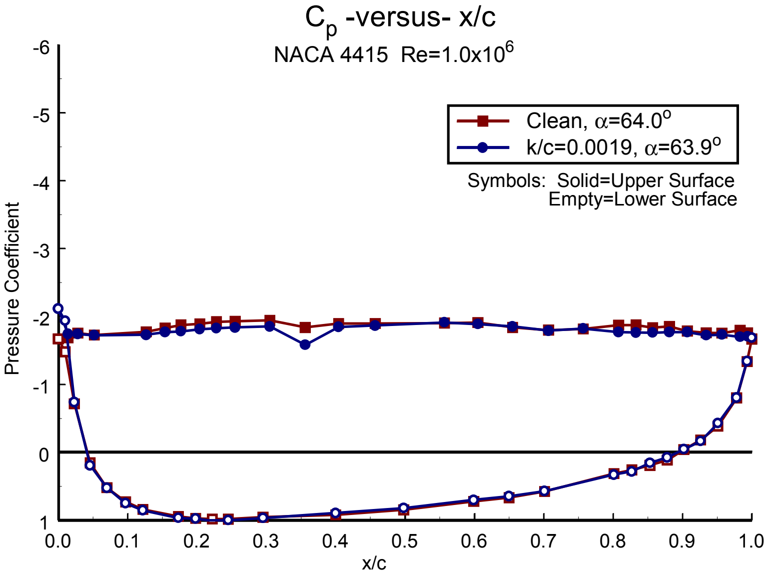

Figure B60. □□ 64°

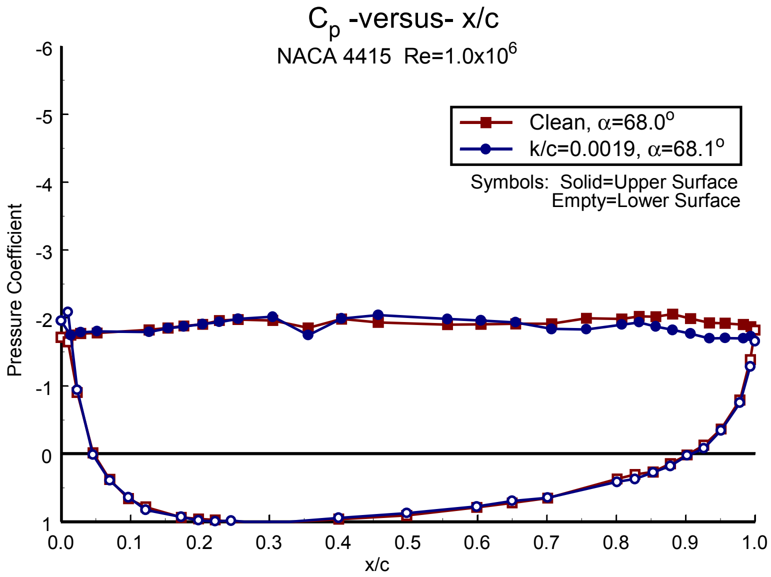

Figure B61. □□ 68°

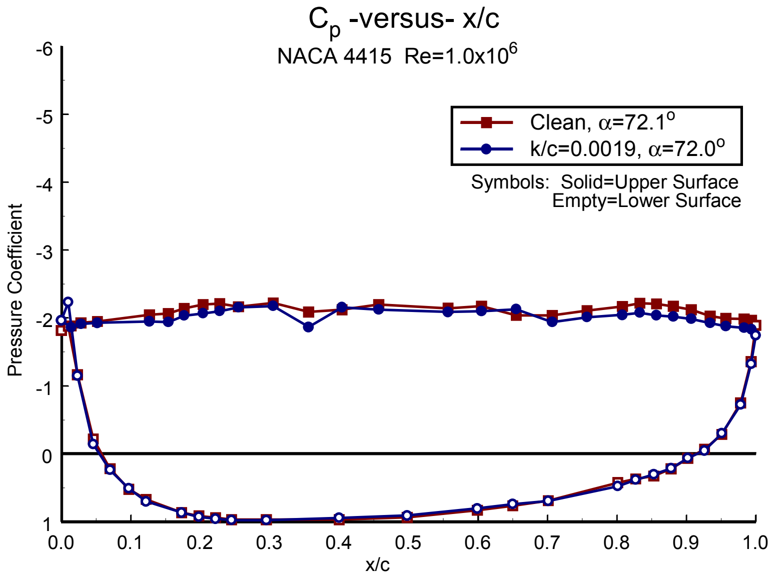

Figure B62. □□ 72°

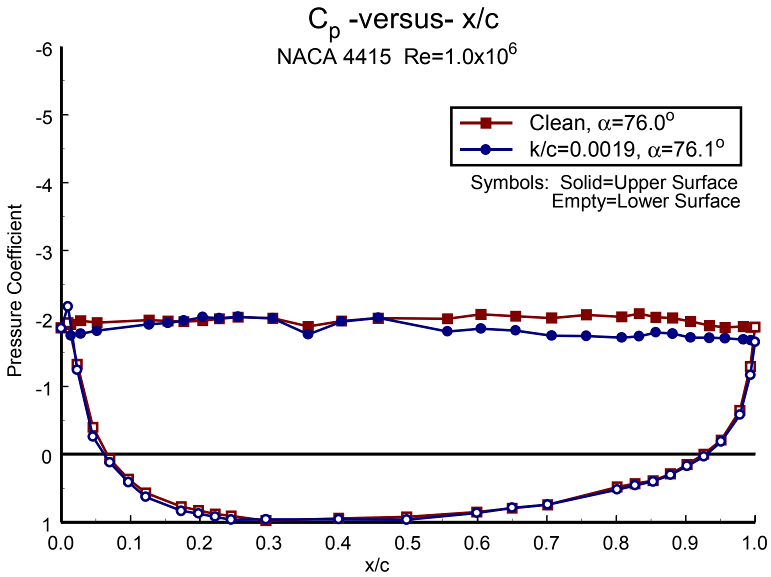

Figure B63. □□ 76°

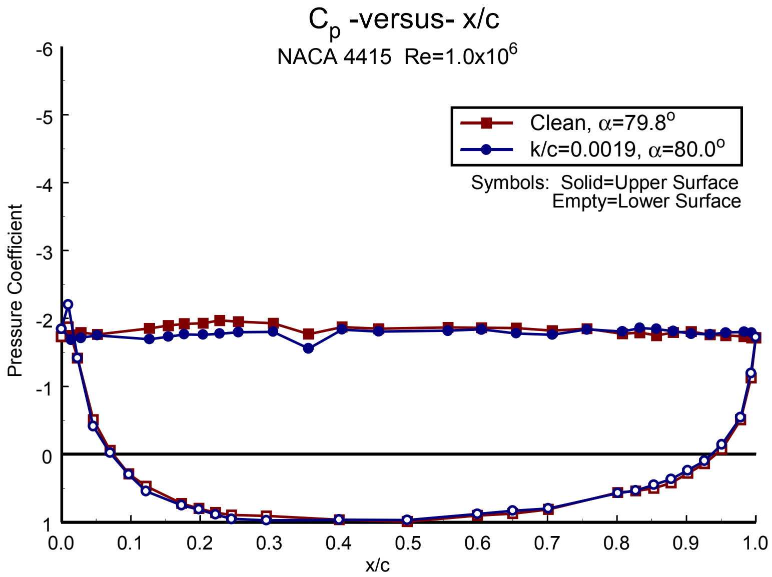

Figure B64. □□ 80°

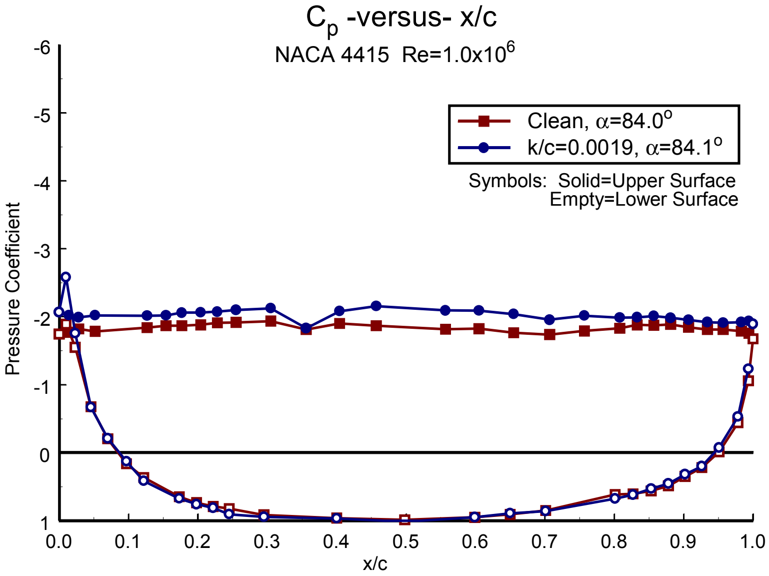

Figure B65. α = 84°

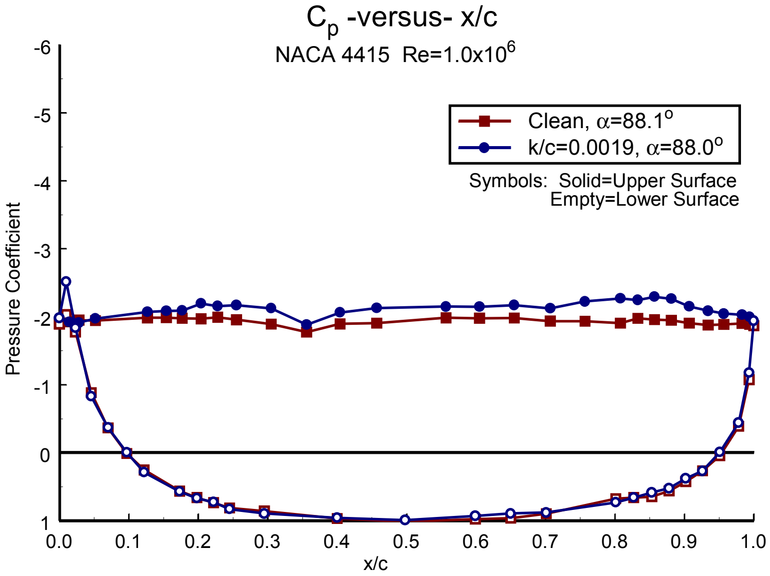

Figure B66. α = 88°

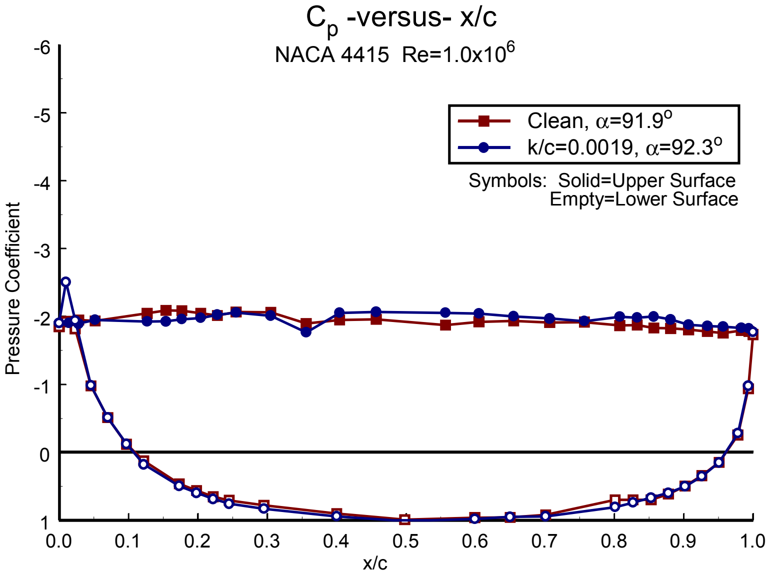

Figure B67. α = 92°

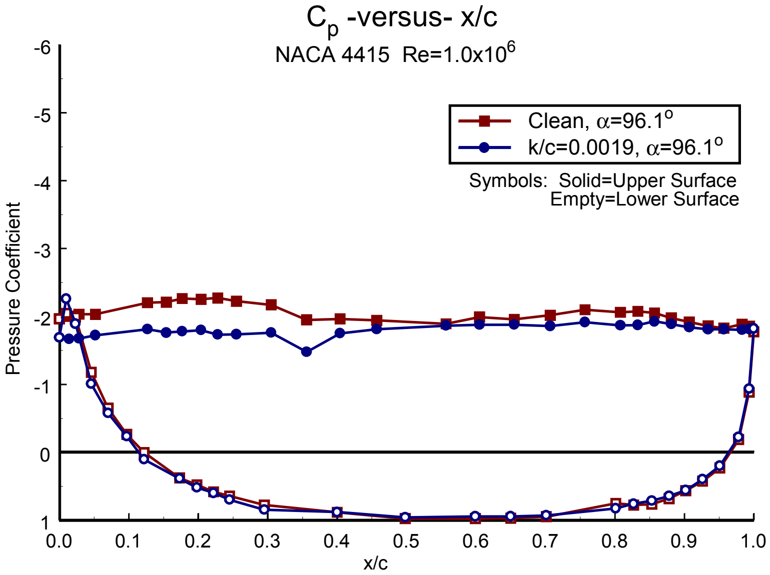

Figure B68. α = 96°

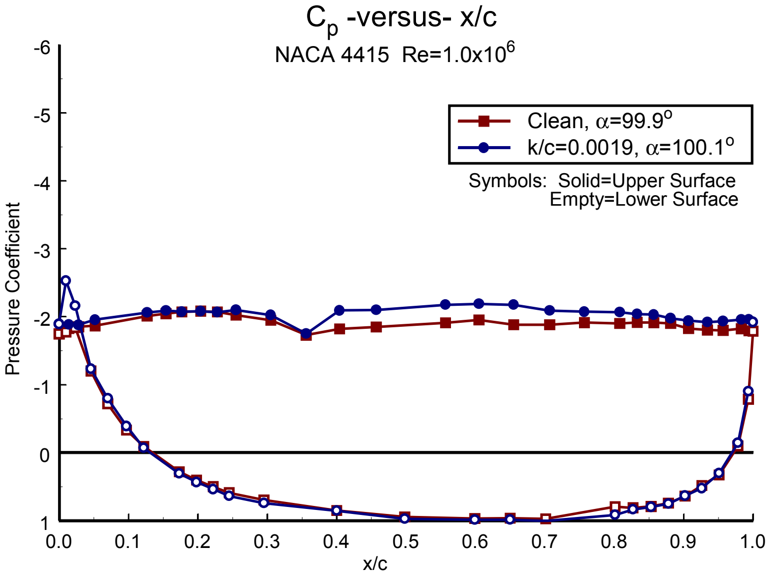

Figure B69. □□ 100°

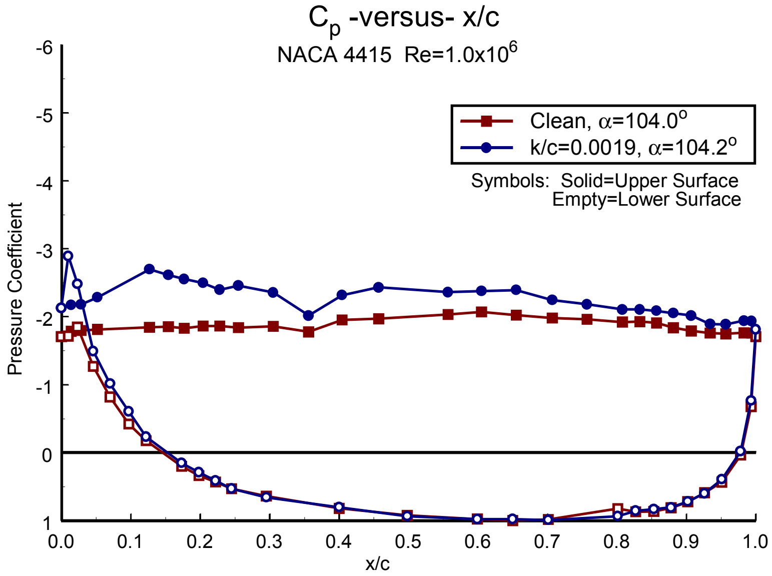

Figure B70. □□ 104°

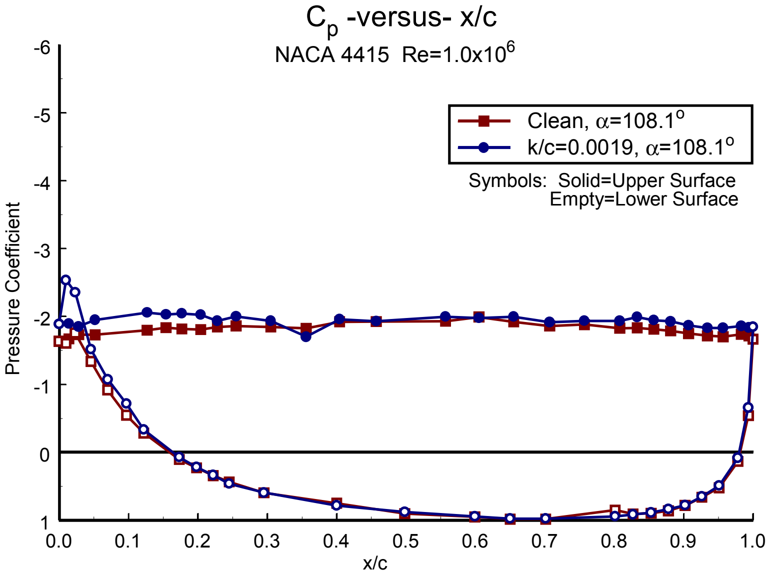

Figure B71. □□ 108°

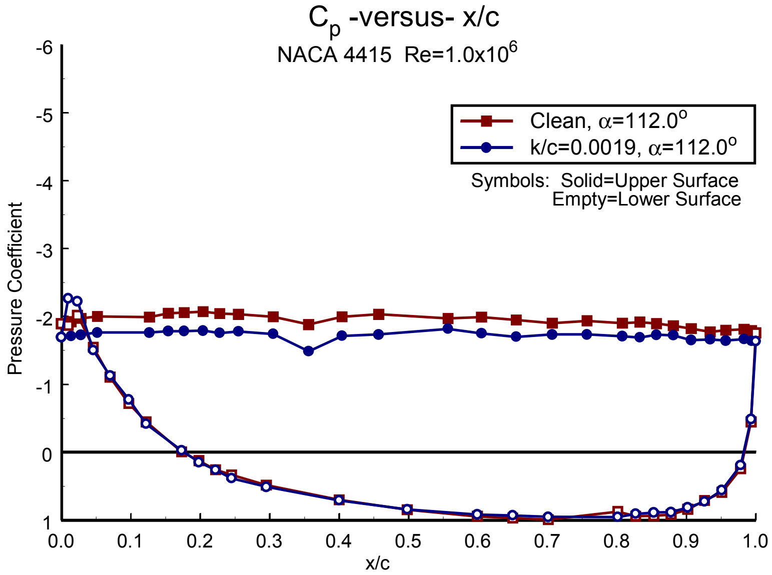

Figure B72. □□ 112°

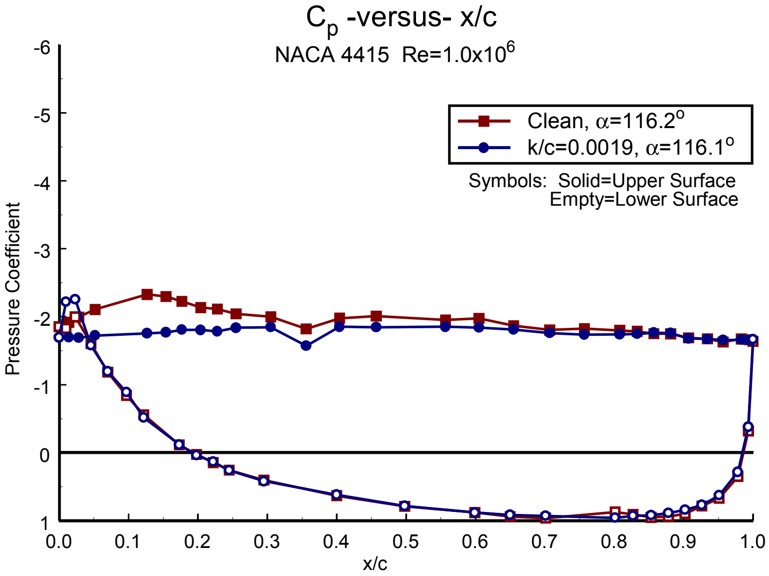

Figure B73. □□ 116°

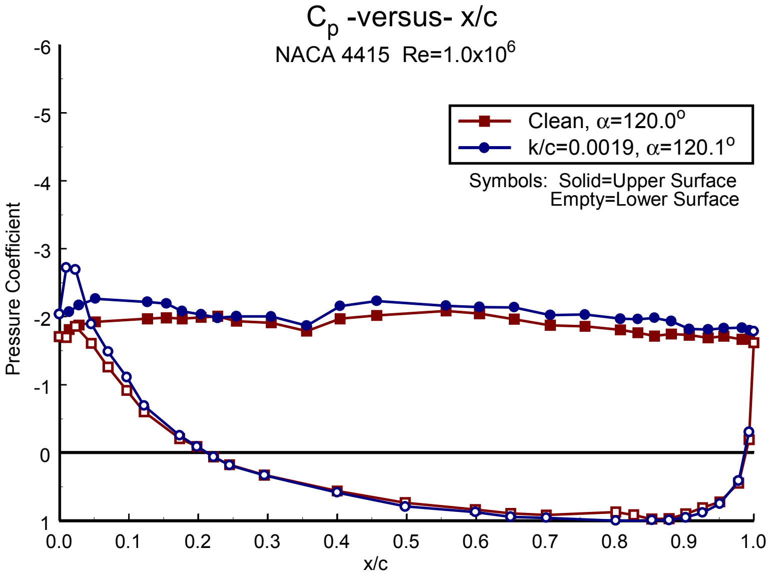

Figure B74. □□ 120°

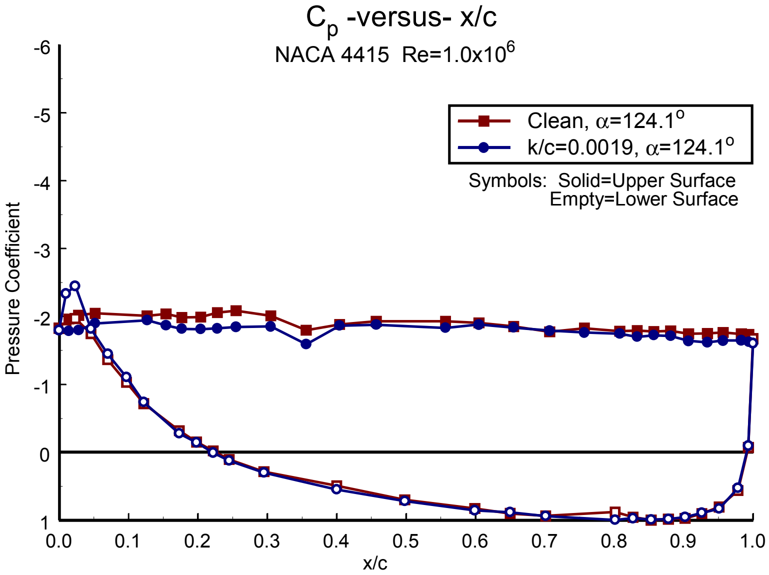

Figure B75. □□ 124°

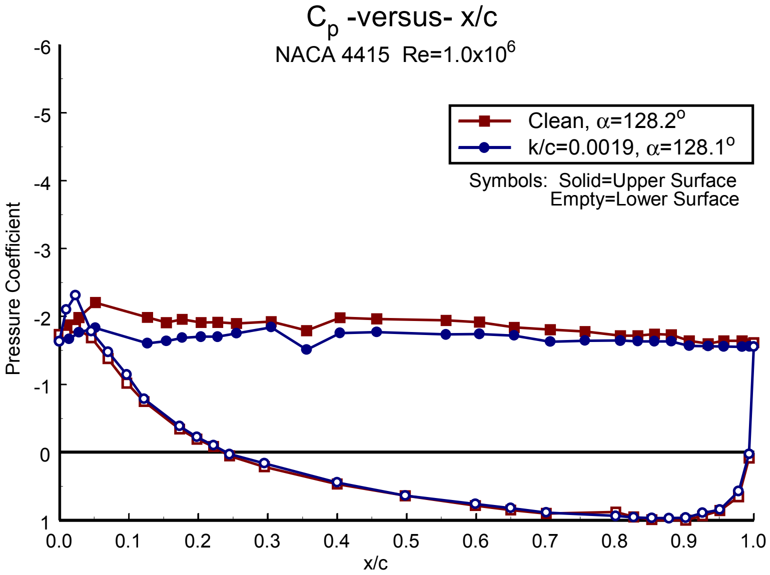

Figure B76. □□ 128°

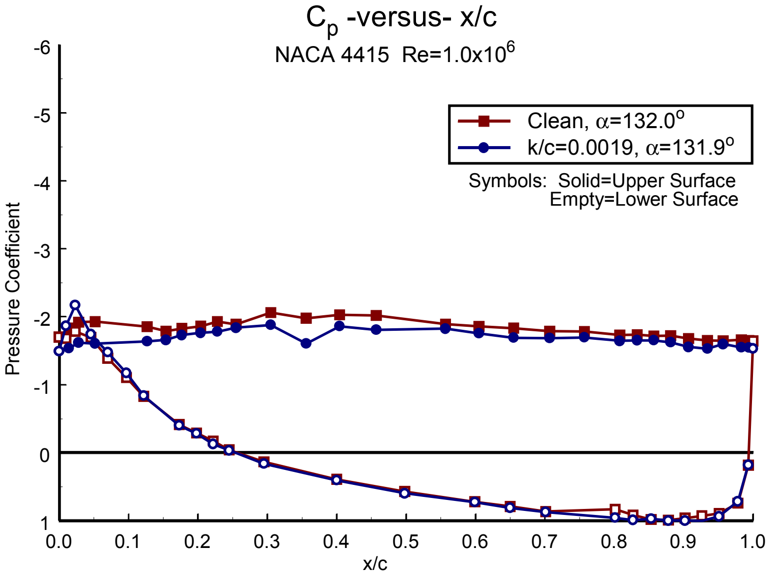

Figure B77. □□ 132°

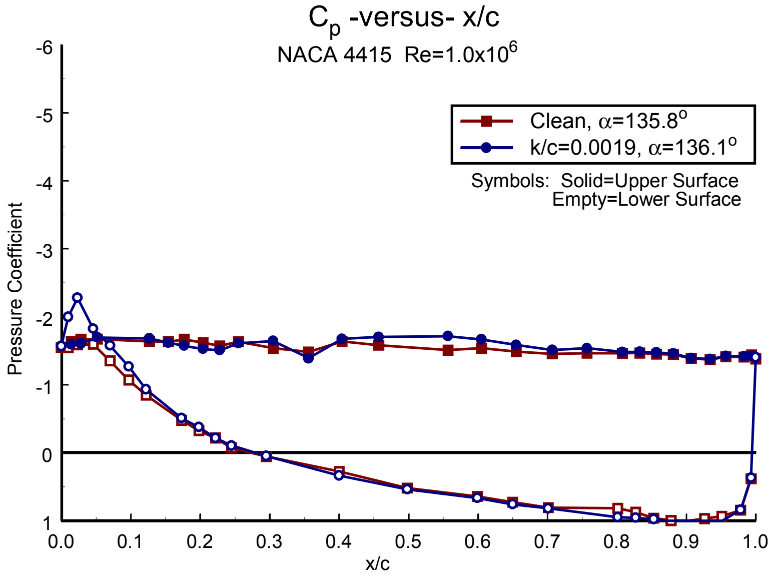

Figure B78. □□ 136°

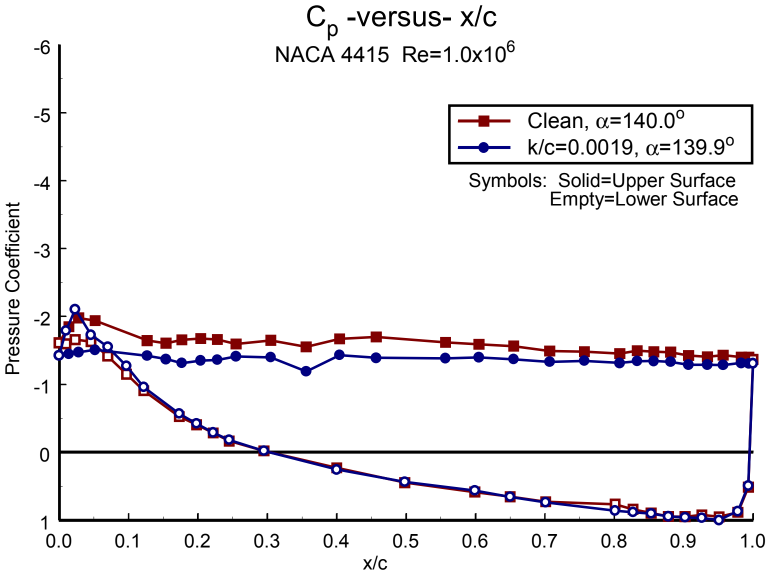

Figure B79. □□ 140°

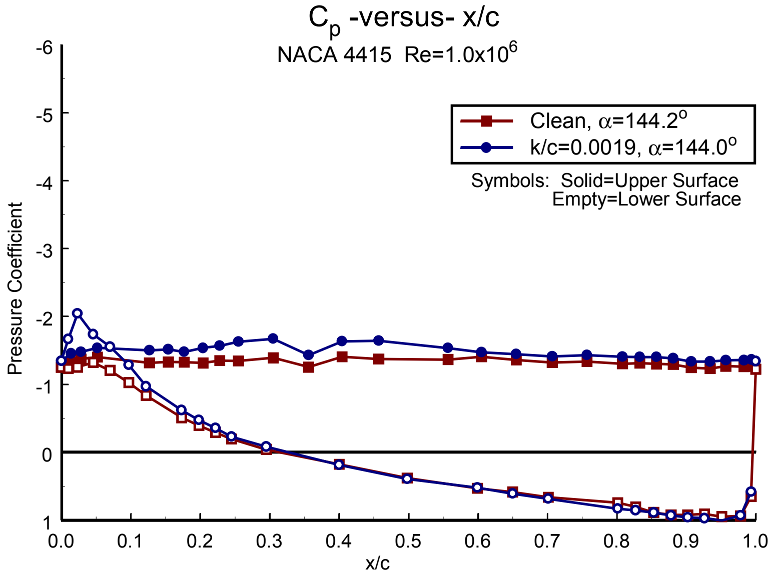

Figure B80. □□ 144°

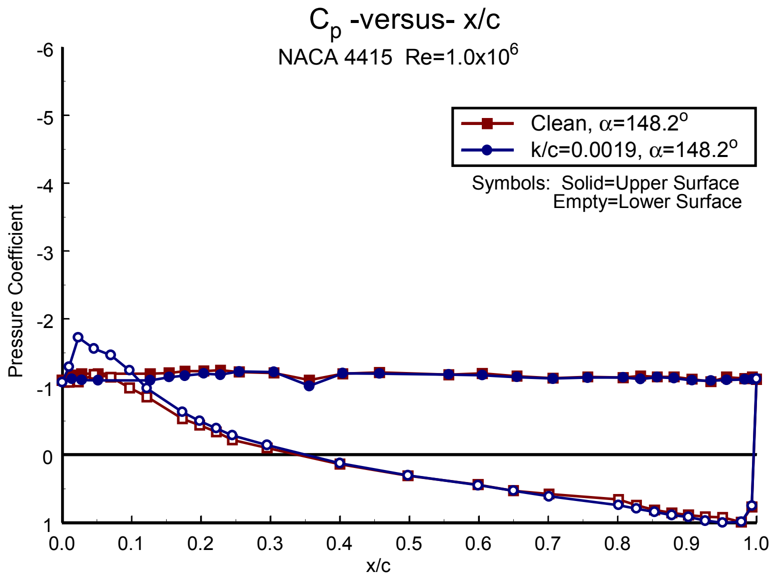

Figure B81. □□ 148°

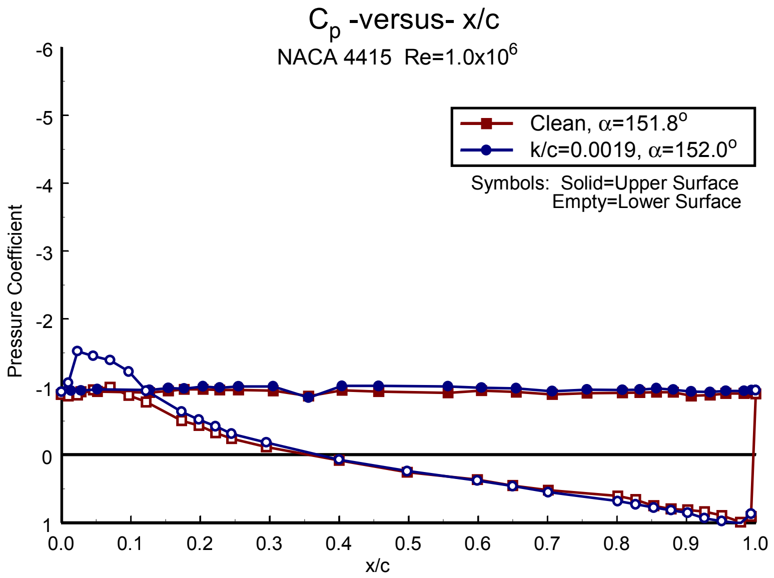

Figure B82. □□ 152°

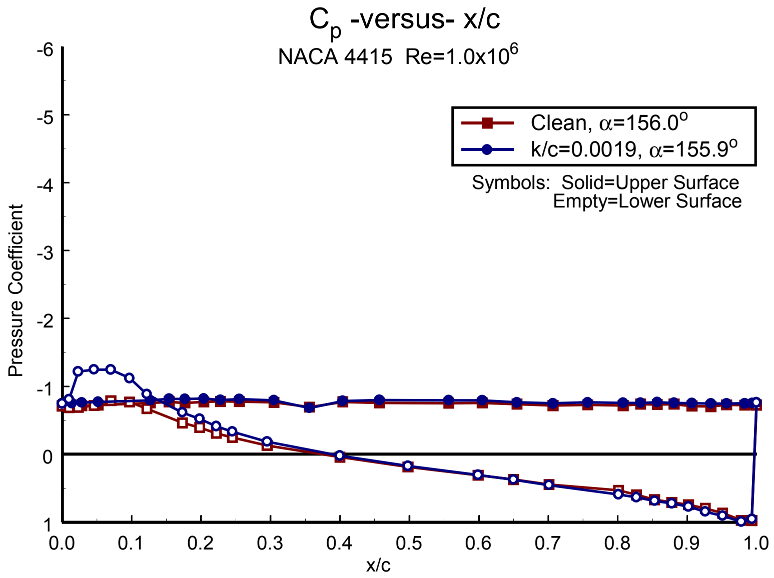

Figure B83. □□ 156°

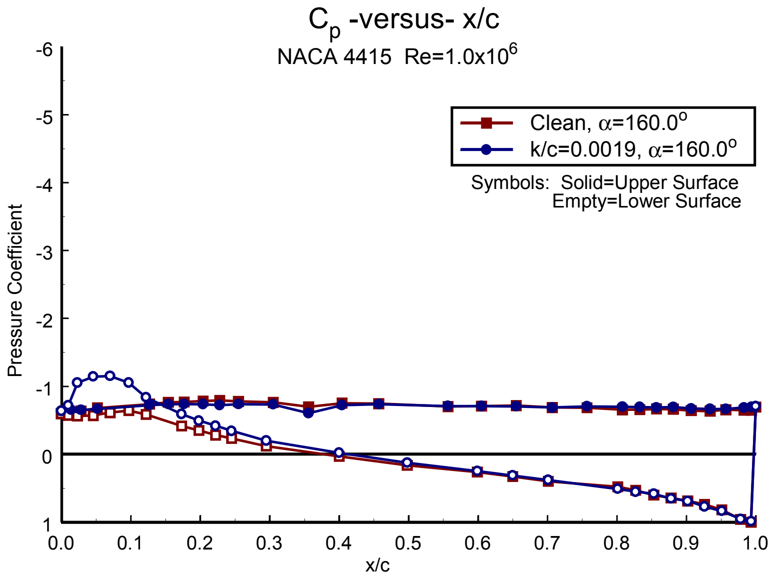

Figure B84. □□ 160°

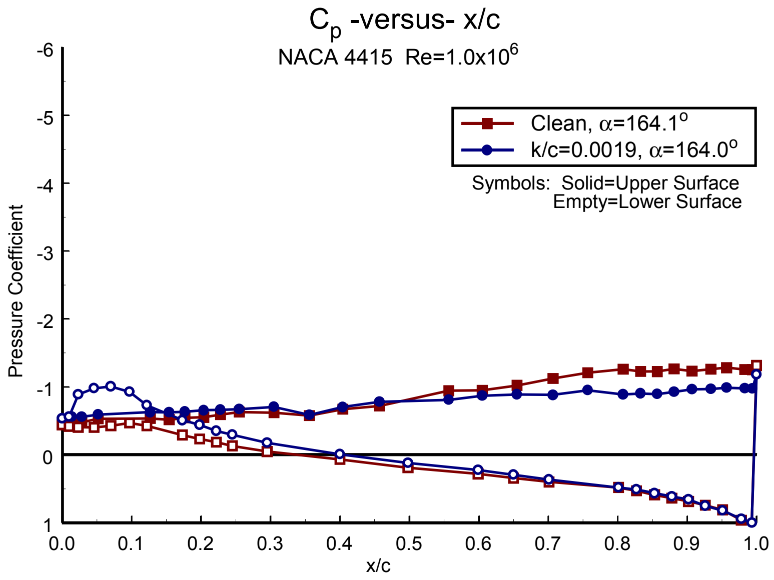

Figure B85. □□ 164°

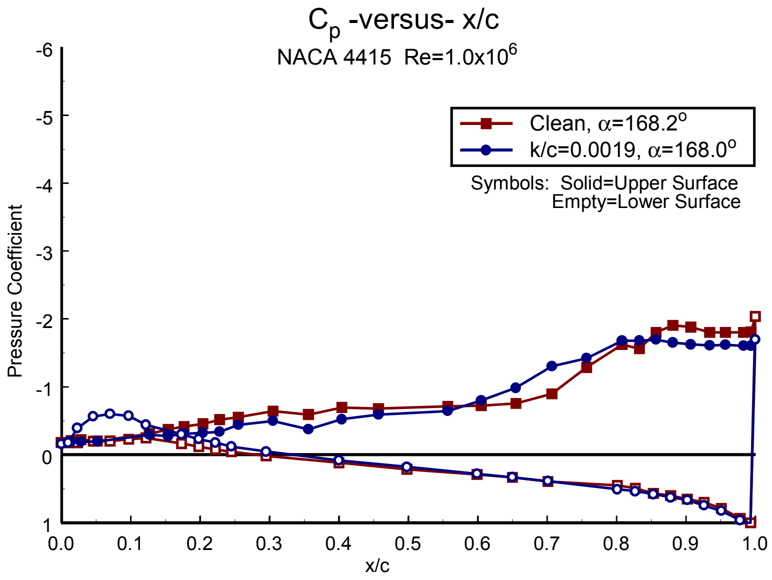

Figure B86. □□ 168°

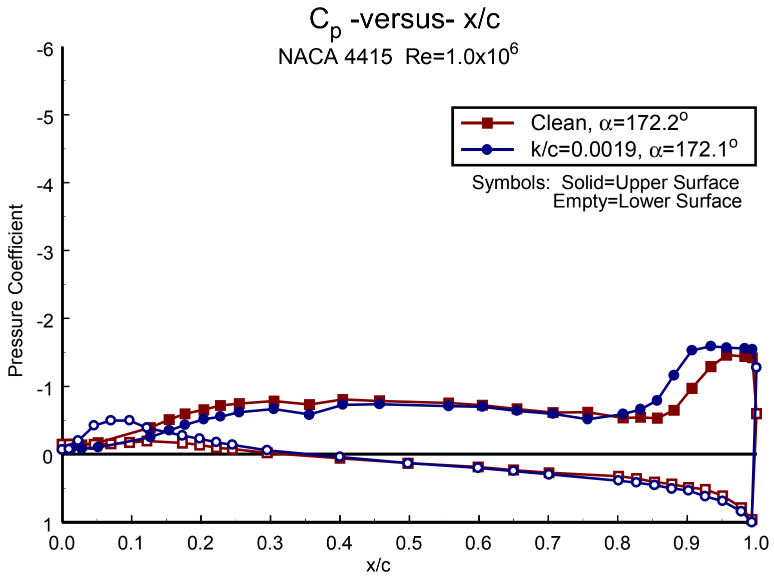

Figure B87. □□ 172°

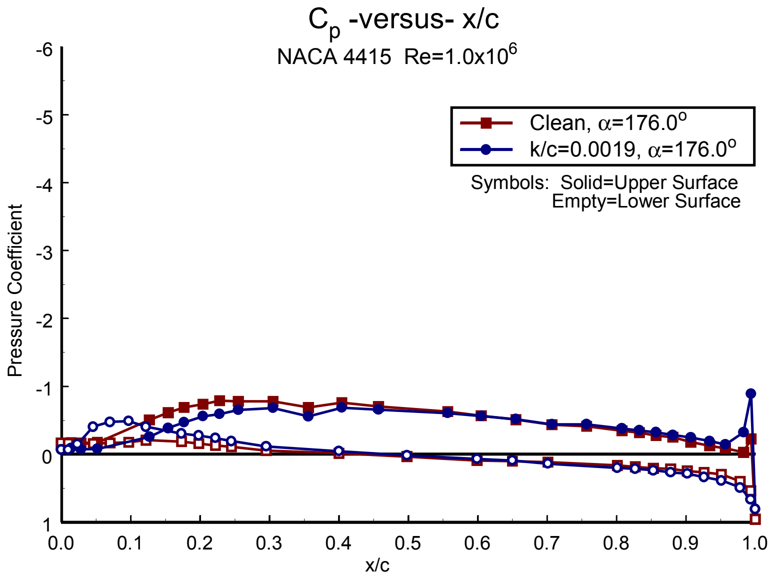

Figure B88. □□ 176°

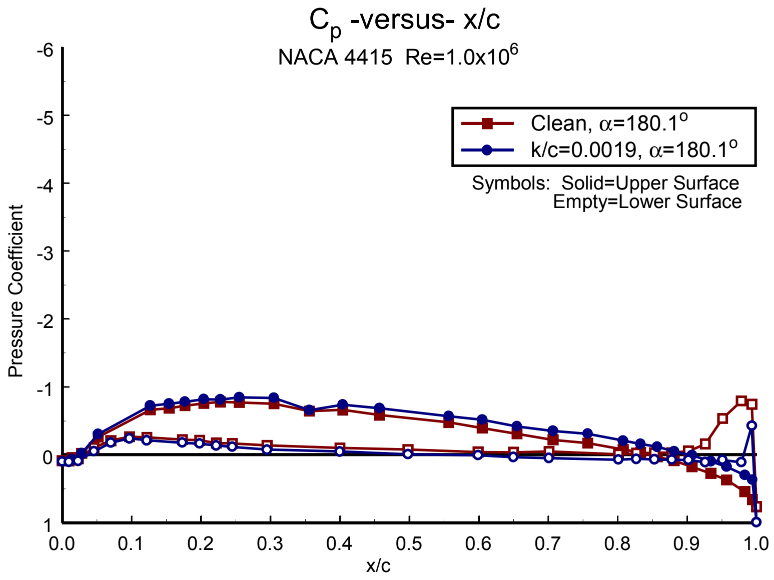

Figure B89. □□= 180°

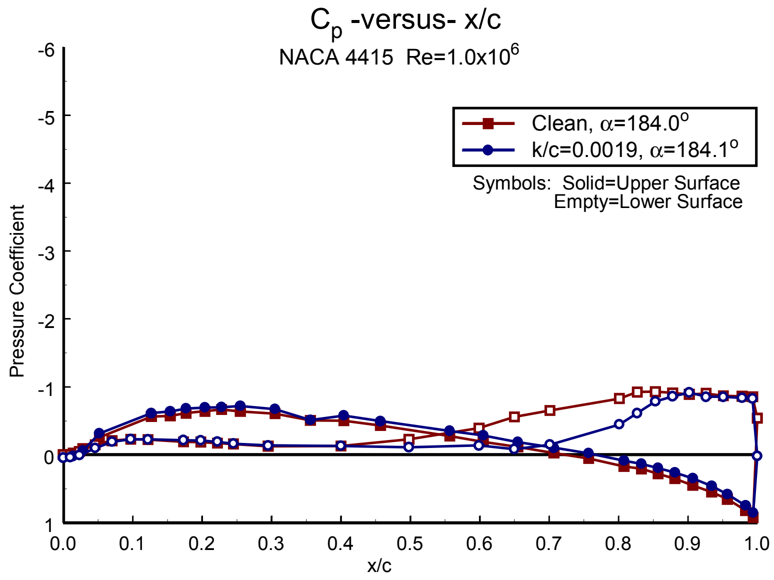

Figure B90. □□= 184°

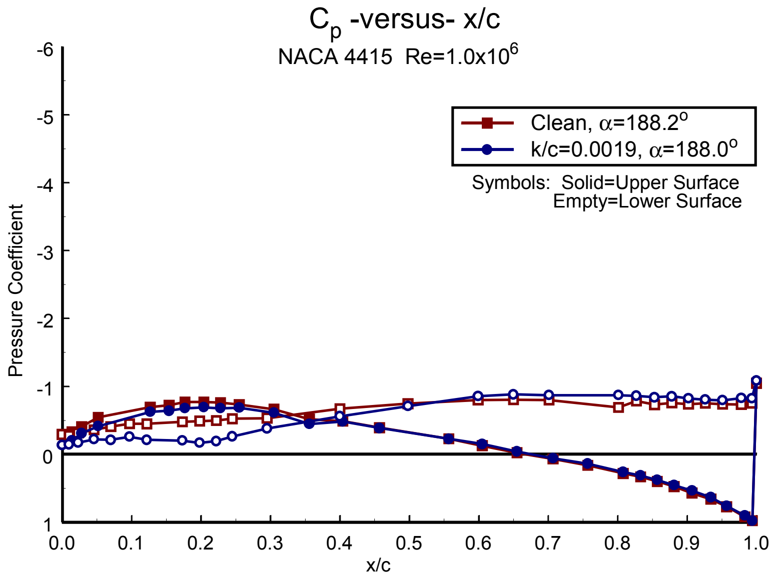

Figure B91. □□= 188°

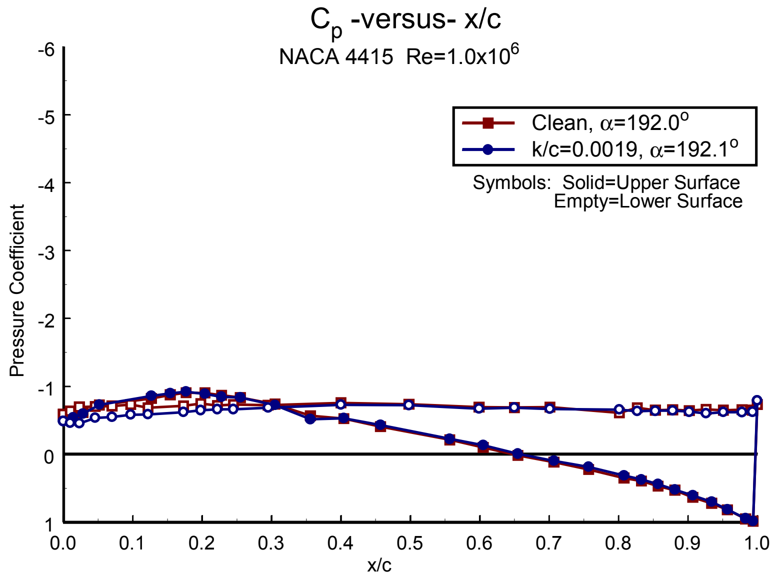

Figure B92. □□= 192°

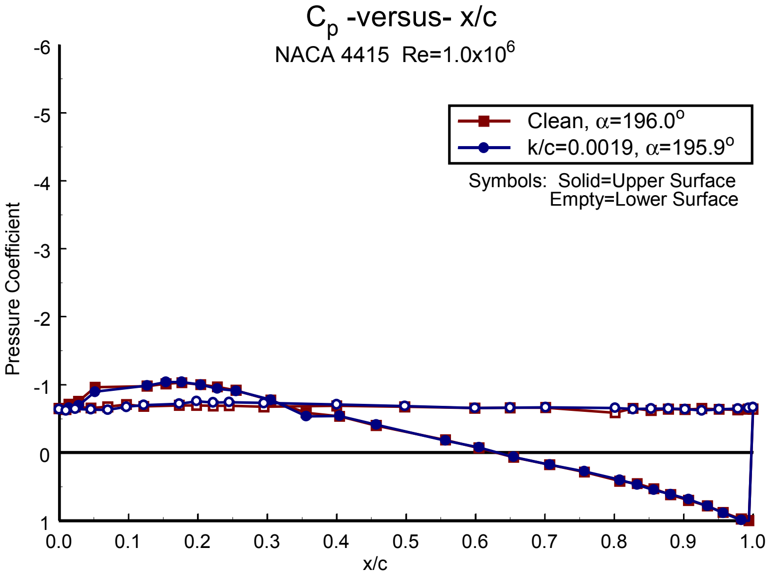

Figure B93. □□ 196°

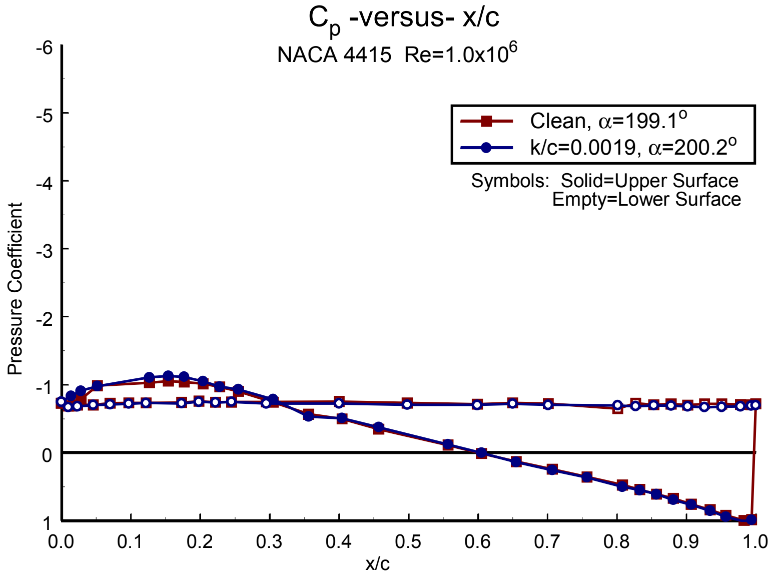

Figure B94. □□ 200°

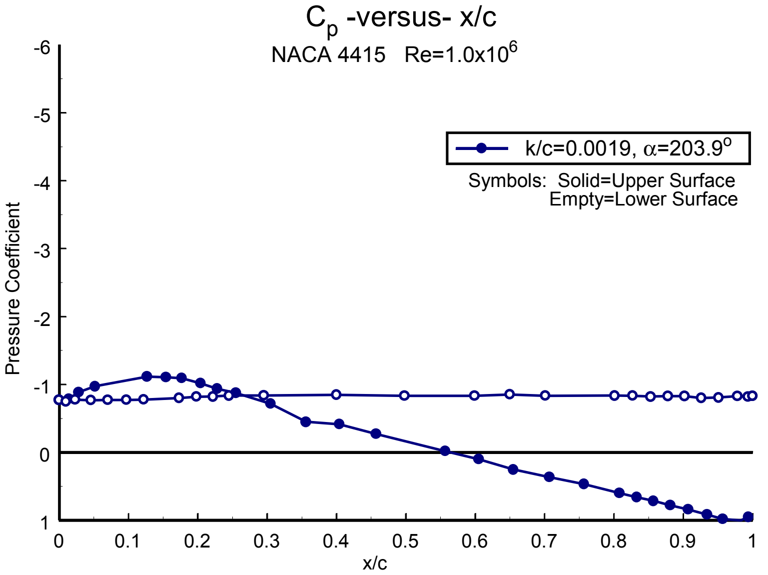

Figure B95. □□ 204°

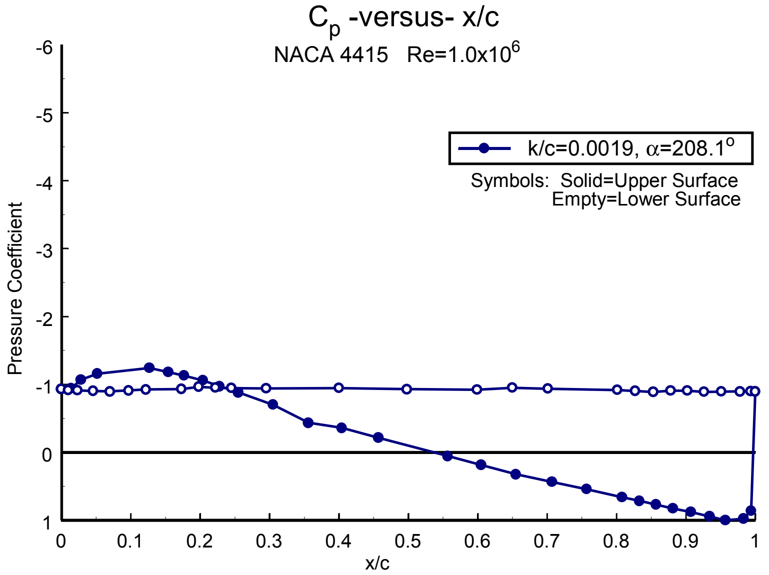

Figure B96. □□ 208°

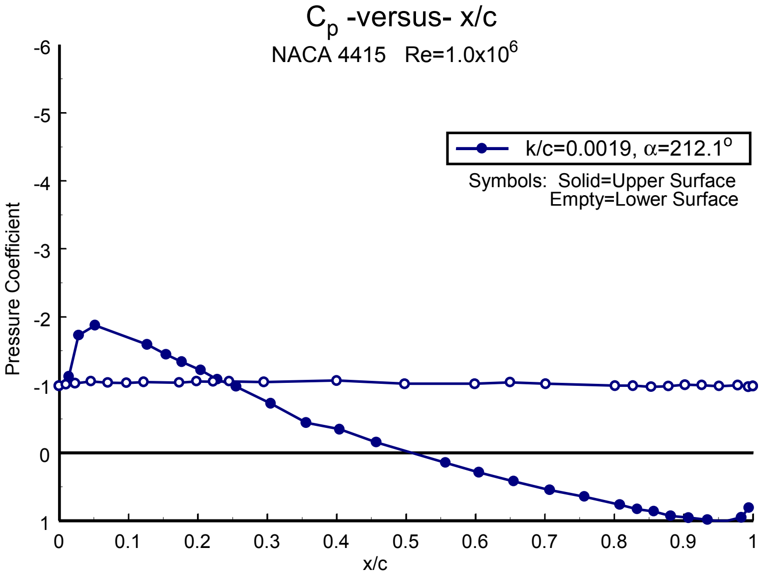

Figure B97. □□ 212°

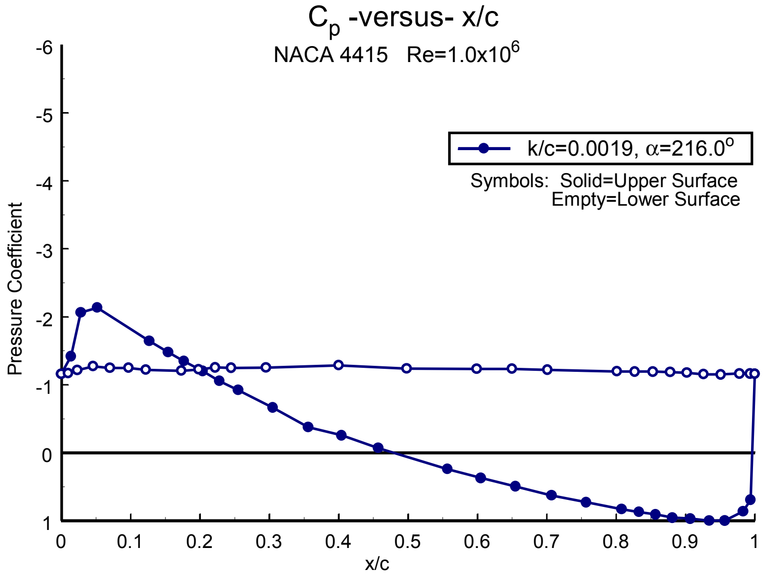

Figure B98. □□ 216°

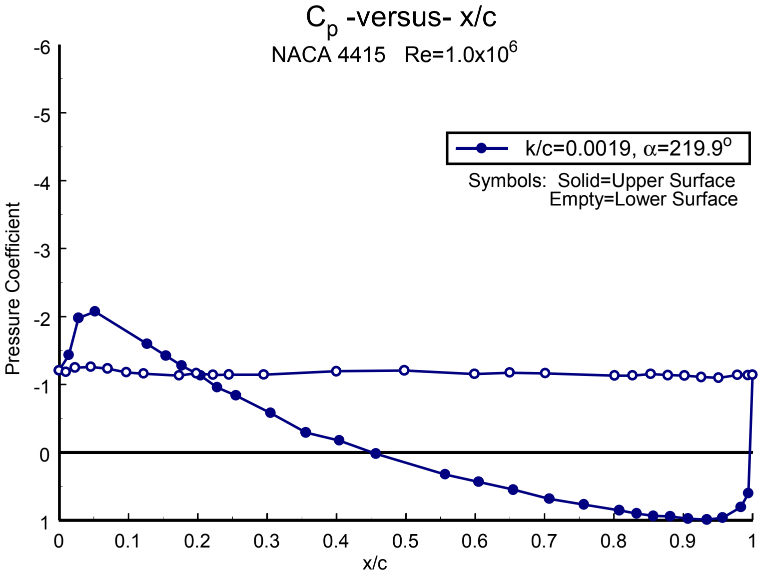

Figure B99. □□ 220°

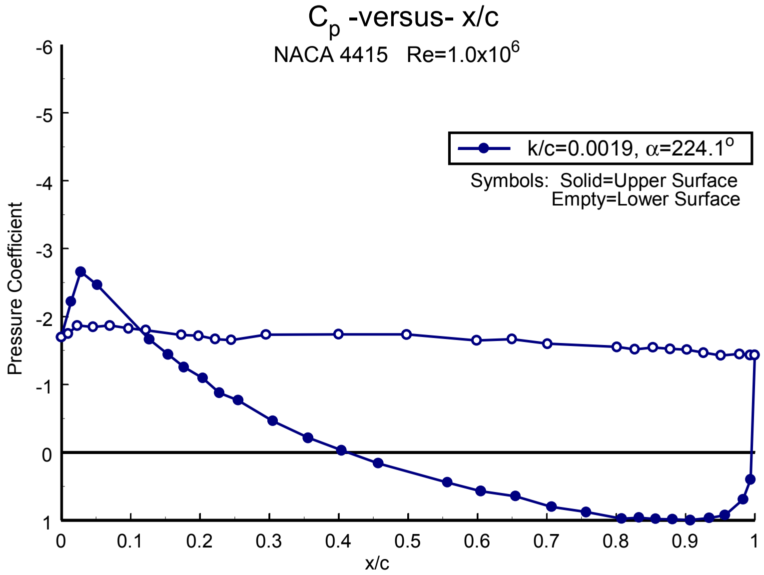

Figure B100. □□ 224°

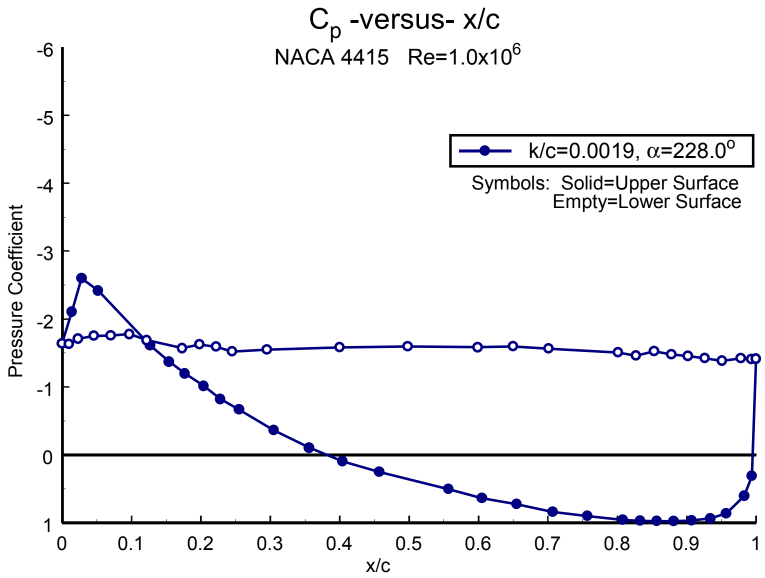

Figure B101. □= 228°

Steady-State Pressure Distributions

Re = 1.5 million

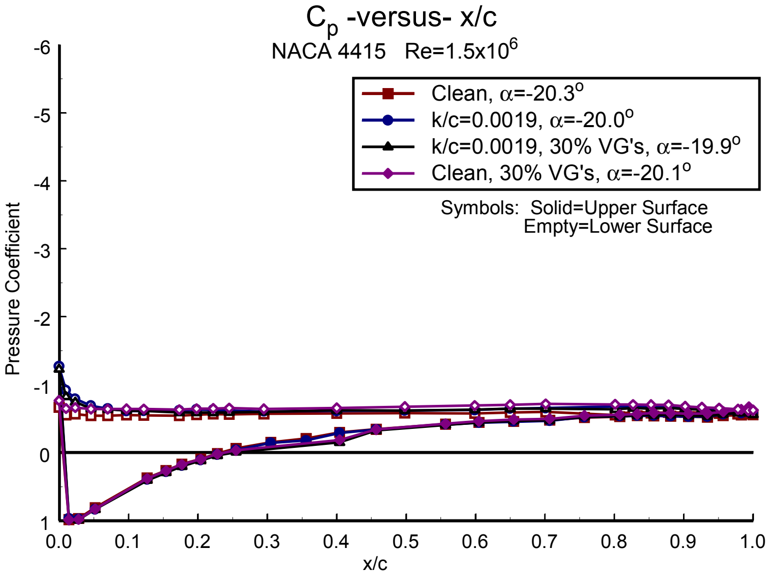

Figure B102. α = -20°

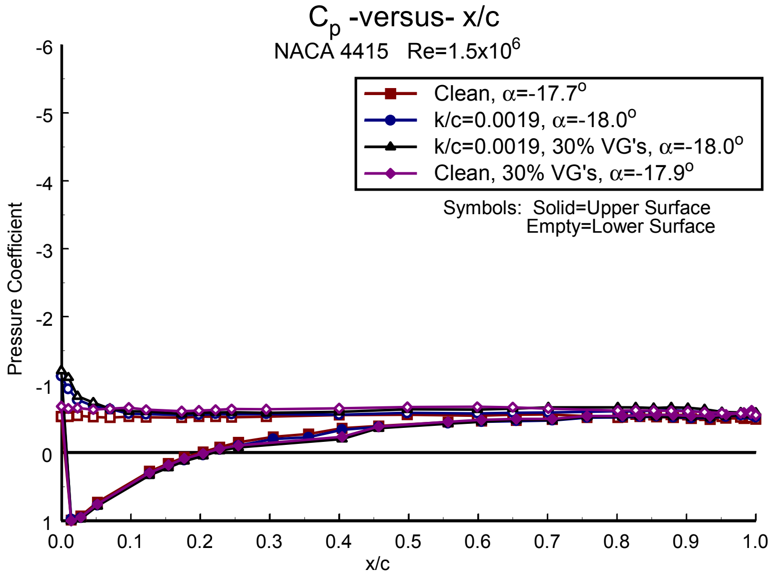

Figure B103. α = -18°

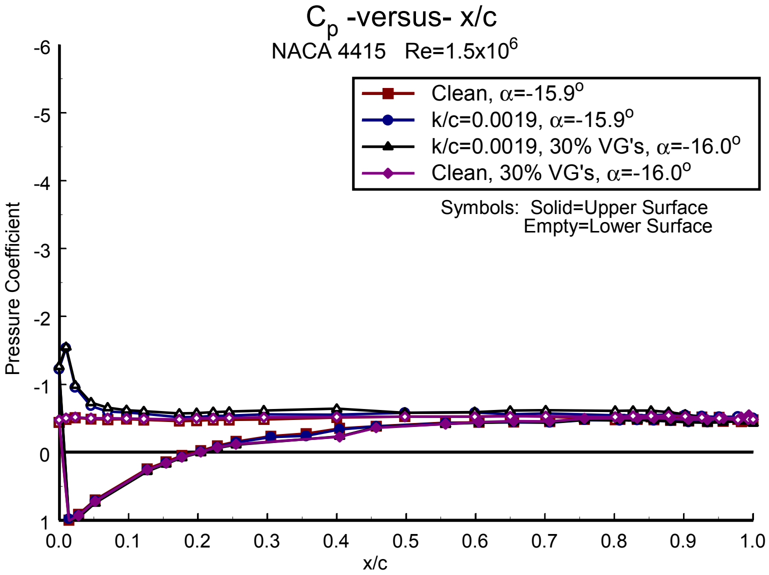

Figure B104. α = -16°

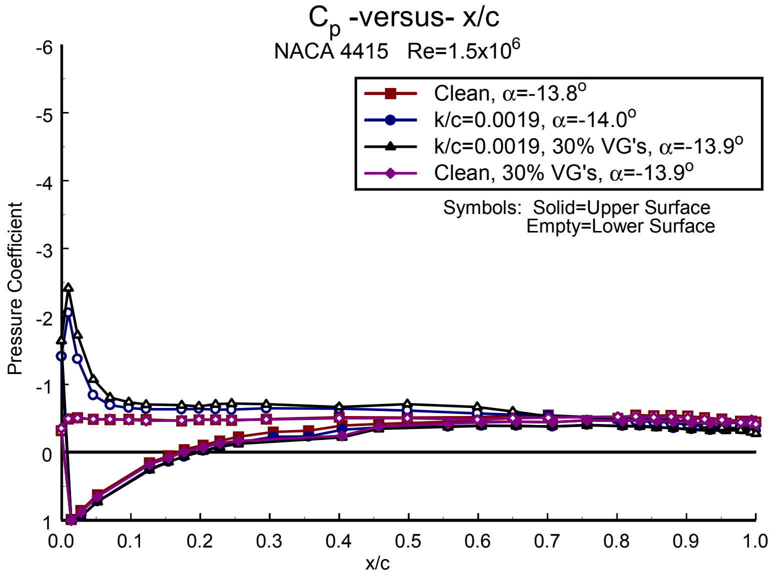

Figure B105. α = -14°

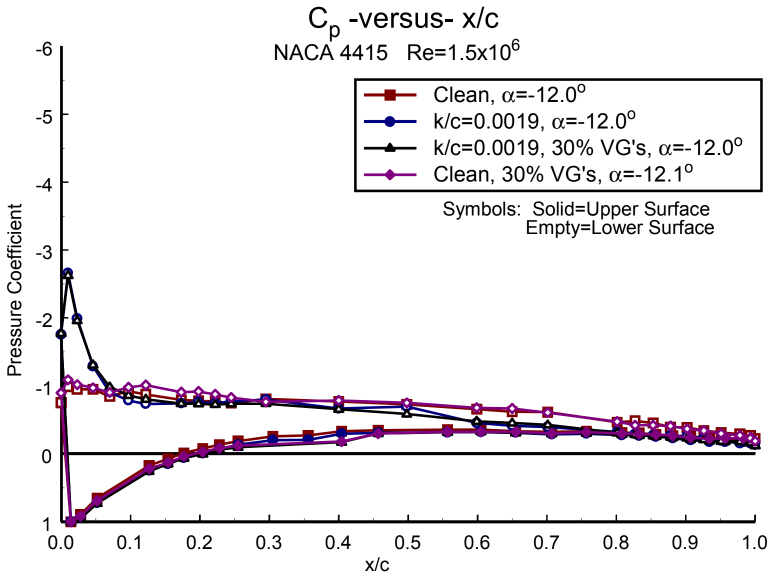

Figure B106. □□= -12°

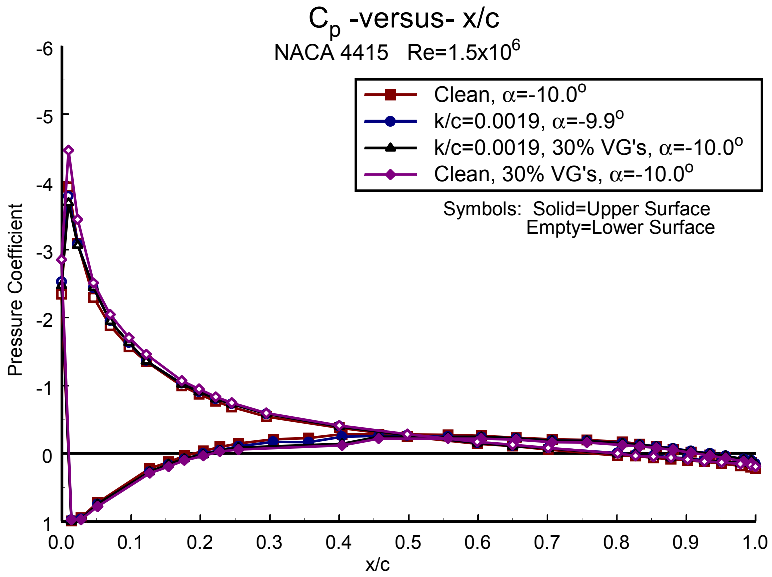

Figure B107. □□= -10°

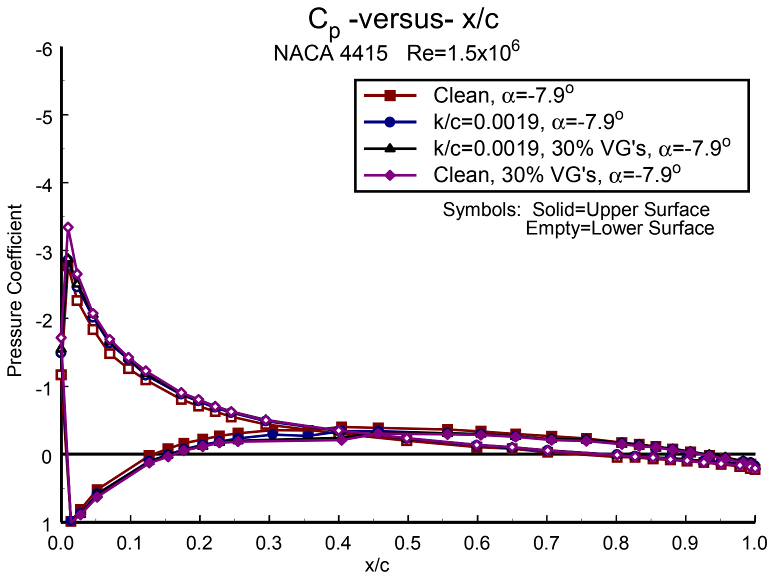

Figure B108. □□= -8°

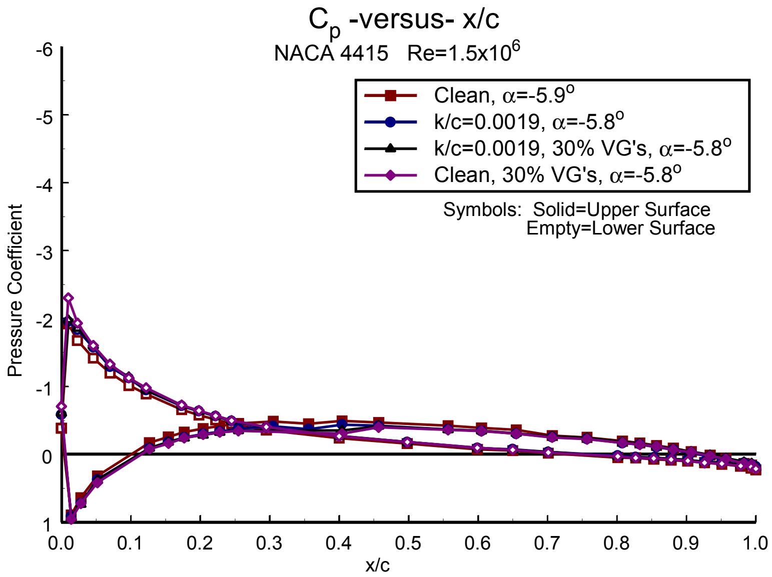

Figure B109. □□= -6°

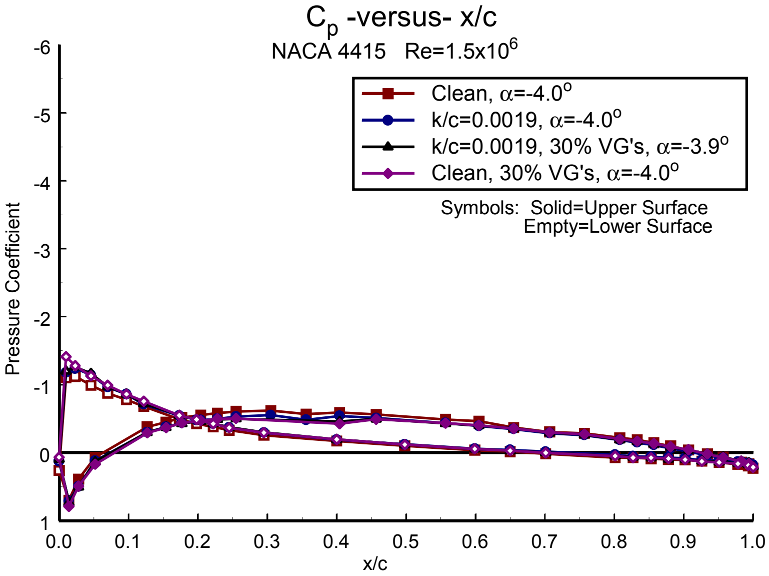

Figure B110. □□ -4°

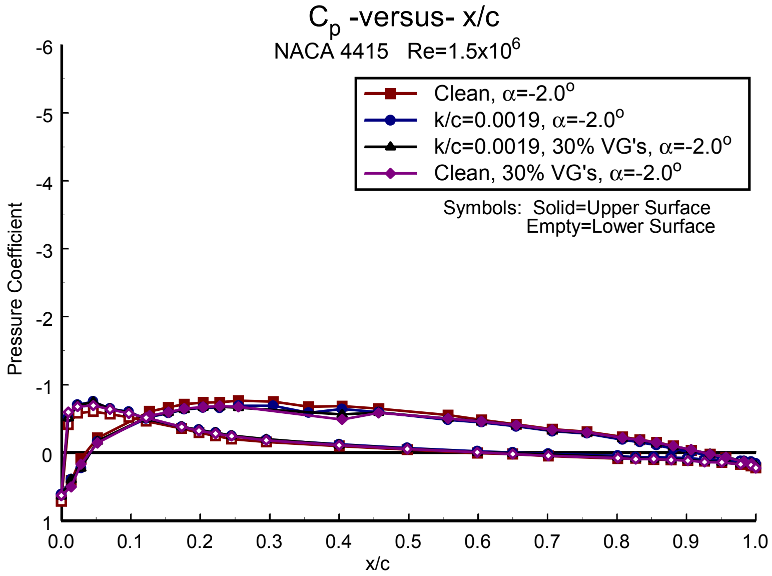

Figure B111. □□ -2°

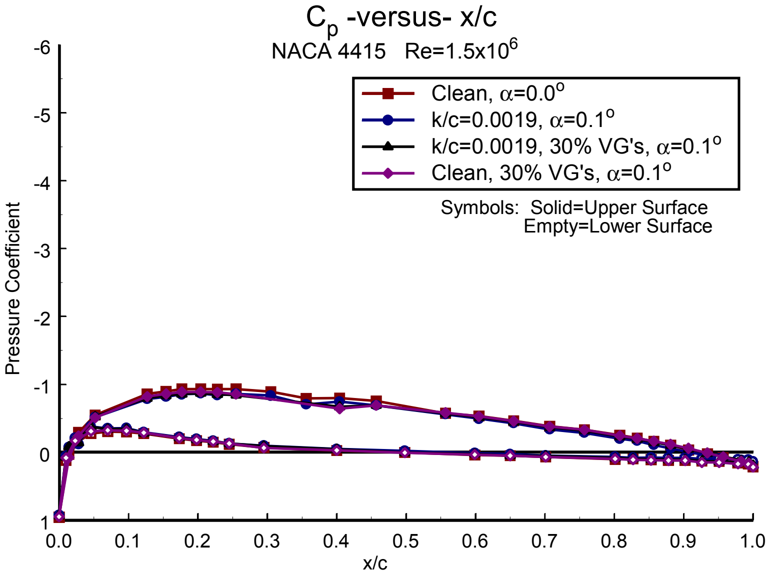

Figure B112. □□ 0°

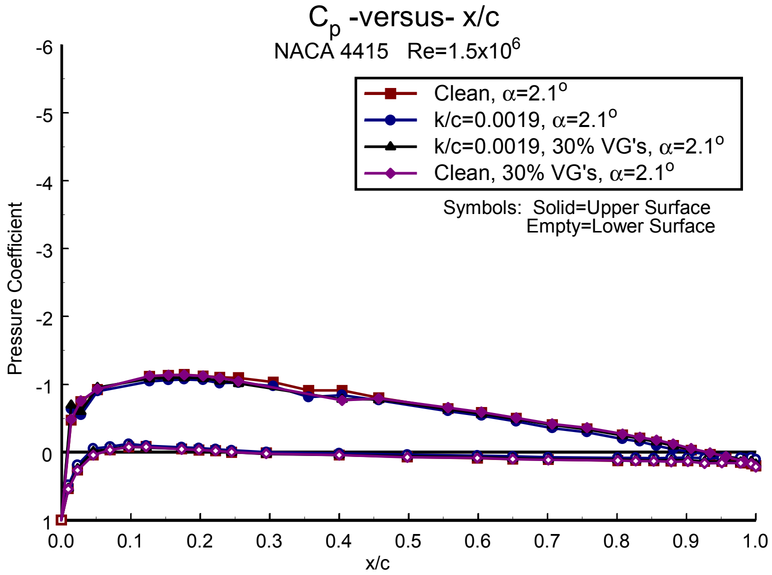

Figure B113. □□ 2°

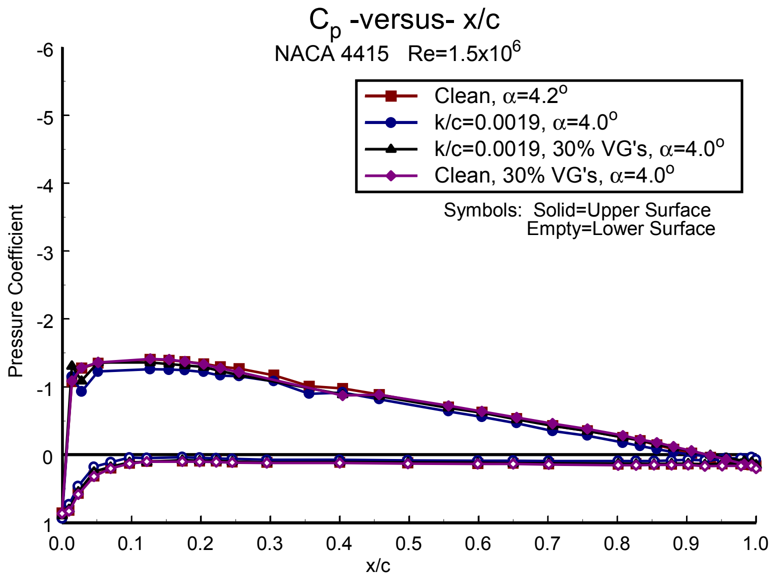

Figure B114. α = 4°

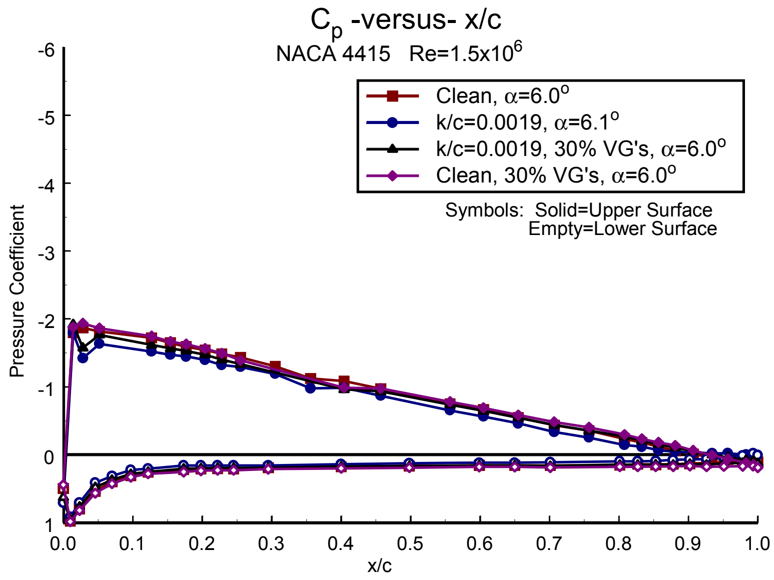

Figure B115. α = 6°

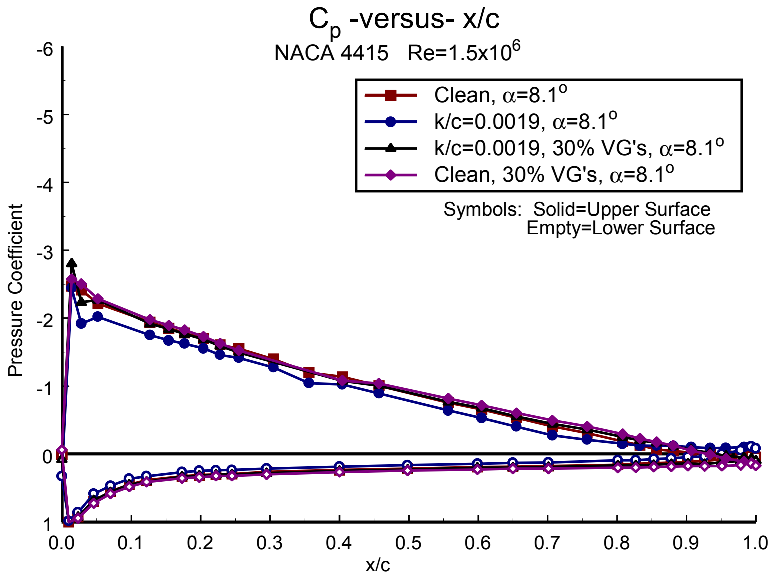

Figure B116. α = 8°

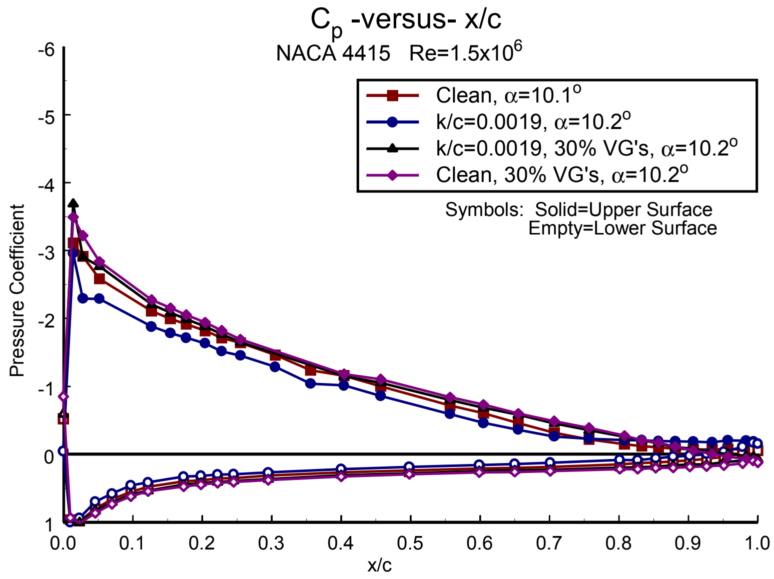

Figure B117. α = 10°

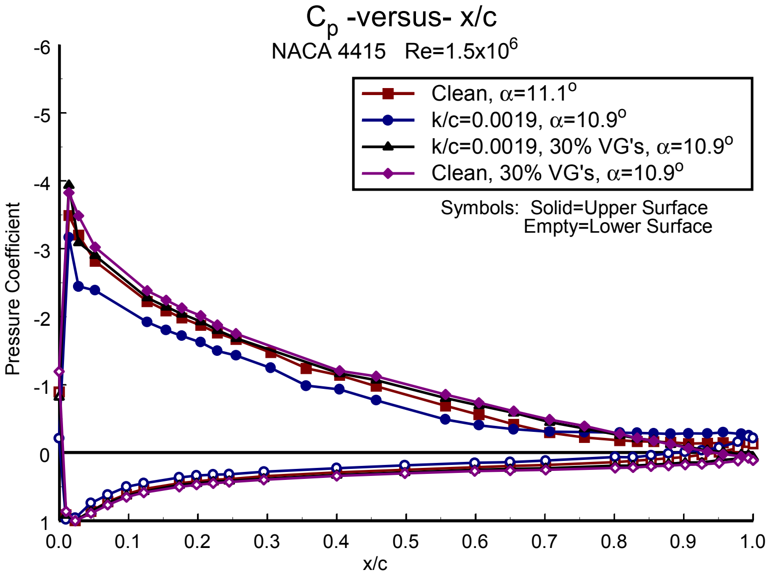

Figure B118. α = 11°

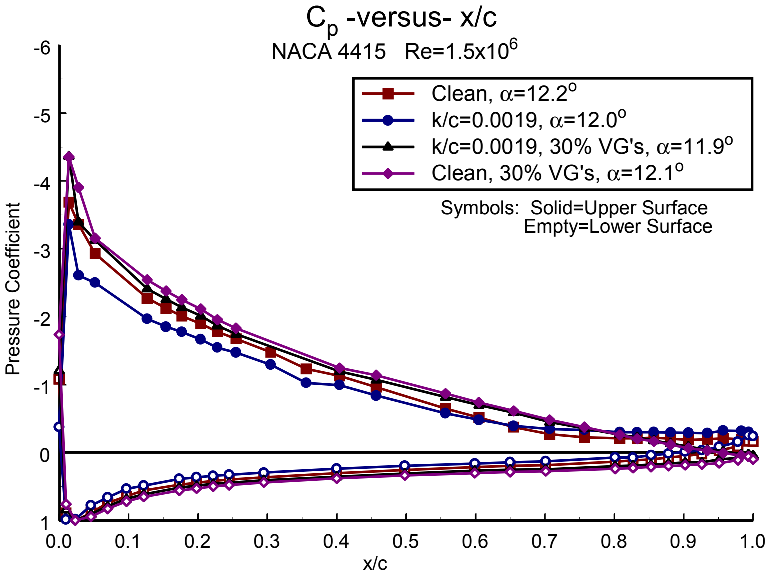

Figure B119. α = 12°

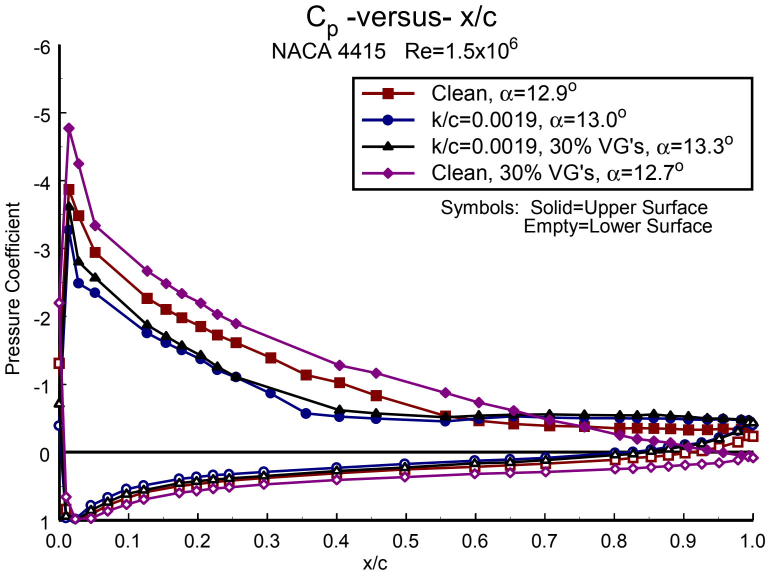

Figure B120. α = 13°

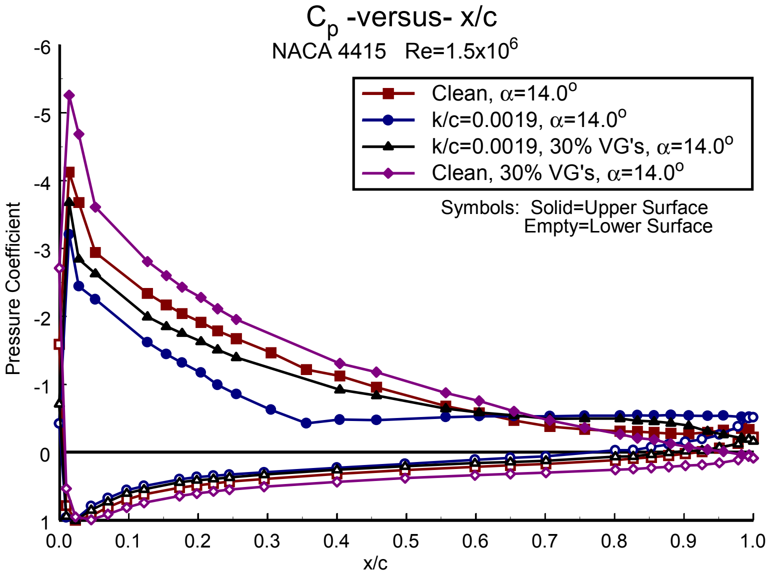

Figure B121. α = 14°

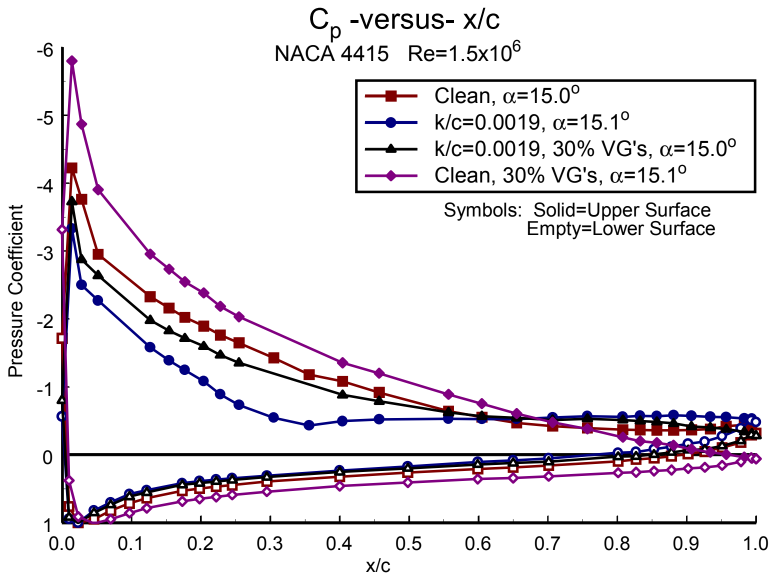

Figure B122. α = 15°

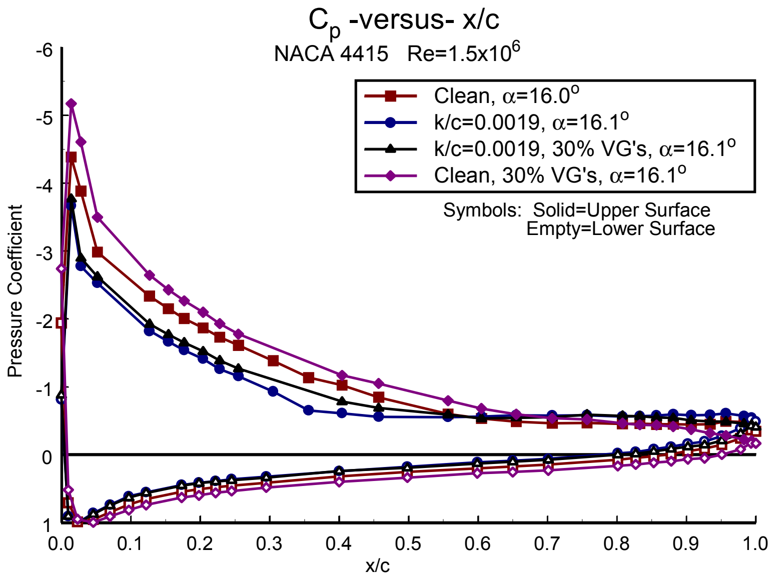

Figure B123. α = 16°

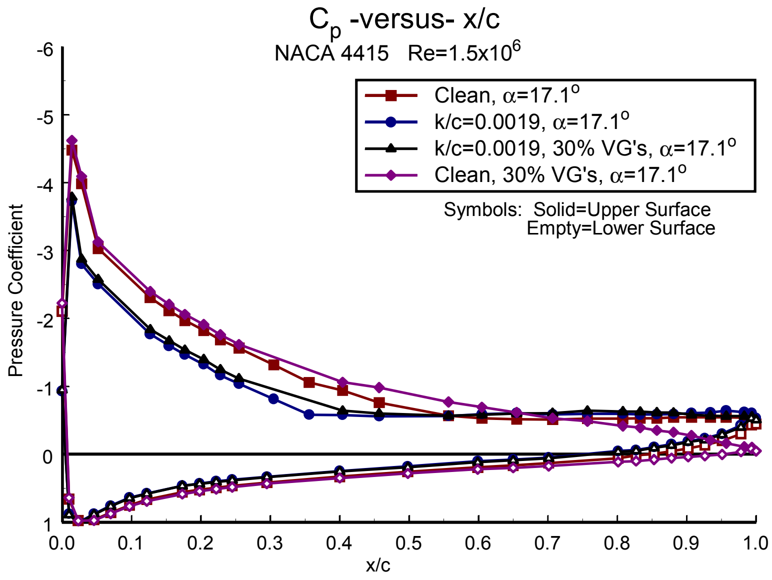

Figure B124. α = 17°

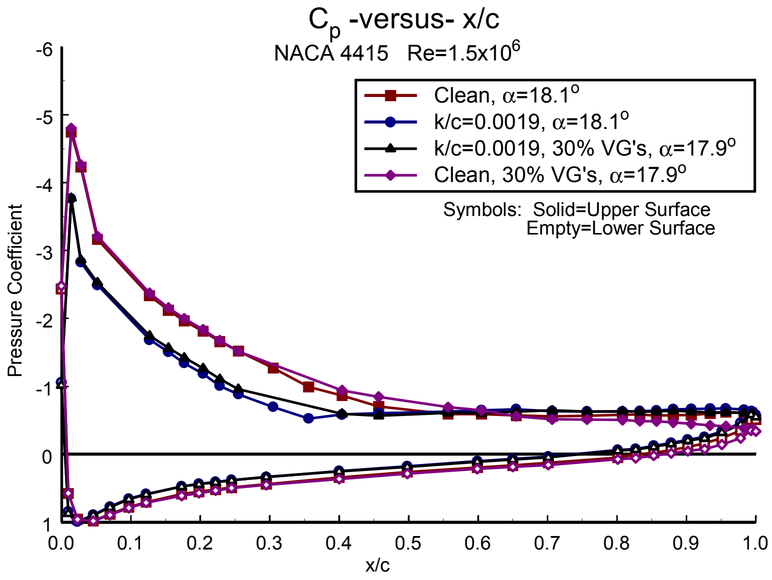

Figure B125. α = 18°

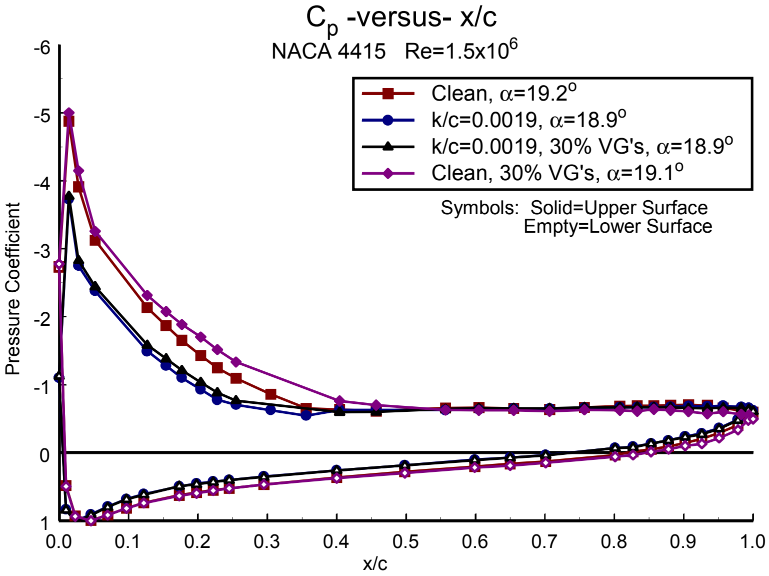

Figure B126. α= 19°

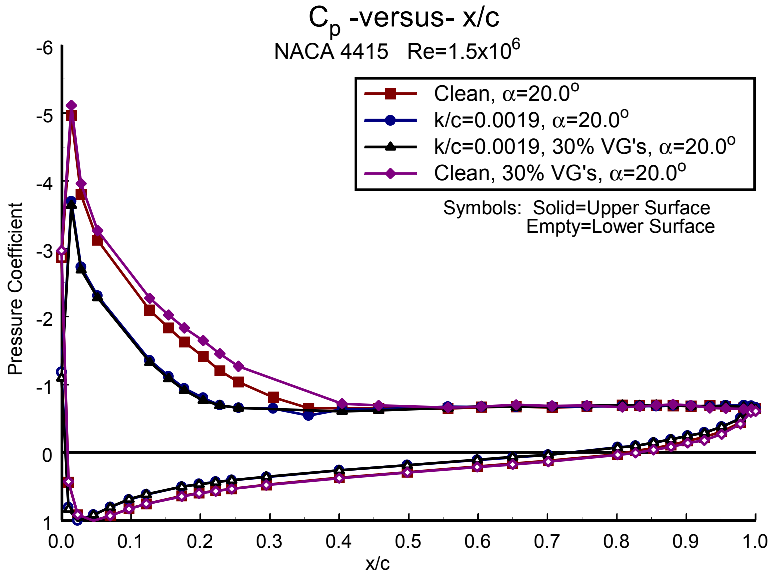

Figure B127. α= 20°

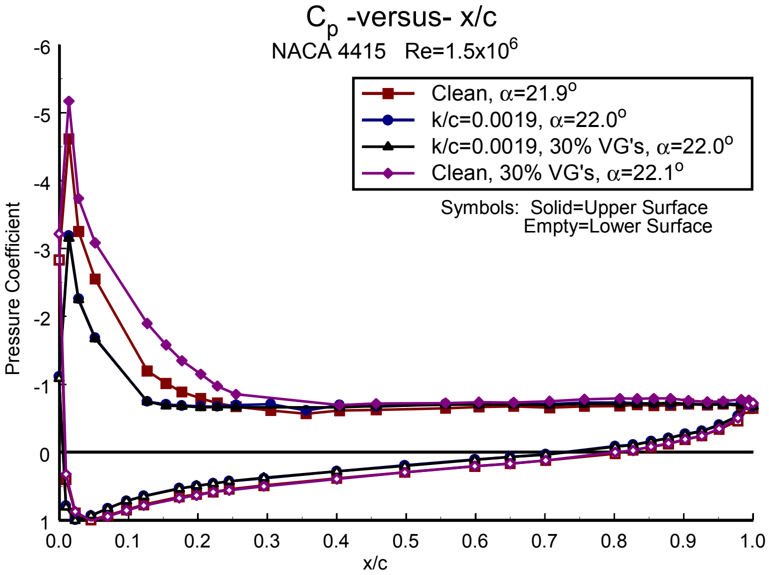

Figure B128. α= 22°

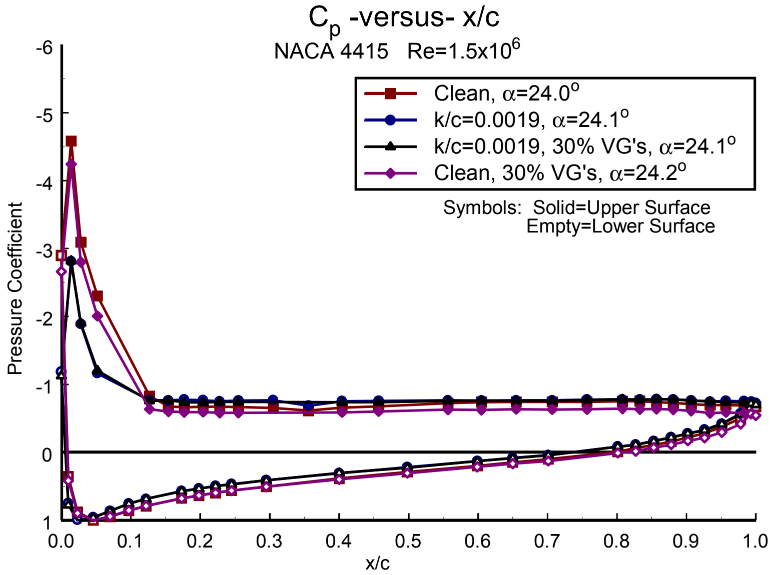

Figure B129. α= 24°

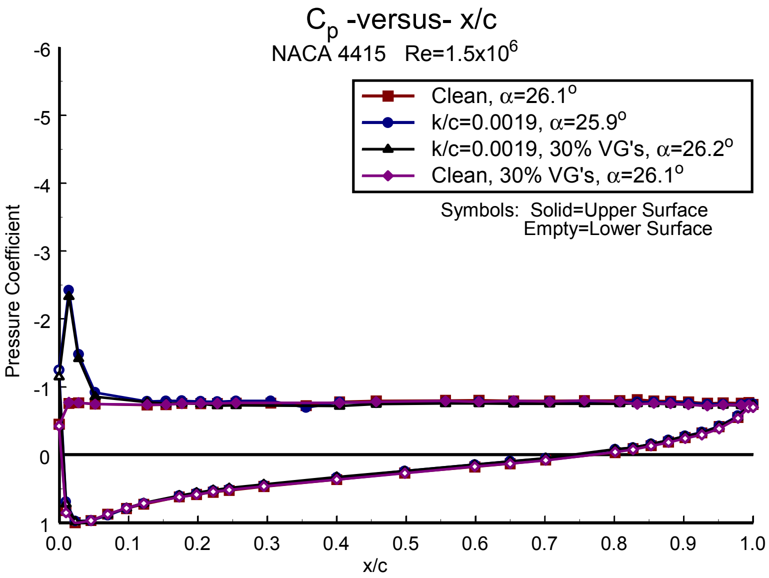

Figure B130. α = 26°

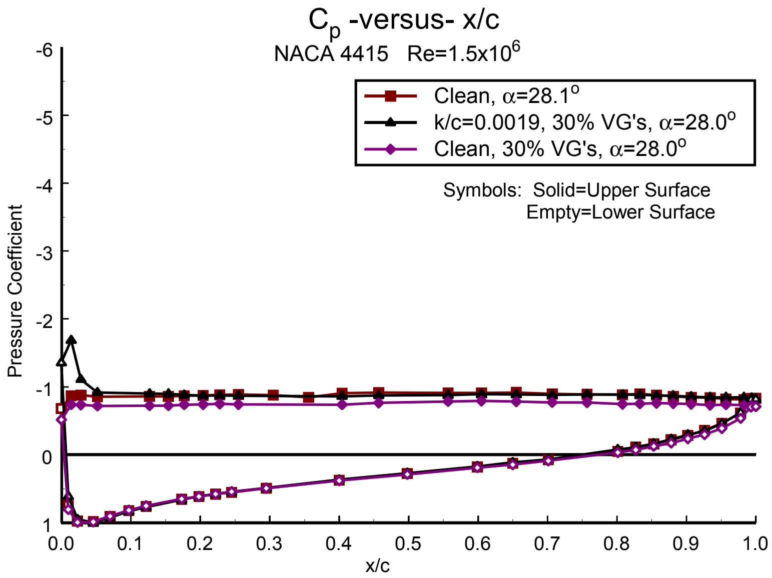

Figure B131. α = 28°

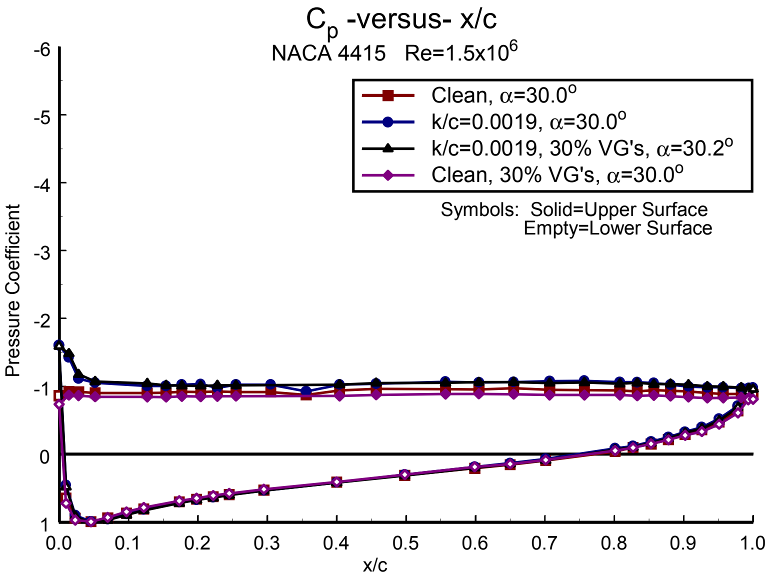

Figure B132. α = 30°

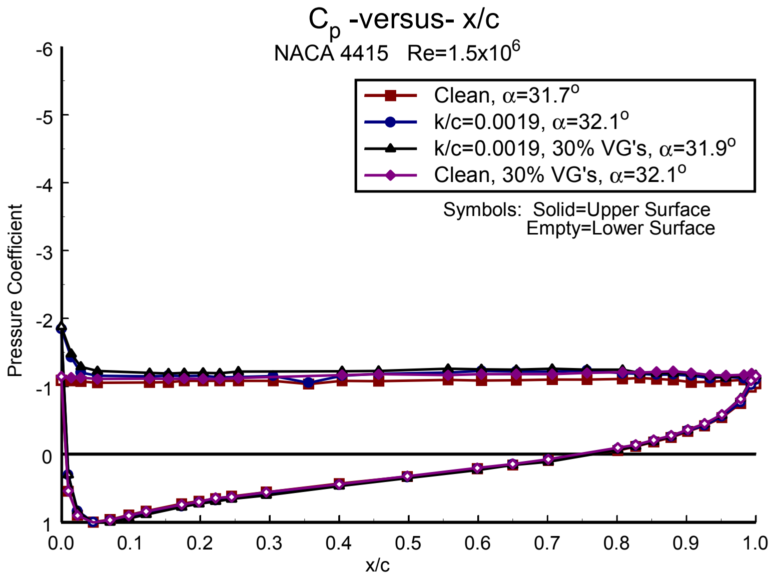

Figure B133. α = 32°

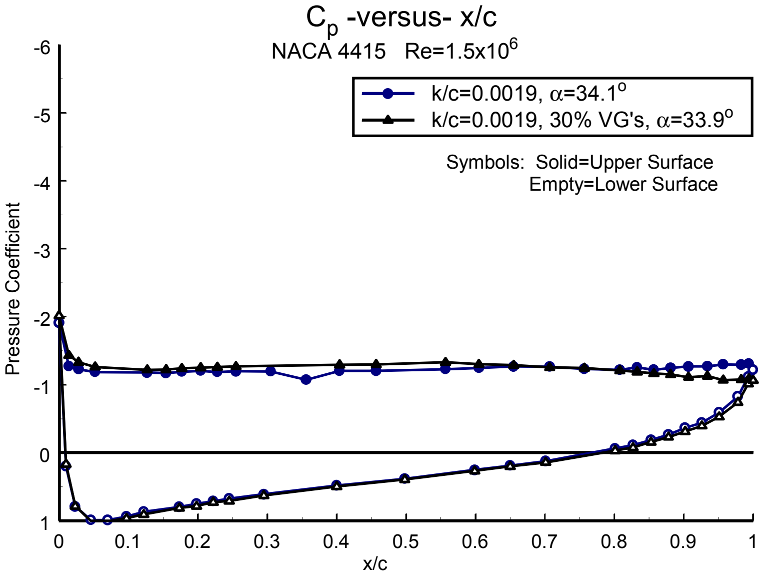

Figure B134. α = 34°

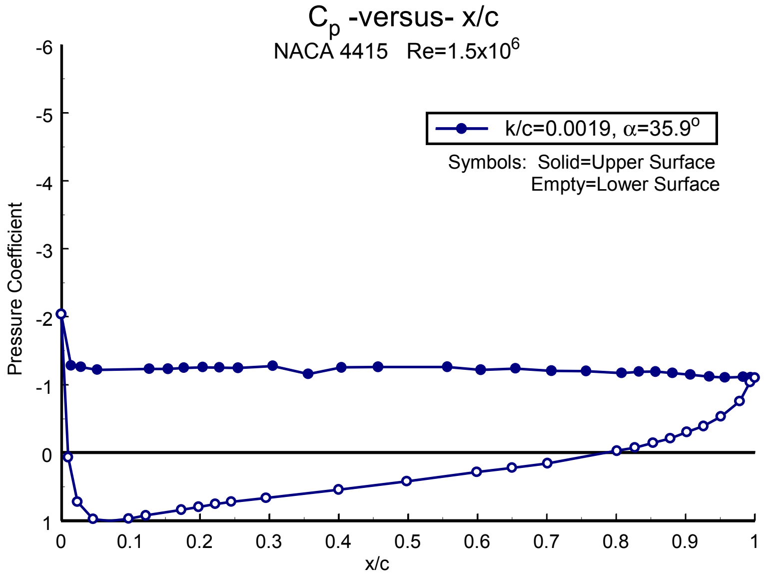

Figure B135. α = 36°

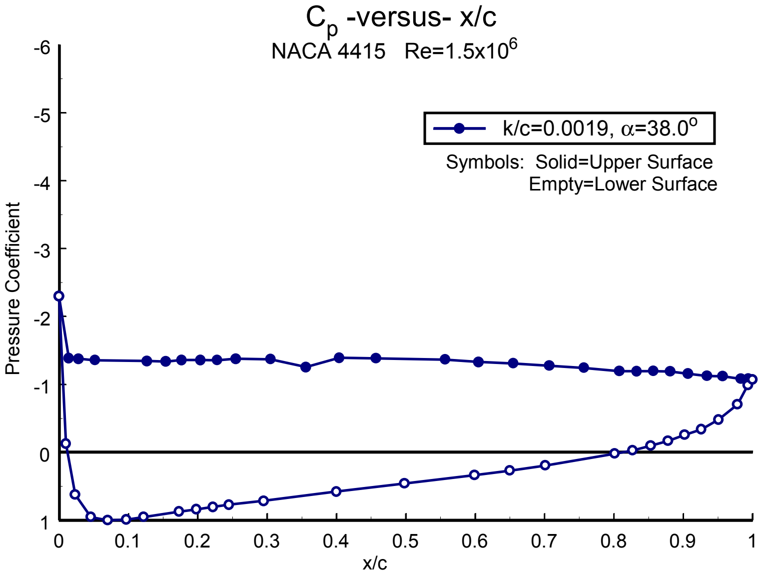

Figure B136. α = 38°

Steady-State Pressure Distributions

Re = 2.0 million

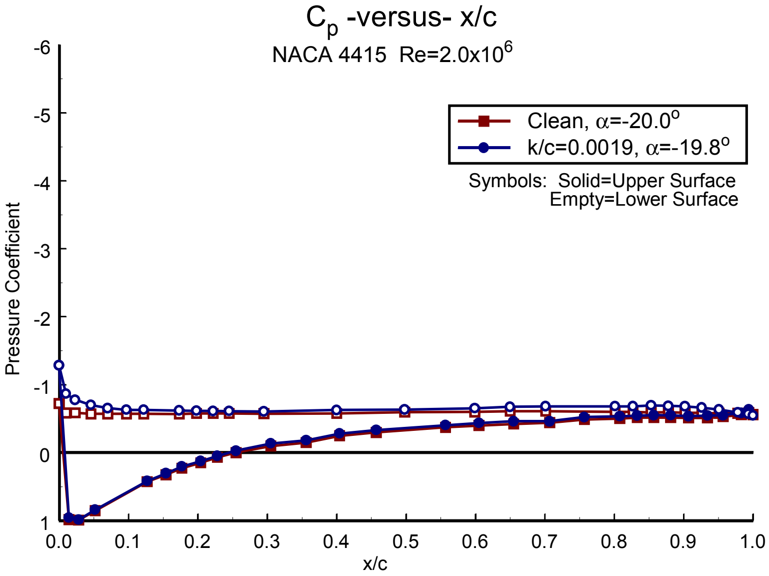

Figure B137. α= -20°

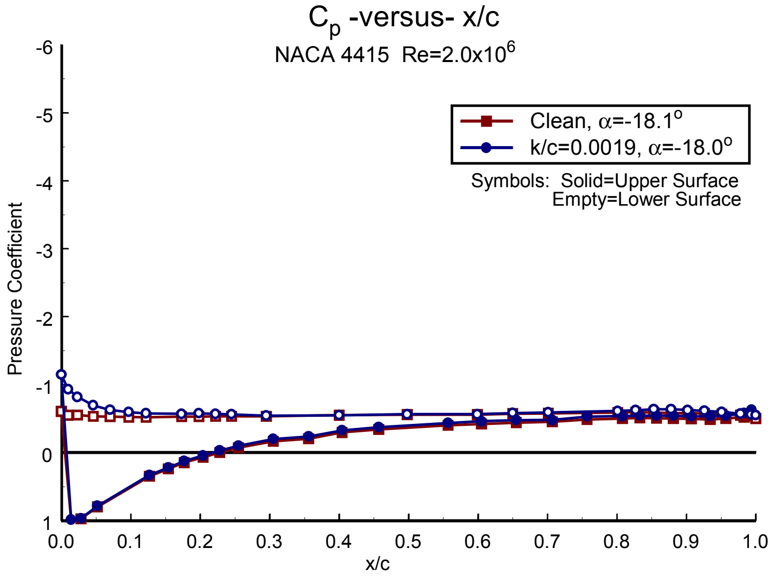

Figure B138. α= -18°

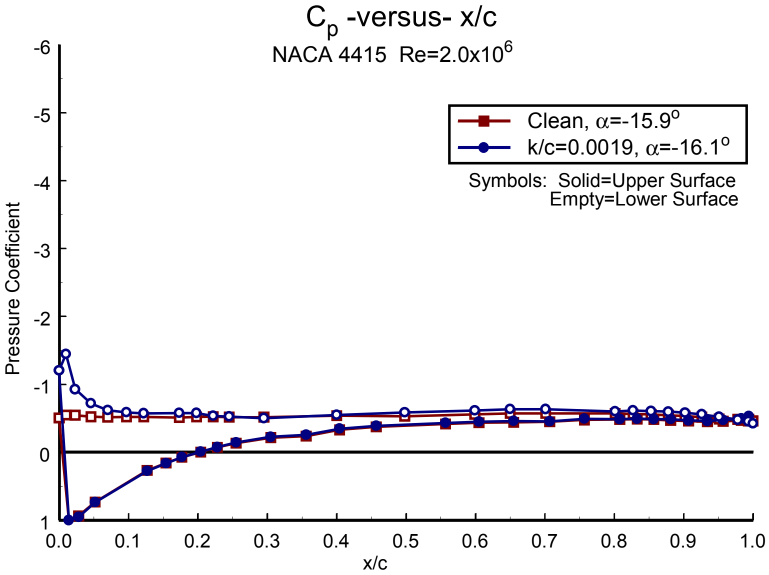

Figure B139. α= -16°

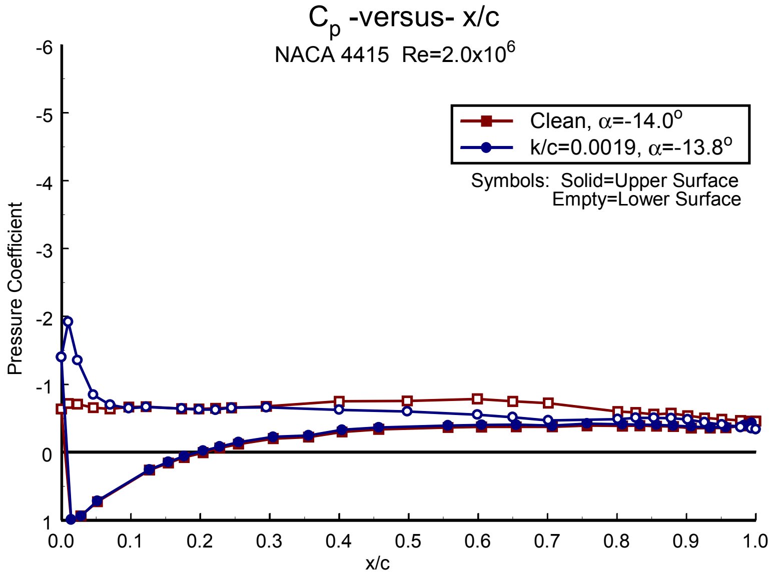

Figure B140. α= -14°

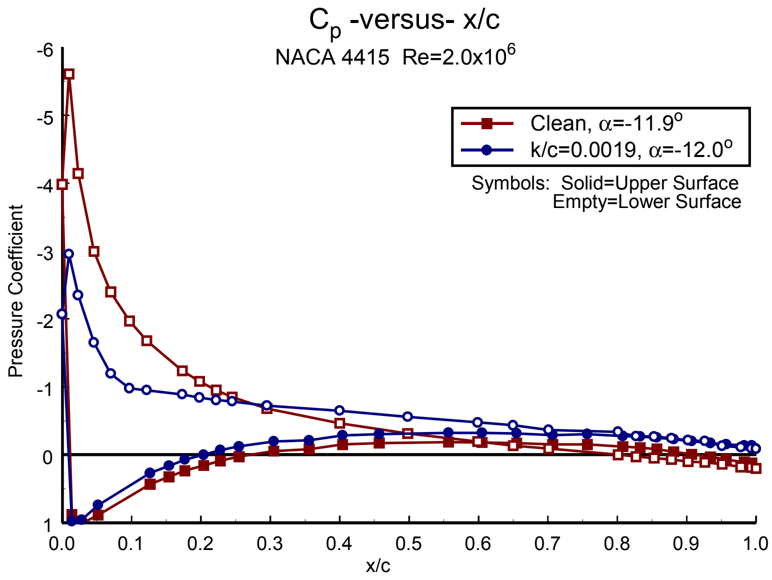

Figure B141. α= -12°

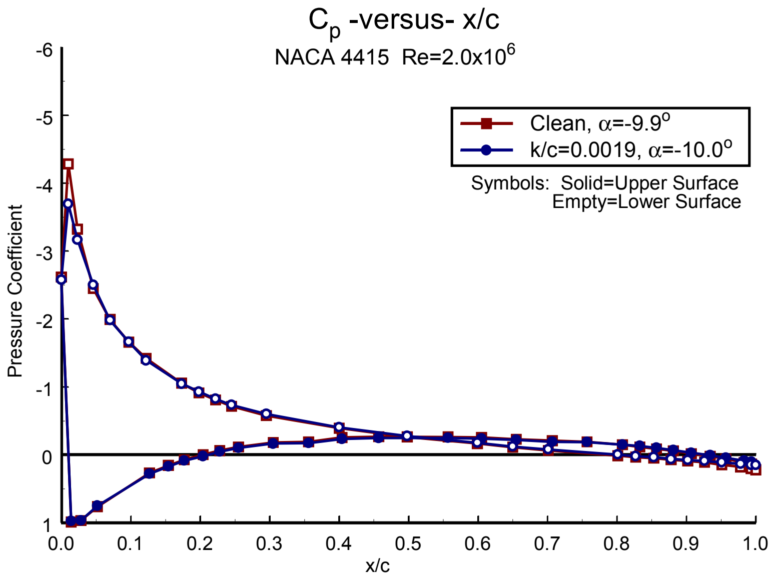

Figure B142. α= -10°

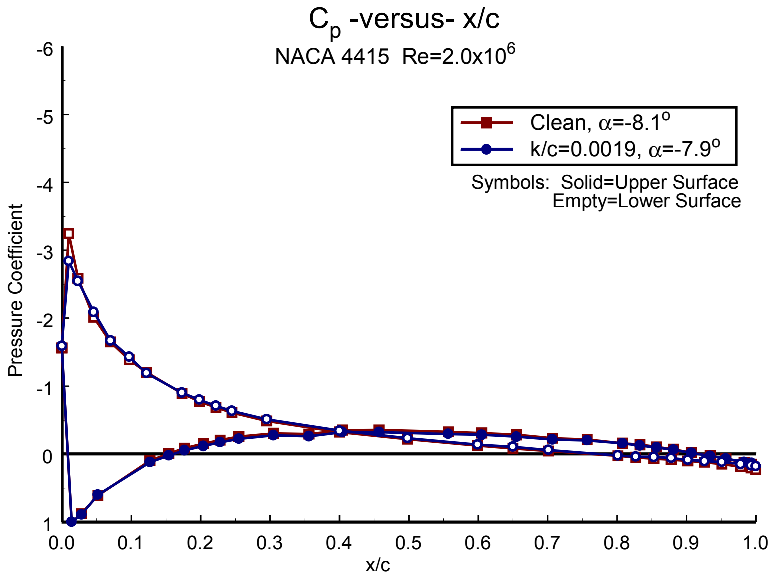

Figure B143. α= -8°

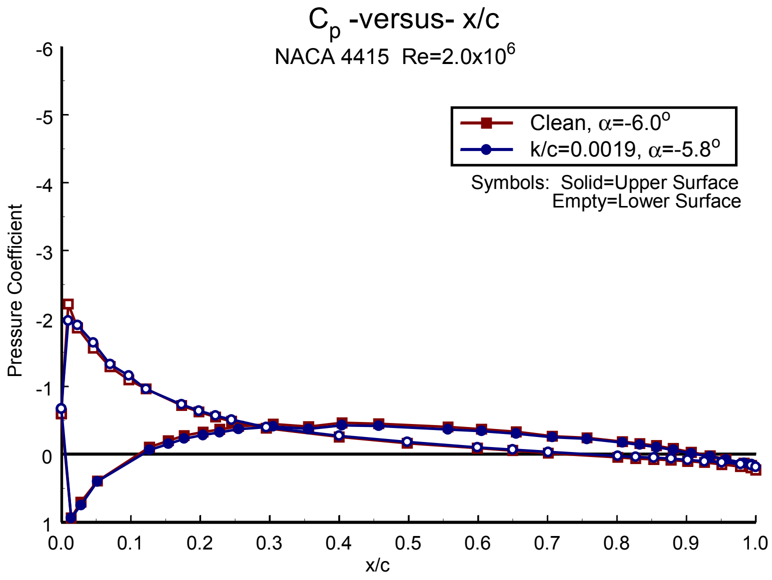

Figure B144. α= -6°

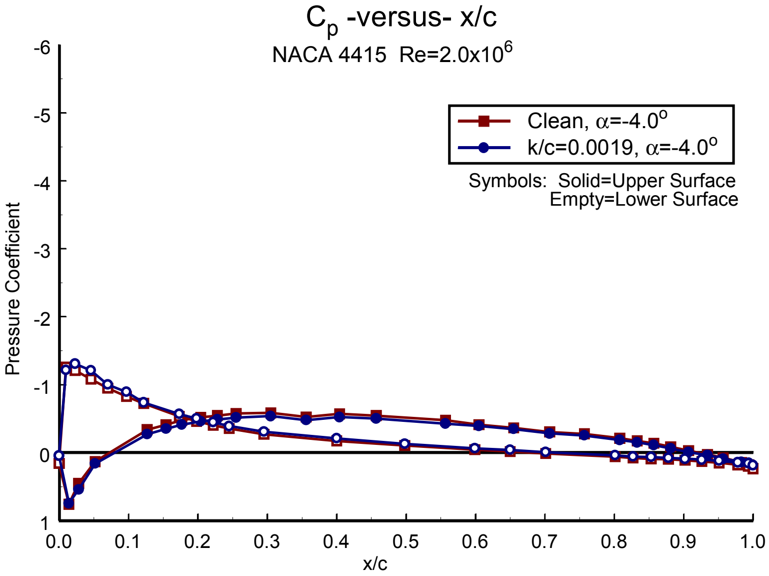

Figure B145. α= -4°

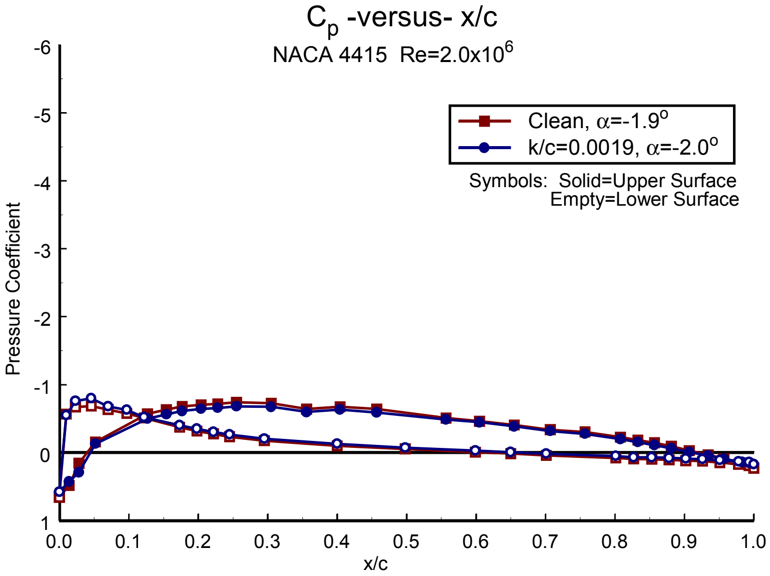

Figure B146. α= -2°

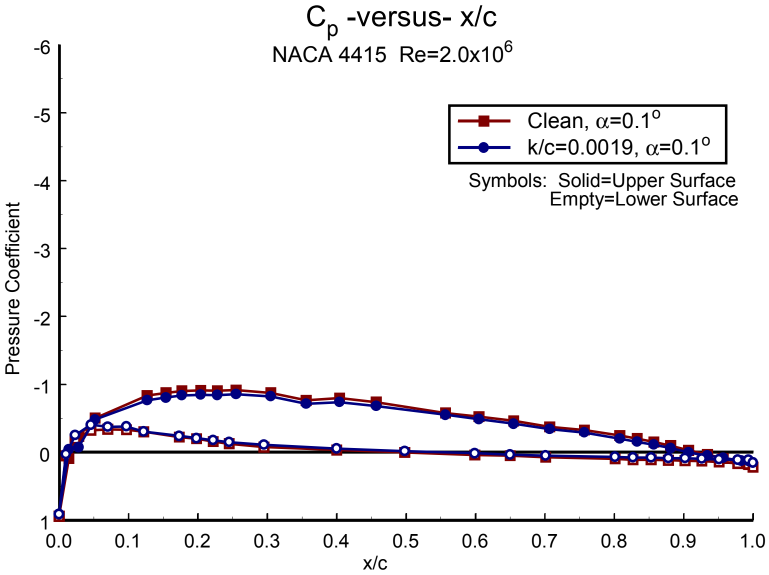

Figure B147. α= 0°

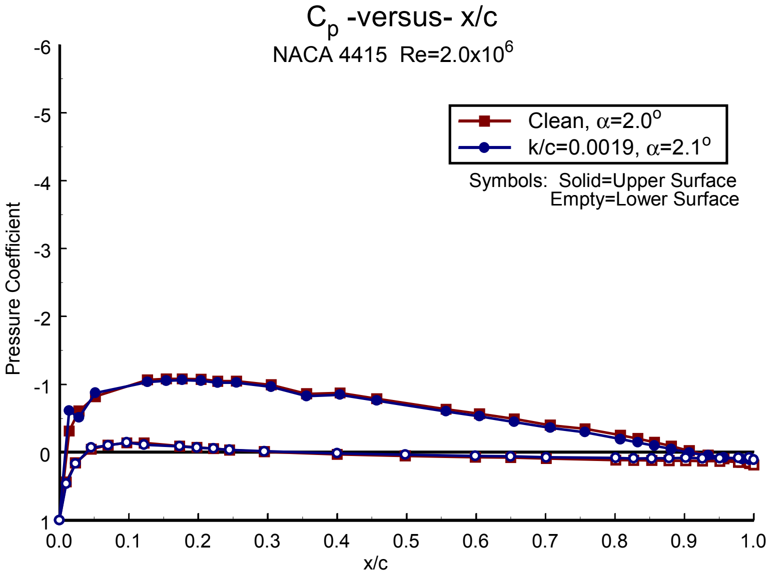

Figure B148. α= 2°

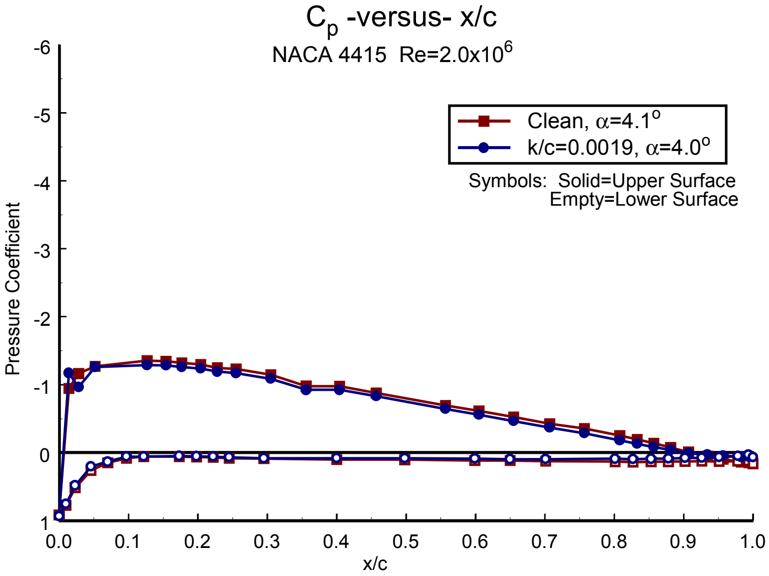

Figure B149. □□= 4°

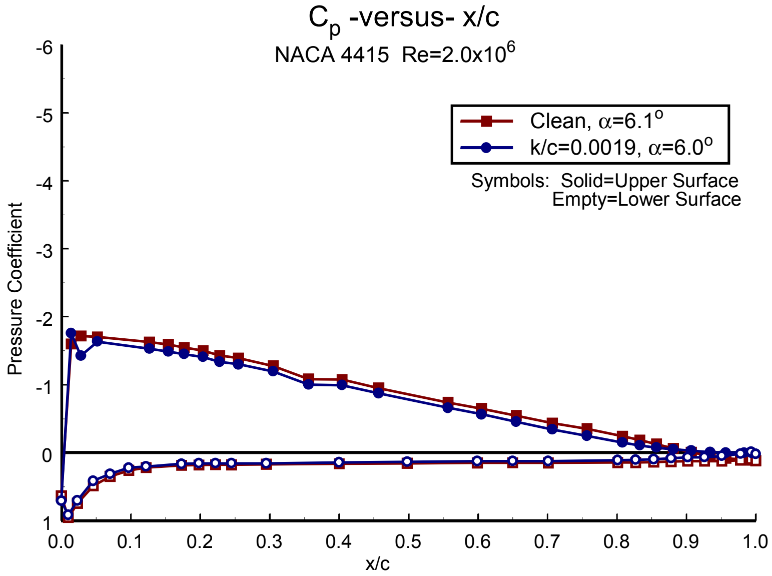

Figure B150. □□= 6°

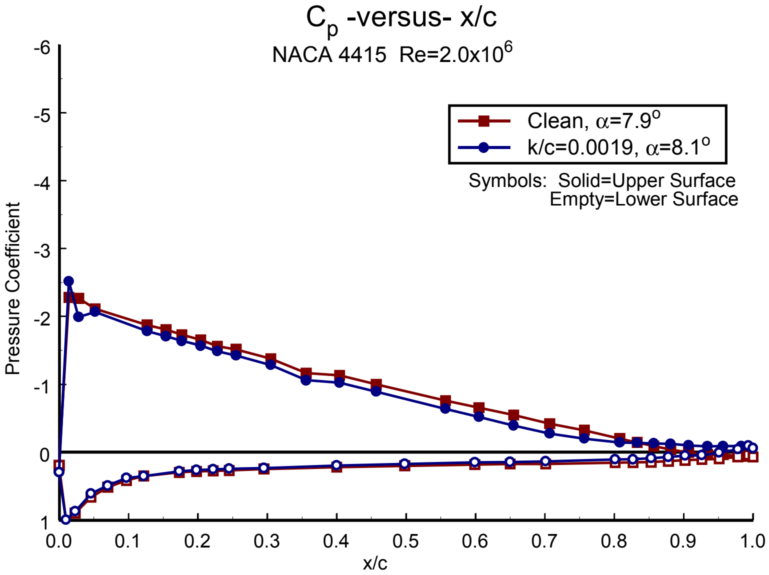

Figure B151. □□= 8°

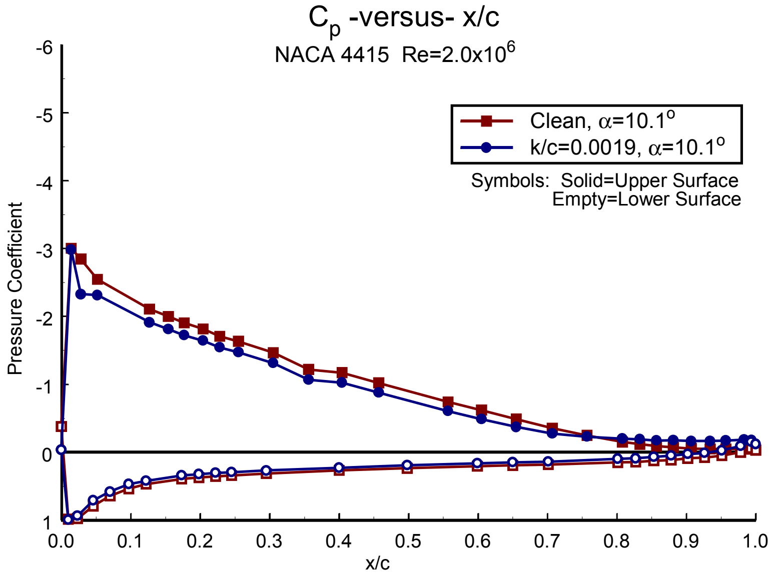

Figure B152. □□= 10°

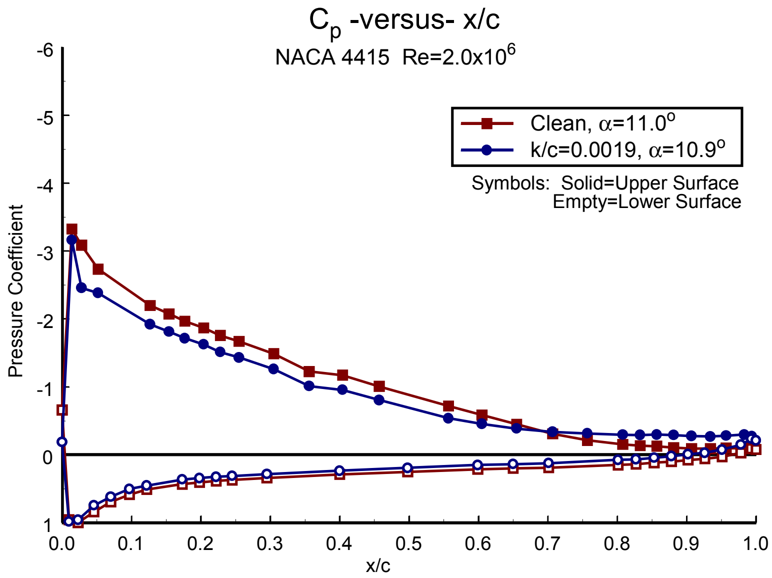

Figure B153. □□= 11°

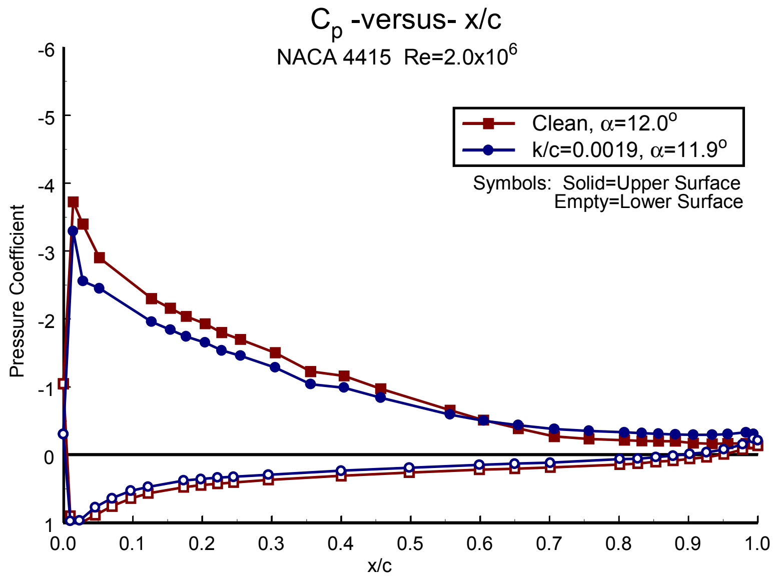

Figure B154. □□= 12°

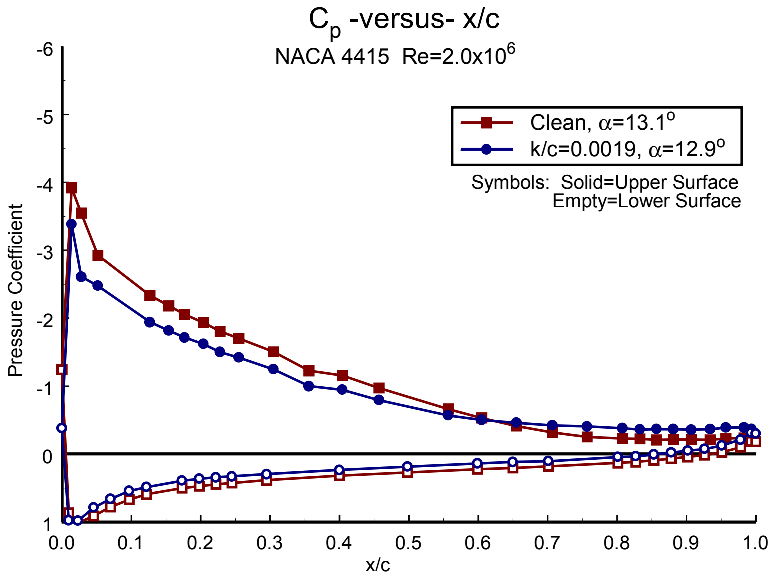

Figure B155. □□= 13°

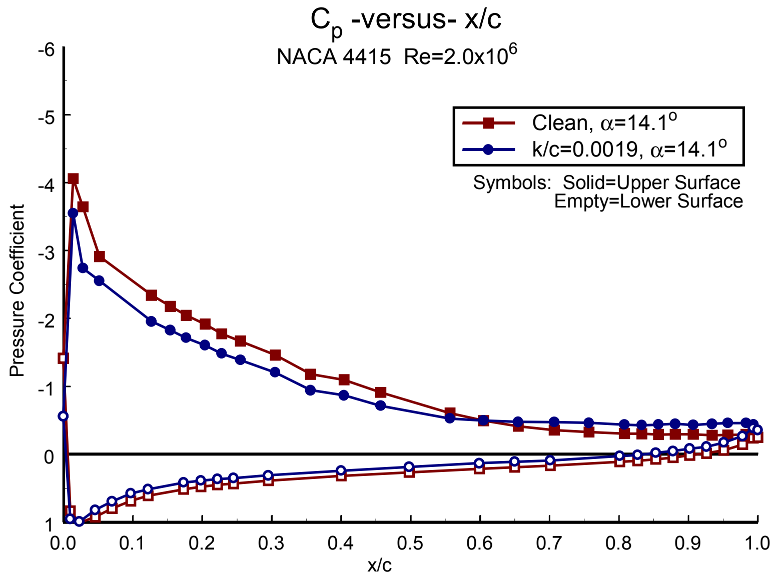

Figure B156. □□= 14°

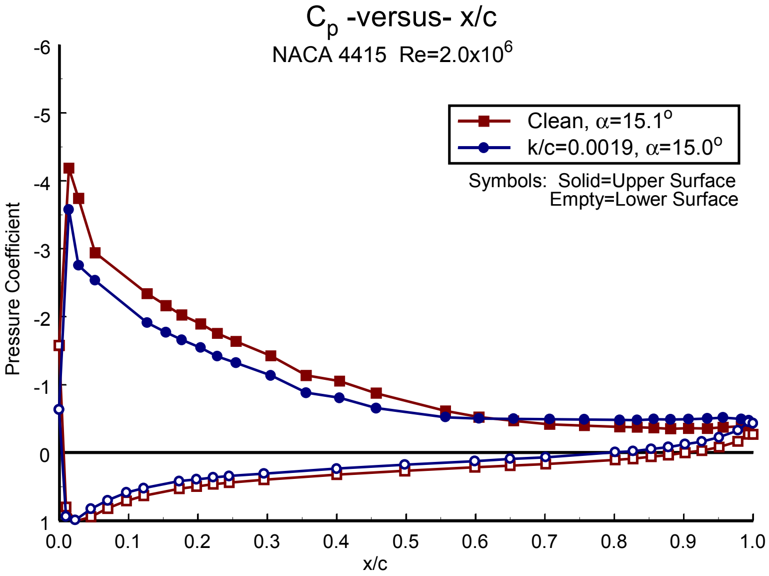

Figure B157. □□= 15°

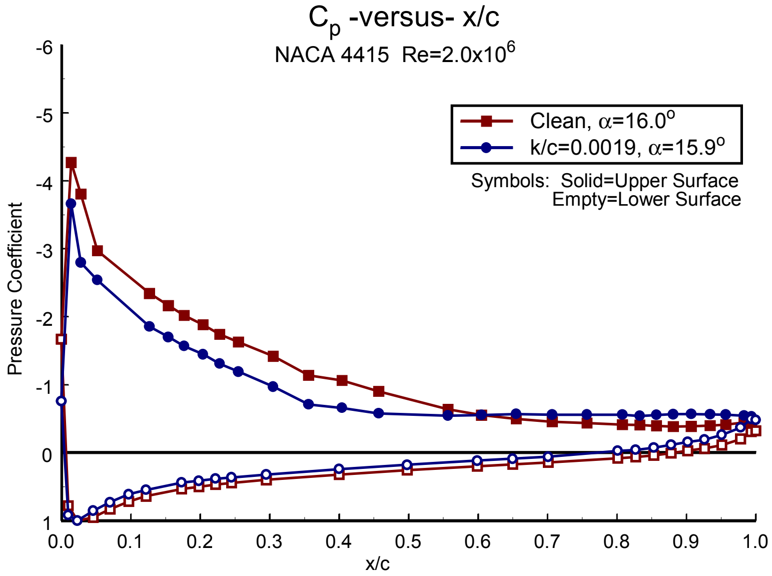

Figure B158. □□= 16°

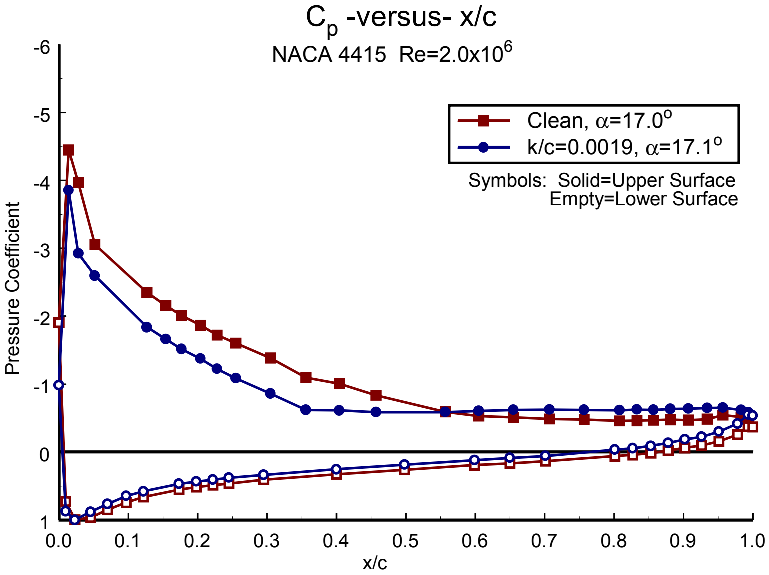

Figure B159. □□= 17°

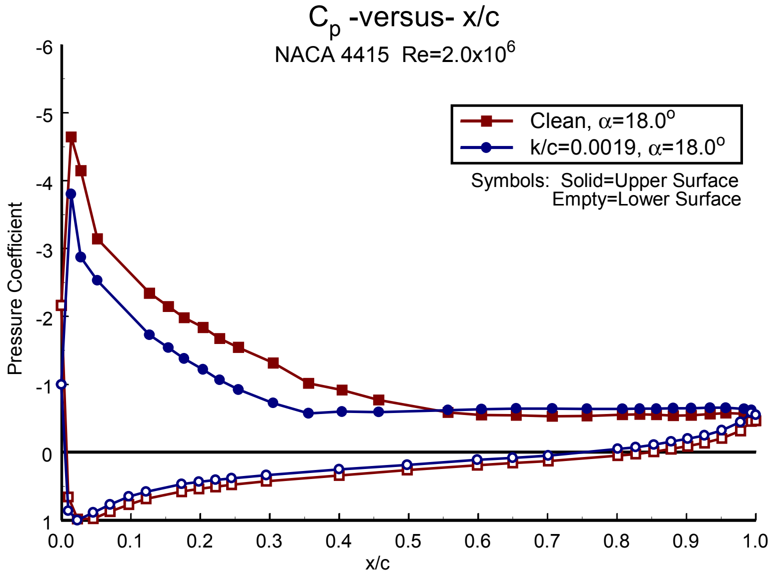

Figure B160. □□= 18°

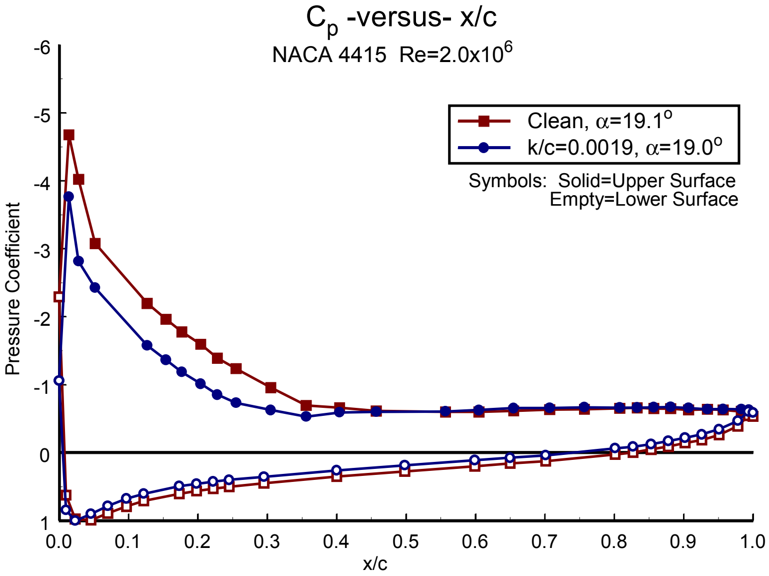

Figure B161. □□= 19°

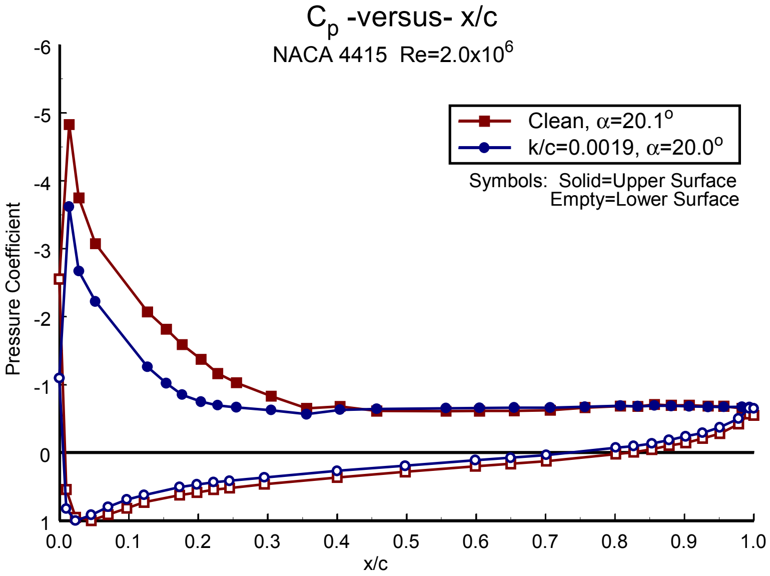

Figure B162. □□= 20°

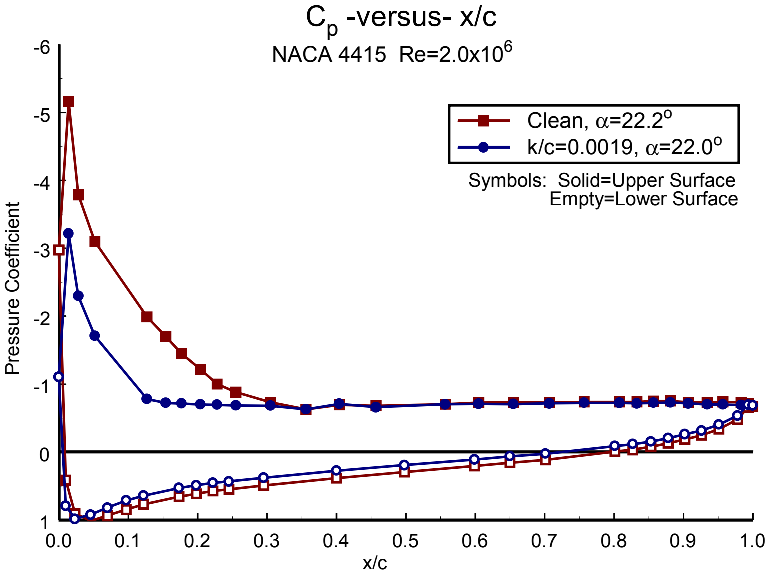

Figure B163. □□= 22°

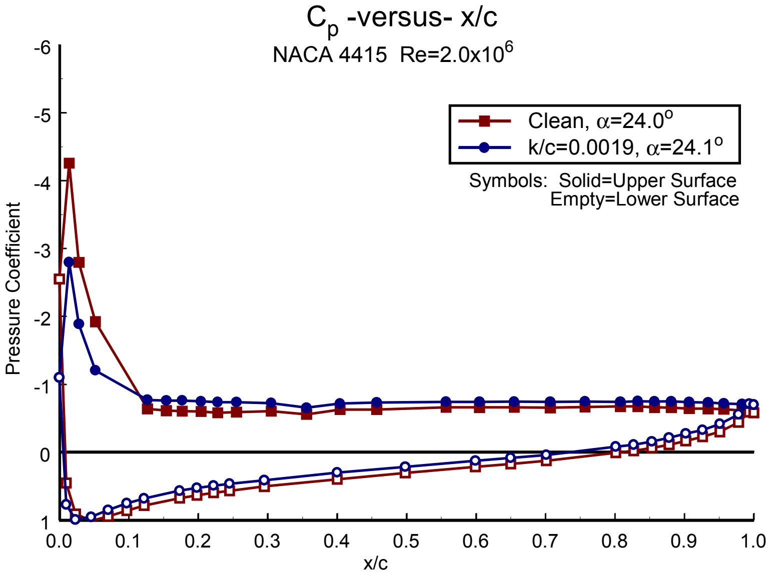

Figure B164. □□= 24°

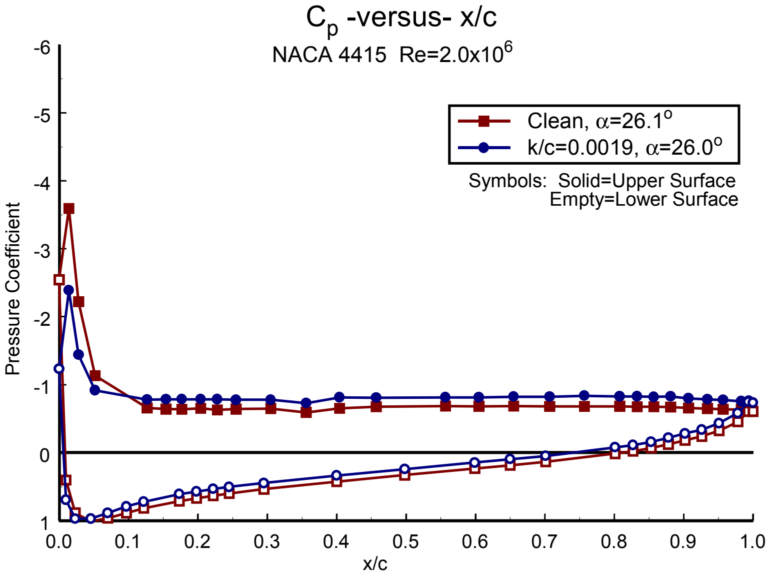

Figure B165. □□ 26°

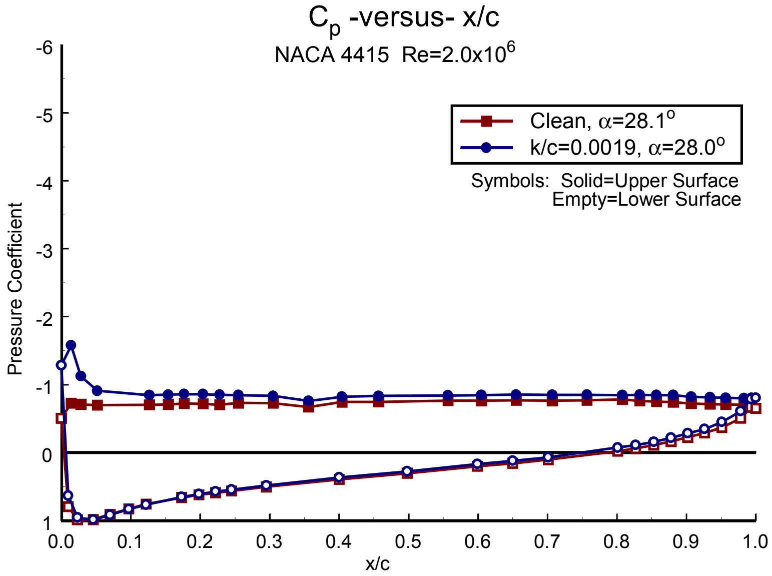

Figure B166. □□ 28°

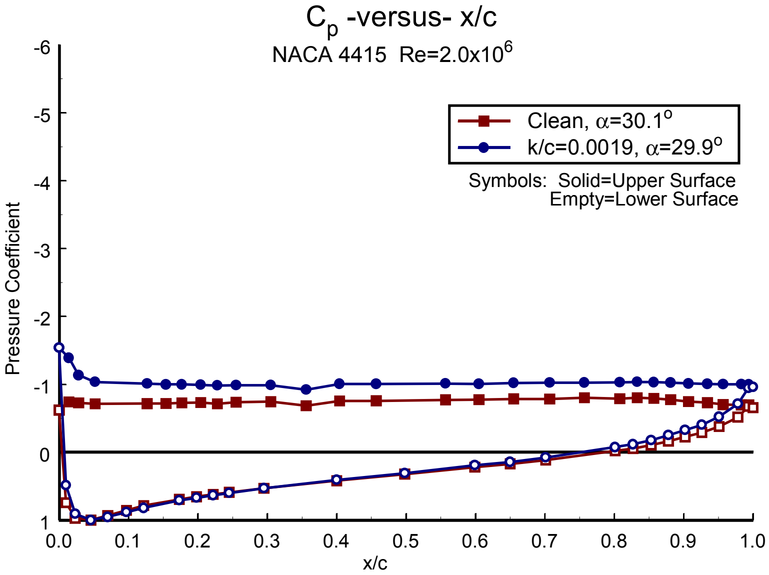

Figure B167. □□ 30°